Complexity

Complexity, Reliability, and Economics of Manufacturing Systems

Lead Guest Editor: Fuli Zhou
Guest Editors: Saurabh Pratap and Ashish Dwivedi

Complexity, Reliability, and Economics of Manufacturing Systems

Complexity

Complexity, Reliability, and Economics of Manufacturing Systems

Lead Guest Editor: Fuli Zhou
Guest Editors: Saurabh Pratap and Ashish Dwivedi

Contents

Hindawi
Complexity
Volume 2024, Article ID 6489087, 28 pages
https://doi.org/10.1155/2024/6489087

WILEY | Hindawi

Research Article

A New Mathematical Model for Cell Layout Problem considering Rotation of Unequal Dimensions of Cells and Machines

Raheleh Alamiparvin, Esmaeil Mehdizadeh, and Hamed Soleimani

Department of Industrial Engineering, Faculty of Industrial and Mechanical Engineering, Qazvin Branch, Islamic Azad University, Qazvin, Iran

Correspondence should be addressed to Esmaeil Mehdizadeh; es.mehdizadeh@iau.ac.ir

Received 26 November 2022; Revised 3 August 2023; Accepted 9 February 2024; Published 12 March 2024

Academic Editor: M. De Aguiar

One of the main concepts in group technology (GT) is the cellular manufacturing system (CMS) with three main problems of cell formation (CF), cell layout (CL), and cell scheduling (CS). This paper studies the cell layout problem (CLP), aiming to find the optimal layout of machines within each cell (intracellular layout) and the optimal layout of cells in each workshop (intercellular layout). To adapt to reality, the dimensions of the cells and machines (inside each cell) were considered unequal, and also the cells and machines could rotate. We believe that a cellular layout that assumes unequal dimensions of the cells and machines can be used for batch production. This kind of production has a wide variety of low to medium demand. Furthermore, a cellular layout can be applied in CMSs and also in noncontinuous industries that have a job shop layout. Our main contribution is considering the possibility of rotating the cells and machines inside the cells. For this purpose, a mixed nonlinear programming model was developed to solve the CLP with the minimum cost of intracellular and intercellular material flows. The proposed nonlinear model was first converted into a linear model, and then a problem was generated and solved with GAMS software to validate the resulting linear model. This model finds the best layout of cells within the workshop and the best layout of machines inside each cell. Then, because of the NP-hardness of the CLP and the fact that even exact methods cannot solve large-scale examples in an acceptable computational time, an imperialist competitive algorithm (ICA) was designed and used to solve the problem. To evaluate the efficiency of the proposed algorithm, its numerical results in small dimensions were compared with the results of GAMS software. In large dimensions, 30 random problems were created, and the results of ICA were compared with the results of the particle swarm optimization (PSO) algorithm and genetic algorithm (GA). Finally, the parameters of the three meta-heuristic algorithms were set by the Taguchi method. Numerical results indicated that ICA was superior to both the PSO algorithm and GA. It could also achieve efficient solutions in a shorter computational time.

1. Introduction

One of the main purposes of manufacturing systems is to convert raw materials, capital, information, labor, and other resources into more value-added goods or services. Manufacturing systems consist of several specifically organized machines to construct different kinds of products. They have different types based on facility layout, flow shop system, job shop system, fixed position layout, and cellular manufacturing system (CMS). In a flow shop system, production facilities are set sequentially. Examples of this flow are metal production industries, refineries, and petrochemical industries. In a job shop production system, similar machines are located next to each other as in automotive and home appliance industries. In fixed position layout, the product is fixed, and each department performs the essential processes. Examples of such systems are aircraft, ship building, and construction industries. The last type of production system, i.e., CMS, is an application of group technology (GT) and comparing to other types of manufacturing systems like the flow shop system, has higher flexibility in the production of different types of products. Also comparing to job shop production system, which is used only for low production volume with high production

and storage cost, CMS enjoys good efficiency with a higher production rate [1].

A cell may contain a group of similar machines in which the components must have the maximum movement within each cell and the minimum movement relating to other cells. This advantage causes in the reduction of material handling costs, process and setup times, and inventory, which ultimately leads to better quality, customer satisfaction, and on-time delivery of the product. For the effective implementation of CMS, there are three important tasks:

(1) Grouping of parts with similar design features or processes in the family of parts, and grouping of machines into machine cells, which is called cell formation (CF).

(2) Finding the optimal layout of machines within each cell (intracellular layout) and the optimal layout of cells in the workshop (intercellular layout), which is collectively called cell layout problem (CLP).

(3) Determining the order of part families in each cell and the order of tasks in each part family, which is called cell scheduling (CS) [2].

The main objective of this paper is to develop a new mixed nonlinear mathematical model for CLP while the cells and machines have unequal dimensions and can rotate. The main questions of the paper are: "How to extend a new mixed nonlinear mathematical model for CLP?" and "How to solve it due to the Np-hardness of the model?" Accordingly, the main contributions of this research can be outlined as follows:

(i) Unlike previous research findings implying that do not rotate, using the model developed in this research, cells and machines can rotate in different directions.

(ii) In order to conform to the reality, unequal dimensions for cells and machines have been considered in this study.

(iii) The main application of cellular layout is in the automotive industries like the Toyota manufacturing industry.

(iv) In the present study, a new mixed nonlinear mathematical model has been proposed for CLP.

The following phases have been done in the present study. The related literature is reviewed in Section 2. Problem statement is explained in Section 3. A mathematical model of the problem is presented in Section 4 to minimize the intercellular and intracellular material flow. Since CLP is very complex and its computational time increases extremely as the size of the problem increases, exact algorithms for solving large-size problems lose their efficiencies; therefore, Section 5 compares the results of ICA with those of (PSO) and (GA). Finally, conclusions, study limitations, and future works presented in Section 6.

2. Literature Review Related to CLPs

CLPs are generally divided into three types: intercellular layout, intracellular layout, and intra- and inter-cellular layout. In the first case, only the layout of cells in the workshop or intercellular layout is considered. The objective function, in this case, is to minimize the cost of material flow between the cells in the workshop. In the second case, the cells' location is already known, and only the layout of machines within each cell or intracellular layout is considered. The objective function of this type of problem is to minimize the cost of material flow between the machines inside the cells. In the third case, the layout of cells in the workshop and the layout of machines inside the cells are considered, which is called intra- and inter-cellular layout. The objective function, in this case, is to minimize the cost of material flow between the cells and the cost of material flow between the machines within each cell. In the following, almost all the work done in the field of CLPs are reviewed. Some studies considered intra- and inter-cellular layout problems under dynamic situations and assumed equal dimensions for cells and machines. Others considered intracellular layout problems. The third group of studies mentioned intercellular layout problems with similar dimensions for cells and machines. Then a mathematical model and a solution method are proposed for the mentioned problems, and numerical results are presented.

Rosenblatt [3] studied factory layout problems under dynamic conditions and equal dimensions for machines. Vakharia and Wemmerlov [4] considered the problem of intracellular layout with equal dimensions and used a coefficient to assess the similarity of parts and the formation of a family of parts and cells. Two years later, Venugopal and Narendran [5] proposed the problem of cell formation (CF) to minimize the intercellular movements of parts, balance the capacity of cells, and solve the problem using GA. Meanwhile, Jajodia et al. [6] developed a new method for intracellular and intercellular layout problems with the equal dimensions for cells and machines. Arvindh and Irani [7] proposed the idea of designing a CMS in intracellular and intercellular layout with equal dimensions for cells and machines and used the production flow technique as a solution. Kim and Kim [8] assumed a model in which the shape of the machine was regular or irregular, its dimensions were fixed, the material handling system was based on an open field, and the objective function had a single criterion.

Vakharia and Cheng [9] developed the CF problem in an intercellular layout. The solution method was based on simulated annealing (SA) and tabu search (TS) algorithms. Consequently, Liang and Zolfaghari [10] proposed a problem for grouping machines with equal dimensions under uncertain and static conditions. Wang et al. [11] proposed a model for solving equipment layout problems in CMSs in which the demand rates changed over the product's life cycle. Lozano et al. [12] developed machine grouping and intercellular layout problems and considered a mathematical programming model to minimize the cost of intercellular

translocation. Solimanpur et al. [13] developed intercellular layout problems as a quadratic assignment. Anders and Lozano [14] proposed CF and intercellular layout problems by assuming a criterion for grouping machines in cells and used PSO algorithm to solve them. Tavakkoli-Moghaddam et al. [15] addressed intracellular and intercellular layout problems by assuming the possible demands and considered the fuzzy linear integer programming model. Hu et al. [16] inspected the intercellular layout problem and developed a model to minimize the cost of intercellular material flow. Chan et al. [17] proposed intercellular and intracellular layout problems by assigning machines within cells and considering equal dimensions for cells and machines. Tavakkoli-Moghaddam et al. [18] considered the problem of dynamic CF and intercellular layout under dynamic conditions. Mahdavi et al. [19] concentrated on the problem of intercellular and intracellular movements and CF in CMS. The following year, Rafiee et al. [20] proposed a CMS considering intracellular and intercellular layout problems in dynamic conditions. Ariafar et al. [21] applied intracellular and intercellular layout problems to CMS. Mahdavi et al. [22] developed a mathematical model for the simultaneous combination of CF and intracellular and intercellular layout. Shiyas and Pillai [1] considered the problem of intercellular layout and used a mathematical model to design manufacturing cells. Asl and Wang [23] developed an intracellular layout problem under uncertain and probabilistic conditions to minimize material flow costs. Mehdizadeh and Rahimi [24] proposed an integrated mathematical model for solving the dynamic CF problem, considering operator allocation and intracellular and intercellular layout problems. Ghosh et al. [25] considered the problem of intercellular layout and proposed a quadratic assignment planning model for such problems. Derakhshan Asl and Wang [26] developed the problem of intracellular layout in static and dynamic conditions, supposing unequal machine dimensions and the possibility of machine rotation. Rabbani et al. [27] hypothesized the problems of CF and intracellular and intercellular layout simultaneously in dynamic conditions and grouping of machines and parts. Feng et al. [28] investigated the CL and CF problems simultaneously and used GA and SA to solve them. Golmohammadi et al. [29] developed intracellular and intercellular layout problems and assumed machines, cells, parts, and batch sizes for transporting parts.

Mahmoodian et al. [30] developed a "smart" PSO algorithm for CLPs. Danilovic and Illic [31] worked on a hybrid algorithm to solve CLPs. Paramasamy et al. [32] developed a GA to form families of machine parts and cells and solved CLPs.

Rahimi et al. [33] considered CF, intercellular layout, and cell scheduling problems for CMSs. Zhao et al. [34] proposed a new layout methodology for the multifloor linear cellular manufacturing layout and a mathematical model. Neufeld et al. [35] pointed out several characteristics that specify the distinctiveness of cell scheduling. Golmohammadi et al. [36] developed a biobjective optimization model to integrate CF and intercellular or intracellular layouts. Rostami et al. [37] presented a multiobjective mathematical model for the simultaneous integration of virtual cellular manufacturing with the supply chain and new product development. Ayough et al. [38] integrated job assignment and job rotation scheduling problems and presented a novel multiperiod nonlinear mixed integer model.

Goli et al. [39] designed a fuzzy mixed-integer linear programming model for CF problems in CMS. Salimpour et al. [40] developed CF, intracellular and intercellular layout problems, and machines of unequal dimensions. Golmohammadi et al. [41] considered the problem of facility layout by integrating CF in continuous space and intercellular and intracellular layouts. Mondal et al. [42] hypothesized the problems of intercellular layout and CF in CMS and offered a model for minimizing cell load variation and reducing intercellular movements. Razmjoei et al. [43] hypothesized an intercellular layout in CMS. Hazarika [44] proposed an intercellular layout in CMS and surveyed the problem of machine CF. Mansour et al. [45] studied cellular manufacturing and intracellular and intercellular layout problems at the same time. Fakhrzad et al. [46] simultaneously addressed CF and intercellular layout problems in terms of scheduling, labor assignment, and limited financial resources. Finally, Forghani and Fatemi Ghomi [47] addressed CF and group layout problems and proposed a mixed integer programming model. A summary of the results of the above works are presented in Table 1.

As shown in Table 1, the current research was conducted on CLPs, including intracellular and intercellular layouts where the dimensions of cells and machines are considered unequal and rotation of cells and machines are allowed. However, in the previous research studies, these six factors were not considered simultaneously.

2.1. Research Gap. As explained above, a comprehensive review of the literature within the last three decades clarifies that no research has examined CLPs under unequal dimensions of cells and machines within each cell and the possibility of rotation of cells and machines. Hence, this study was designed to examine these types of problems.

3. Problem Statement

In CLP problem, to find the layout of cells in the workshop and that of machines within each cell, first the number of cells and machines and then the dimensions of the workshop, cells, and machines are determined. Next, the number of machines inside each cell is specified. Lastly, the material flow between the cells and between the machines is determined. For example, assume we have three cells and ten machines. The cells are positioned in a workshop (1.5 m in length and 1.5 m in width). The length of the first cell is 50 cm and its width is 45 cm, and the length of the second cell is 45 cm and its width is 40 cm. The length and width of the third cell are both 40 cm, and the dimensions of the machines are also known. The first, second, third, and fourth machines are inside the first cell, the fifth, sixth, and seventh machines are inside the second cell, and the eighth, ninth, and tenth machines are inside the third cell. There is a material flow between the first, second, and third cells

Table 1: Results of literature review.

Author/Year	Intracellular	Intercellular	Unequal dimension of cells	Unequal dimension of machines	Cells rotation	Machines rotation
Rosenblatt (1986) [3]	• ⟶					
Vakharia and Wemmerlov (1990) [4]	• ⟶	• ⟶				
Venugopal and Narendran (1992) [5]		• ⟶				
Jajodia et al. (1992) [6]	• ⟶	• ⟶				
Arvindh and Irani (1994) [7]	• ⟶	• ⟶				
Kim and Kim (1995) [8]	• ⟶			• ⟶		• ⟶
Vakharia and Chang (1997) [9]		• ⟶				
Liang and Zolfaghari (1999) [10]		• ⟶				
Wang et al. (2001) [11]	• ⟶	• ⟶	• ⟶			
Lozano et al. (2002) [12]		• ⟶				
Solimanpur et al. (2004) [13]		• ⟶				
Anders and Lozano (2006) [14]		• ⟶				
Tavakkoli-Moghaddam et al. (2007) [48]	• ⟶	• ⟶				
Hu et al. (2007) [16]		• ⟶				
Chan et al. (2008) [17]	• ⟶	• ⟶				
Tavakkoli-Moghaddam et al. (2008) [18]		• ⟶				
Mahdavi et al. (2010) [19]	• ⟶	• ⟶		• ⟶		
Rafiee et al. (2011) [20]	• ⟶	• ⟶				
Ariafar et al. (2011) [21]	• ⟶	• ⟶				
Mahdavi et al. (2013) [22]	• ⟶	• ⟶	• ⟶	• ⟶		
Shiyas and Pillai (2014) [1]	• ⟶	• ⟶				
Asl and Wong (2015) [23]	• ⟶			• ⟶		• ⟶
Mehdizadeh and Rahimi (2016) [24]	• ⟶	• ⟶				
Ghosh et al. (2016) [25]		• ⟶				
Derakhshan Asl, Wong (2017) [26]	• ⟶			• ⟶		• ⟶
Rabbani et al. (2016) [27]	• ⟶	• ⟶				
Feng et al. (2018) [28]		• ⟶		• ⟶		
Golmohammadi et al. (2019) [29]	• ⟶	• ⟶				
Rahimi et al. (2020) [33]		• ⟶				
Mahmoodian et al. (2019) [30]	• ⟶	• ⟶				
Danilovich and Illich (2019) [31]	• ⟶	• ⟶				
Paramasamy (2019) [32]	• ⟶	• ⟶				
Zhao et al. (2020) [34]	• ⟶			• ⟶		
Neufeld et al. (2020) [35]		• ⟶				
Golmohammadi et al. (2020) [36]	• ⟶	• ⟶				
Rostami et al. (2020) [37]		• ⟶				
Ayough et al. (2020) [38]	• ⟶					
Salimpour et al. (2021) [40]	• ⟶	• ⟶	• ⟶	• ⟶		
Golmohammadi et al. (2021) [41]	• ⟶	• ⟶				
Goli et al. (2021) [39]		• ⟶				
Mondal et al. (2021) [42]		• ⟶				
Razmjoei et al. (2021) [43]		• ⟶				
Hazarika (2022) [44]		• ⟶				

Table 1: Continued.

Author/Year	Intracellular	Intercellular	Unequal dimension of cells	Unequal dimension of machines	Cells rotation	Machines rotation
Mansour et al. (2022) [45]	• ⟶	• ⟶		• ⟶		
Fakhrzad et al. (2022) [46]		• ⟶				
Forghani et al. (2022) [49]	• ⟶	• ⟶	• ⟶	• ⟶		
Present research	• ⟶	• ⟶	• ⟶	• ⟶	• ⟶	• ⟶

called *intercellular material flow*. There is also a material flow between the machines inside each cell, called *intracellular material flow*. The layout of the first, second, and third cells in the workshop area is called *intercellular layout*, and the machine's layout inside each cell is called *intracellular layout*. It is also possible to rotate all machines and cells. Figure 1 schematically displays an integrated intercellular and intracellular layout.

This study examines CLPs when the cells are located in the workshop and do not go beyond the workshop area, and the machines are located inside the cells and do not go outside. In addition, the cells and machines should not overlap. As you know, in the real world, cells and machines have unequal dimensions; so, in this study, in order to get closer to reality, the dimensions of cells and machines inside each cell have been considered to be unequal. Another considered aspect in this research is that, unlike previous studies where cells and machines did not rotate, here, they can rotate in different directions. The present study suggests a new mixed nonlinear mathematical model for CLPs. Because the proposed model is nonlinear, to solve small CLPs using GAMS software, the model was linearized, and the results were compared with the ICA results.

Since CLPs are NP-hard, we used ICA and other metaheuristic algorithms like PSO and GA to solve large-scale problems. Finally, the results of ICA were compared with the results of the two other algorithms (PSO and GA).

3.1. Assumptions. In this research, a new mixed nonlinear mathematical programming model is proposed to solve intracellular and intercellular layout problems with unequal dimensions for cells and machines. The assumptions of the proposed mathematical model are as follows:

(1) Manufacturing cells should be enclosed inside the workshop with exact dimensions.

(2) Location of the cells inside the workshop is not predetermined.

(3) Dimensions of the cells and machines are known and not equal (i.e., it is not an assignment problem).

(4) The cells are not located over each other and do not overlap.

(5) The machines used to produce various parts are enclosed inside the cells.

(6) The machines are not located over each other and do not overlap.

(7) Structural cells can rotate.

(8) Machines can also rotate.

(9) Material entry and exit points are always in the center of the cells and machines.

3.2. Notations

3.2.1. Indices

i, k: Cell index

j, p: Machine index

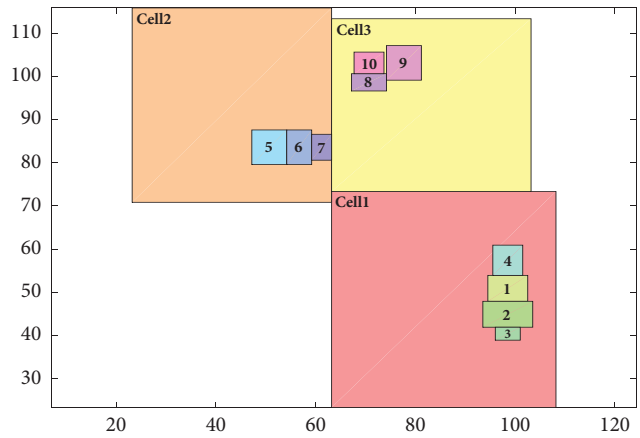

FIGURE 1: Integrated inter-cellular and intracellular layout for three cells and ten machines.

3.2.2. Parameters

W: Length of the workshop

H: Width of the workshop

N: Number of cells

w_i: Length of the i^{th} cell $i = \{1, \ldots, N\}$

h_i: Width of the i^{th} cell $i = \{1, \ldots, N\}$

w'_{ij}: Length of the j^{th} machine in the i^{th} cell $i = \{1, .., N\}, j = \{1, \ldots, M\}$

h'_{ij}: Width of the j^{th} machine in the i^{th} cell $i = \{1, .., N\}, j = \{1, \ldots, M\}$

M_i: Number of the machines in the i^{th} cell $i = \{1, .., N\}$

f_{ik}: Material flow between the i^{th} and k^{th} cells $i = \{1, .., N\}, k = \{1, \ldots, N\}, i \neq k$

f_{ijp}: Material flow between the j^{th} and p^{th} machines in cell i $i = \{1, .., N\}, j = \{1, \ldots, M\}, p = \{1, \ldots, M\}, j \neq p$

3.2.3. Decision Variables

x_i: Center coordinates of the i^{th} cell along the x-axis $i = \{1, \ldots, N\}$

y_i: Center coordinates of the i^{th} cell along the y-axis $i = \{1, \ldots, N\}$

x'_{ij}: Center coordinates of the j^{th} machine in the i^{th} cell along the x-axis $i = \{1, .., N\}, j = \{1, \ldots, M\}$

y'_{ij}: Center coordinates of the j^{th} machine in the i^{th} cell along the y-axis $i = \{1, .., N\}, j = \{1, \ldots, M\}$

d_{ik}: Rectilinear distance between i and k cells, a function of x_i and y_i $i = \{1, .., N\}, k = \{1, \ldots, N\}, i \neq k$

d_{ijp}: Rectilinear distance between j and p machines, a function of x'_{ij} and y'_{ij} $i = \{1, .., N\}, j = \{1, \ldots, M\}, p = \{1, \ldots, M\}, j \neq p$

$$r_i = \begin{cases} 1, \text{if cell } i \text{ direction changes compared to its original direction} \\ 0, \text{otherwise} \end{cases}$$

$i = \{1, \ldots, N\}$

$$r'_{ij} = \begin{cases} 1, \text{if machine } j \text{ direction in cell } i \text{ changes compared to its original direction} \\ 0, \text{otherwise} \end{cases}$$

$i = \{1, .., N\}, j = \{1, \ldots, M\}$

3.3. Preliminaries. This model aims to find the best layout of cells in the workshop and the best layout of machines inside each cell.

3.4. Mixed Nonlinear Programming Model. Based on the above information, the mixed nonlinear programming model for intracellular and intercellular layout problems is as follows:

$$f_1 = \mathrm{Min}\left(\sum_{i=1}^{N}\sum_{k=1}^{N} f_{\mathrm{ik}}\, d_{\mathrm{ik}}\right) = \mathrm{Min}\left(\sum_{i=1}^{N}\sum_{k=1}^{N} f_{ik}\left(\left|x_i - x_k\right| + \left|y_i - y_k\right|\right)\right), \tag{1}$$

$$f_2 = \mathrm{Min}\left(\sum_{i=1}^{N}\left(\sum_{j=1}^{M_i}\sum_{p=1}^{M_i} f_{\mathrm{ijp}}\left(\left|x'_{\mathrm{ij}} - x'_{\mathrm{ip}}\right| + \left|y'_{\mathrm{ij}} - y'_{\mathrm{ip}}\right|\right)\right)\right), \tag{2}$$

$$\min Z = f_1 + f_2 = \mathrm{Min}\left(\sum_{i=1}^{N}\sum_{k=1}^{N} f_{\mathrm{ik}}\left(\left|x_i - x_k\right| + \left|y_i - y_k\right|\right) + \sum_{i=1}^{N}\left(\sum_{j=1}^{M_i}\sum_{p=1}^{M_i} f_{\mathrm{ijp}}\left(\left|x'_{\mathrm{ij}} - x'_{\mathrm{ip}}\right| + \left|y'_{\mathrm{ij}} - y'_{\mathrm{ip}}\right|\right)\right)\right), \tag{3}$$

$$\frac{w_i}{2}(1 - r_i) + \frac{h_i}{2} r_i \le x_i \le W - \left(\frac{w_i}{2}(1 - r_i) + \frac{h_i}{2} r_i\right) i = 1, 2, \ldots, N, \tag{4}$$

$$\frac{h_i}{2}(1 - r_i) + \frac{w_i}{2} r_i \le y_i \le H - \left(\frac{h_i}{2}(1 - r_i) + \frac{w_i}{2} r_i\right) i = 1, 2, \ldots, N, \tag{5}$$

$$\frac{w'_{\mathrm{ij}}}{2}\left(1 - r'_{\mathrm{ij}}\right) + \frac{h'_{\mathrm{ij}}}{2} r'_{\mathrm{ij}} \le x'_{\mathrm{ij}} \le w_i - \left(\frac{w'_{\mathrm{ij}}}{2}\left(1 - r'_{\mathrm{ij}}\right) + \frac{h'_{\mathrm{ij}}}{2} r'_{\mathrm{ij}}\right) i = 1, 2, \ldots, N, \quad j = 1, 2, \ldots, M_i, \tag{6}$$

$$\frac{h'_{\mathrm{ij}}}{2}\left(1 - r'_{\mathrm{ij}}\right) + \frac{w'_{\mathrm{ij}}}{2} r'_{\mathrm{ij}} \le y'_{\mathrm{ij}} \le h_i - \left(\frac{h'_{\mathrm{ij}}}{2}\left(1 - r'_{\mathrm{ij}}\right) + \frac{w'_{\mathrm{ij}}}{2} r'_{\mathrm{ij}}\right) i = 1, 2, \ldots, N, \quad j = 1, 2, \ldots, M_i, \tag{7}$$

$$\left|x_i - x_k\right| + \left|y_i - y_k\right| \ge \left(\frac{w_i}{2}(1 - r_i) + \frac{h_i}{2} r_i + \frac{w_k}{2}(1 - r_k) + \frac{h_k}{2} r_k\right) + \left(\frac{h_i}{2}(1 - r_i) + \frac{w_i}{2} r_i + \frac{h_k}{2}(1 - r_k) + \frac{w_k}{2} r_k\right) i, k = 1, 2, \ldots, N, \quad i \ne k, \tag{8}$$

$$\left|x'_{\mathrm{ij}} - x'_{\mathrm{ip}}\right| + \left|y'_{\mathrm{ij}} - y'_{\mathrm{ip}}\right| \ge \left(\frac{w'_{\mathrm{ij}}}{2}\left(1 - r'_{\mathrm{ij}}\right) + \frac{h'_{\mathrm{ij}}}{2} r'_{ij} + \frac{w'_{\mathrm{ip}}}{2}\left(1 - r'_{\mathrm{ip}}\right) + \frac{h'_{\mathrm{ip}}}{2} r'_{\mathrm{ip}}\right) + \left(\frac{h'_{\mathrm{ij}}}{2}\left(1 - r'_{\mathrm{ij}}\right) + \frac{w'_{\mathrm{ij}}}{2} r'_{\mathrm{ij}} + \frac{h'_{\mathrm{ip}}}{2}\left(1 - r'_{\mathrm{ip}}\right) + \frac{w'_{\mathrm{ip}}}{2} r'_{\mathrm{ip}}\right) i = 1, 2, \ldots, N, j, p = 1, 2, \ldots, M_i, \quad j \ne p, \tag{9}$$

$$x_i \ge 0\, i = 1, 2, \ldots, N, \tag{10}$$

$$y_i \ge 0\, i = 1, 2, \ldots, N, \tag{11}$$

$$x'_{\mathrm{ij}} \ge 0\, i = 1, 2, \ldots, N, j = 1, 2, \ldots, M, \tag{12}$$

$$y'_{\mathrm{ij}} \ge 0\, i = 1, 2, \ldots, N, j = 1, 2, \ldots, M, \tag{13}$$

$$r_i \in \{0, 1\}\, i = 1, 2, \ldots, N, \tag{14}$$

$$r'_{ij} \in \{0,\ 1\}\ i = 1,\ 2, \ldots, N,\ j = 1,\ 2, \ldots, M. \tag{15}$$

In the proposed model, the objective function consists of two parts. The first part shows minimizing the cost of material flow between cells, and the second part states minimizing the cost of material flow between machines located inside the cell. Equation (1) indicates minimizing the sum of material flow costs between cells, and equation (2) represents minimizing the sum of material flow costs between machines. In equations (1) and (2), the cost is considered one per unit distance. Equation (3) indicates intracellular and inter-cellular cost minimization. Inequalities (4) and (5) show that each cell is enclosed inside the workshop along the x- and y-axes. Inequalities (6) and (7) express that the machines of each cell are enclosed in the corresponding cell along the x- and y-axes. Inequality (8) indicates the nonoverlap of cells, while Inequality (9) expresses the nonoverlap of machines inside the cells. Inequalities (10) and (11) express that the center coordinates of the i^{th} cell along the x- and y-axes are equal to or greater than 0. Inequalities (12) and (13) indicate that the center coordinates of the j^{th} machine located in the i^{th} cell, along the x- and y-axes, are equal to or greater than 0. Constraints (14) and (15) ensure that the decision variables, r_i and r'_{ij} are binary variables.

3.5. Linearization of the Mixed Nonlinear Programming Model. Since the proposed model is nonlinear, we should linearize the model. For this purpose, the following variables were changed in the objective function and constraints as shown in Table 2.

After applying the changes in the above variables, the objective function and model constraints were transformed into equations (16)–(21):

$$f_1 = \sum_{i=1}^{N} \sum_{k=1}^{N} f_{ik}\, d_{ik} = \sum_{i=1}^{N} \sum_{k=1}^{N} f_{ik}\left(Z1_{ik} + Z2_{ik} + Z3_{ik} + Z4_{ik}\right), \tag{16}$$

$$f_2 = \sum_{i=1}^{N} \left(\sum_{j=1}^{M_i} \sum_{p=1}^{M_i} f_{ijp}\left(Z5_{ijp} + Z6_{ijp} + Z7_{ijp} + Z8_{ijp}\right) \right), \tag{17}$$

$$\min Z = f_1 + f_2, \tag{18}$$

$$\begin{aligned} Z1_{ik} - Z2_{ik} + Z3_{ik} - Z4_{ik} \geq{}& \left(\frac{w_i}{2}\left(1 - r_i\right) + \frac{h_i}{2} r_i + \frac{w_k}{2}\left(1 - r_k\right) + \frac{h_k}{2} r_k \right) \\ &+ \left(\frac{h_i}{2}\left(1 - r_i\right) + \frac{w_i}{2} r_i + \frac{h_k}{2}\left(1 - r_k\right) + \frac{w_k}{2} r_k \right) i, k = 1,\ 2, \ldots, N, \quad i \neq k, \end{aligned} \tag{19}$$

$$Z5_{ijp} - Z6_{ijp} + Z7_{ijp} - Z8_{ijp} \geq \left(\frac{w'_{ij}}{2}\left(1 - r'_{ij}\right) + \frac{h'_{ij}}{2} r'_{ij} + \frac{w'_{ip}}{2}\left(1 - r'_{ip}\right) + \frac{h'_{ip}}{2} r'_{ip} \right) i = 1,\ 2, \ldots, N\ j, p = 1,\ 2, \ldots, M_i, \quad j \neq p, \tag{20}$$

$$Z1_{ik}, Z2_{ik}, Z3_{ik}, Z4_{ik}, Z5_{ijp}, Z6_{ijp}, Z7_{ijp}, Z8_{ijp} \geq 0. \tag{21}$$

3.6. Solution Method. Ballakur and Steudel [50] described that CLPs are complex and increase in complexity when the cells and machines are unequally sized. For this reason, exact methods cannot solve the problems explained above during an acceptable computational time. Therefore, to test our proposed model, meta-heuristic algorithms should be used. To our knowledge, ICA has not been used until now in CLPs. Hence, this algorithm was implemented on CLPs, and its numerical results were compared with the numerical results of PSO and GA.

ICA creates an initial set of random solutions, known as chromosomes in GA, as particles in PSO, and as countries in ICA. Convergence rates and achieving near-optimal solutions are other advantages of ICA [51, 52].

3.6.1. Implementation of ICA to Solve the Problem. ICA was first introduced by Atashpaz-Gargari and Lucas in 2007 [51]. It is designed based on population. The original population is generated randomly, each member of which is known as a country. It steadily improves the initial answers (countries), and finally, creates the suitable answer to the optimization problem (optimal country). In the concept of optimization, some of the best members of the population that have the lowest cost are selected as imperialist countries, and the rest of the population is allocated as a colony to the imperialist country. Colonies in the original population are divided between the imperialist countries based on their power. The power of any imperialist is inversely related to the fitness (cost) of that country. Colonies and imperialist

Table 2: Changes of variables for linearization.

Changing the variables applied to the constraints	Changing the variables applied to the objective function
$x_i - x_k = Z1_{ik} - Z2_{ik}$	$x_i - x_k = Z1_{ik} + Z2_{ik}$
$y_i - y_k = Z3_{ik} - Z4_{ik}$	$y_i - y_k = Z3_{ik} + Z4_{ik}$
$x'_{ij} - x'_{ip} = Z5_{ijp} - Z6_{ijp}$	$x'_{ij} - x'_{ip} = Z5_{ijp} + Z6_{ijp}$
$y'_{ij} - y'_{ip} = Z7_{ijp} - Z8_{ijp}$	$y'_{ij} - y'_{ip} = Z7_{ijp} + Z8_{ijp}$

countries form empires [53, 54]. The steps to implementation of ICA are as follows.

(1) Creating Initial Solutions and Forming Empires. ICA is implemented in four phases, and each phase is executed to the maximum number of repetitions. In each iteration, the amount of material flow cost is calculated for all population members and selected as the number of empires from the countries with the lowest material flow cost, as imperialist countries. The selection of the best countries in our case was made using Roulette's wheel method [55]. The remaining countries were then assigned as colonies to the imperialist country, and primary empires were created.

(2) Solution Representation. Previous studies have shown that displaying solutions as continuous is efficient and provides better solutions in terms of facility layout [23]. Therefore, in the present study, solutions were displayed in a continuous and linear manner. To implement the algorithm, in displaying shadow solutions for each decision variable, a number between 0 and 1 was mentioned. Four parts were used to represent the solution. The first part consists of 9 numbers; the first three of which are the shadow of the center coordinates of the cells along the x-axis $(\widehat{x}_i, i = 1, \ldots, N)$, the second three are the shadow of the center coordinates of the cells along the y-axis $(\widehat{y}_i, i = 1, \ldots, N)$, and the last three numbers show the shadow of rotation or nonrotation of the cells in relation to their original direction $(\widehat{r}_i, i = 1, \ldots, N)$. The second part contains the next 15 numbers; the first five numbers in this section are the shadow of the center coordinates of the machines in the first cell along the x-axis $(\widehat{x}_j, j = 1, \ldots, M)$, the second five numbers are the shadow of the center coordinates of the machines in the first cell along the y-axis $(\widehat{y}_j, j = 1, \ldots, M)$, and the last five numbers are the shadow of rotation or nonrotation of the machines in the first cell $(\widehat{r}_j, j = 1, \ldots, M)$. The third part includes the next 12 numbers; the first four numbers in this section are the shadow of the center coordinates of the machines in the second cell along the x-axis $(\widehat{x}_j, j = 1, \ldots, M)$, the second four numbers are the shadow of the center coordinates of the machines in the second cell along the y-axis $(\widehat{y}_j, j = 1, \ldots, M)$, and the last four numbers are the shadow of the orientation of the machines in the second cell $(\widehat{r}_j, j = 1, \ldots, M)$. The fourth part comprises the numbers 36 to 45; the first three numbers in this section are the shadow of the center coordinates of the machines in the third cell along the x-axis $(\widehat{x}_j, j = 1, \ldots, M)$, the second three numbers are the shadow of the center coordinates of the machines in the third cell along the y-axis $(\widehat{y}_j, j = 1, \ldots, M)$, and the last three numbers are the shadow of the orientation of the machines in the third cell $(\widehat{r}_j, j = 1, \ldots, M)$. Then, by inserting the obtained shadow coordinates in equations (22)–(24), we can determine the center coordinates of the machines along the x-axis $(\widehat{x}_j)$, the center coordinates of the machines along the y-axis $(\widehat{y}_j)$ in the corresponding cell, and their orientation relative to their original direction $(\widehat{r}_j)$:

$$x_j = x\min_j + \left(x\max_j - x\min_j\right)\widehat{x}_j \longrightarrow \begin{cases} x\min_j = \dfrac{w_j}{2}\left(1 - r_j\right) + \dfrac{h_j}{2} r_j, \\ x\max_j = W - \left(\dfrac{w_j}{2}\left(1 - r_j\right) + \dfrac{h_j}{2} r_j\right), \end{cases} \quad j = 1, \ldots, M, \tag{22}$$

$$y_j = y\min_j + \left(y\max_j - y\min_j\right)\widehat{y}_j \longrightarrow \begin{cases} y\min_j = \dfrac{h_j}{2}\left(1 - r_j\right) + \dfrac{w_j}{2} r_j, \\ y\max_j = H - \left(\dfrac{h_j}{2}\left(1 - r_j\right) + \dfrac{w_j}{2} r_j\right), \end{cases} \quad j = 1, \ldots, M, \tag{23}$$

$$r_j = \begin{cases} 0, & 0 \le \widehat{r}_j \le 0.5 \text{ اگر}, \\ 1, & 0.5 \le \widehat{r}_j \le 1 \text{ اگر}, \end{cases} \quad j = 1, \ldots, M. \tag{24}$$

In this type of solution representation, a matrix with 1 row and $3 \times M$ columns is applied. The above process is also used to display the solution for the cells. For example, in displaying the solution for three cells and 12 machines, a matrix with one row and 45 columns is utilized. Figure 2 displays the shadow of the center coordinates of machines and cells, while Figure 3 displays their actual center coordinates.

0.3488	0.3596	0.3689	0.1260	0.9741	0.5759	0.1419	0.2785	0.6787	0.8430	0.8430	0.6483	0.6483	0.4816	..
0.9616	0.7878	0.7878	0.9616	0.7693	0.1712	0.0971	0.7431	0.7952	0.2238	0.9741	0.9194	0.6502	0.6953	..
0.7753	0.5472	0.7753	0.5384	0.4218	0.1270	0.9649	0.0357	0.8905	0.4853	0.7003	0.2904	0.2671	0.2794	0.9572	..
0.6324	0.8491														

Figure 2: Displaying the shadow of the center coordinates of cells, machines, and their orientations.

27.449	21.949	21.949	16.949	31.349	25.849	25.849	31.349	25.849	0	40.174	40.174	40.174	25.693	..
83.193	55.693	0	0	1	27.449	0	1	1	0	25.906	25.906	18.906	18.906	..
21.884	16.228	21.884	15.884	0	0	1	0	20.707	12.207	16.707	8.308	8.308	8.308	..
1	1	1												

Figure 3: Displaying the actual center coordinates of cells, machines, and their orientations.

(3) Improving the Solution Space. At this phase, the position of the imperialist countries is changed using the absorption operator. By using the revolution operator, random changes are made in the material flow cost of the imperialist and colony countries to attain better and more diverse solutions. The movement of the colonies towards the imperialist country (following a policy of absorption) is done using the following equation:

$$x' = x + \beta(t - x), \tag{25}$$

where x' is the secondary position of the colony, x is the primary position of the colony, β is the simulation coefficient, t is the value of the imperialist or the objective value, and $0 \le \beta \le 2$. The absorption policy about colonies is shown in Figure 4.

(4) Replacement of the Colony and the Imperialist with Each Other in case of Meeting Relevant Conditions. Next, the material flow cost of the colonies is compared with the relevant imperialist country, and if the material flow cost of the colony is better than the material flow cost of the imperialist, the position of the colony and the imperialist country will be changed (the intragroup competition).

(5) Transfer of Colonies and Imperialists to Another Empire in case of Meeting Relevant Conditions. At this step, empires are first evaluated using equation (26) in order to obtain the index for each empire:

$$f(\text{Empires}) = f(\text{imperialist}) + \xi \text{Mean}(f(\text{colonies})), \tag{26}$$

where $f(\text{imperialist})$ refers to the value of the imperialist objective function, $\text{Mean}(f(\text{colonies}))$ denotes the average value of the objective function for the colonies, and ξ is the zeta coefficient, the value of which is set by parameter setting.

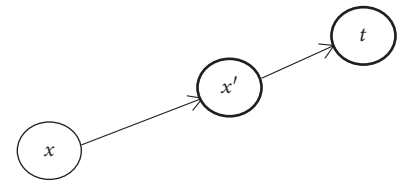

Figure 4: Application of absorption policy in the case of colonies.

The weakest colony is removed from the weakest empire, and accidently, moved to a more powerful empire (intergroup or inter-empire competition). If the weakest empire has no colony, the imperialist, as a colony, is transferred to another empire. Then the value of the objective function of the empires is updated, and the same process is repeated.

(6) Reporting the Best Solution Found. In this section, the best solution found in the output of MATLAB software is shown.

(7) Checking the Stop Condition. Although there are several conditions for stopping the algorithm, in this paper, reaching a certain number of iterations or reaching the maximum iteration (MaxIt) in implementing the ICA is considered a stop condition. The pseudocode of the proposed ICA is presented in Figure 5.

4. Results

4.1. Computational Results. Here, numerical examples as well as the results of running them with GAMS (win32 24.1.3) and MATLAB R2015 are presented.

4.1.1. Solving a Small-Scale Problem to Assess the Proposed Model's Validity. To evaluate the model's validity, a small-scale problem was solved with GAMS software. The data of this example were taken from the Asl and Wong article [23].

Step 1: generating the primary countries and calculating the material flow cost of the countries.
Step 2: Selecting the countries with the lowest cost as imperialists and assigning other countries to them (creation of primary empires).
Step 3: Movement of the colonies to the imperialist country using the absorption or simulation operator follows: $x' = x + \beta\ (t - x)$
Step 4: Applying random changes to the material flow costs of countries using the revolution operator.
Step 5: Comparing the cost of the colony countries with the cost of the respective imperialist country and changing the status of the colony country with the imperialist country if the material flow cost of the colony country is better than that of the imperialist country.
Step 6: Evaluating the empires using the following equation:
f (empires) = f (imperialist) + ξ Mean (f (colonies))
Step 7: Removing the weakest colony from the weakest empire and transferring it to the strongest empire.
Step 8: Eliminating the powerless empires.
Step 9: If there is just one empire, go to Step 10; otherwise, go to Step 3.
Step 10: Reporting the best solution found.
Step 11: Checking the stop condition.

Figure 5: Pseudocode of the imperialist competitive algorithm.

This example comprised three cells and 12 machines. The cells were set in a 100 cm wide × 100 cm long workshop. Other parameters of the problem are presented in Tables 3–9.

The small-scale problem was solved by the above model in GAMS software. Since CLPs are very complex and exact solution methods cannot solve them in a reasonable computational time, we solved them using ICA, and the results were compared with those of GAMS software as shown in Table 10. The layout of cells in the workshop and the layout of machines inside each cell are shown in Figure 6.

4.2. Parameter Setting for Meta-Heuristic Algorithms Using the Taguchi Method. In meta-heuristic algorithms, several parameters must be set. Parameter setting is important because better solutions can be created using the right parameter setting. In this paper, parameter setting for ICA, PSO, and GA was performed using the Taguchi method [56]. In the Taguchi method, the factors and parameters of each algorithm are categorized into two groups of *controllable* and *uncontrollable*, and the effect of uncontrollable factors is minimized. Then, the parameters of the assumed algorithms are adjusted by considering the output of the Taguchi method, which is the *main effects plot* for the signal-to-noise ratios.

4.2.1. Parameter Setting for the ICA. ICA has two operators and eight parameters. The following symbols are used to set the parameters of this algorithm: *MaxIt*, *npop*, *nEmp*, *alpha*, *beta*, *PRevolution*, *mu*, and *zeta*, where *MaxIt* is the highest number of iterations, *npop* is the population size, *nEmp* is the number of empires, *alpha* is selection pressure, *beta* is similarity coefficient, *PRevolution* is the probability of revolution operator, *mu* is the revolution operator rate, and *zeta* is the average cost factor of colonies. The parameters of ICA are set according to Figures 7 and 8, and the results are presented in Table 11.

4.2.2. Parameter Setting for PSO. There are five parameters for PSO, and *MaxIt*, *nPop*, C_1, C_2, and W symbols are applied to regulate its parameters: *MaxIt* is the highest number of iterations, *nPop* is the number of particles, C_1 is the acceleration coefficient of the best personal answer, C_2 is the acceleration coefficient of the best overall answer, and W is the inertia weight coefficient. The results are presented in Table 12.

Table 3: Length and width of machines.

Machines	1	2	3	4	5	6	7	8	9	10	11	12
Length of machine (w'_j)	5	7	6	4	6	5	10	7	6	5	5	6
Width of machine (h'_j)	4	5	5	4	6	4	7	5	5	5	5	4

Table 4: Length and width of manufacturing cell.

Cells	Cell 1	Cell 2	Cell 3
Length of cell (w_i)	35	30	25
Width of cell (h_i)	35	30	25

Table 5: Number of machines inside each cell.

Cell number	Machine number
1	3-5-9-10-11
2	2-4-6-7
3	1-8-12

Table 6: Material flow between cells.

Intercellular material flow	1	2	3
1	0	5	7
2	0	0	0
3	0	9	0

Table 7: Material flow between machines in the first cell.

Machines	3	5	9	10	11
3	0	0	10	20	0
5	20	0	0	10	0
9	0	10	0	0	20
10	20	0	20	0	0
11	0	0	0	10	0

Table 8: Material flow between machines in the second cell.

Machines	2	4	6	7
2	0	15	25	0
4	40	0	0	15
6	0	0	0	40
7	10	40	15	0

Table 9: Material flow between machines in the third cell.

Machines	1	8	12
1	0	0	80
8	35	0	0
12	0	55	0

Table 10: Results of solving the mathematical model with GAMS and the ICA.

Objective function of ICA	Computational time of ICA	Objective function of GAMS	Computational time of GAMS
3880.0012	79.601018	3880.0012	3101.61

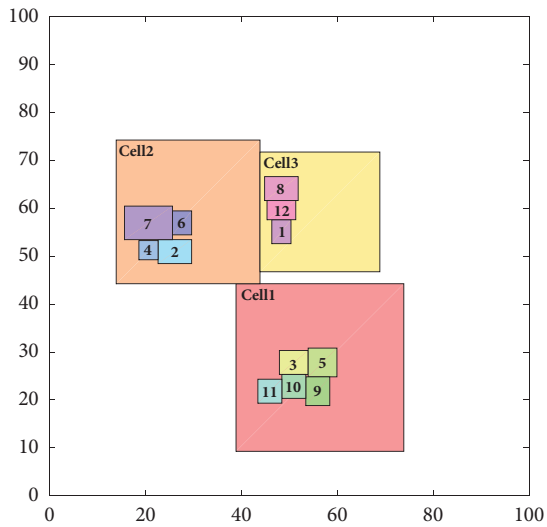

Figure 6: Layout of cells in the workshop and layout of machines inside each cell.

4.2.3. Parameter Setting for GA. GA has five parameters, and *MaxIt*, *nPop*, *Pc*, *Pm*, and *Mu* symbols are used to adjust these parameters: *MaxIt* is the highest number of iterations, *nPop* is the population size, *Pc* is the percentage of intersection operator for population, *Pm* is the percentage of mutation operator for population, and Mu is the percentage of mutation rate for selected chromosomes. The results are presented in Table 13.

4.3. Generating Random Problems. To evaluate the mixed nonlinear programming model and meta-heuristic algorithms, 30 random problems were designed in MATLAB R2015 software and solved by (ICA), (PSO), and (GA). Then, the results were statistically analyzed using analysis of variances. The mean values of the objective function related to three meta-heuristic algorithms are shown in Figure 9 and Table 14.

4.3.1. Results of Running Random Problems. After designing the random problems, we executed them and the center coordinates of cells in the workshop and the center coordinates of machines inside each cell for the 30th random problem after implementation of ICA, PSO, and GA were determined, and the results are shown in Tables 15–17, respectively. Also, the layout of cells in the workshop and the layout of machines inside each cell for the three meta-heuristic algorithms are shown in Figures 10–12, respectively. It is worth noting that the dimensions of problems 26 to 30 are presented in Tables 18 and 19.

To demonstrate a more accurate estimate of the criteria for meta-heuristic algorithms, the mean relative percentage difference ($\overline{\text{RPD}}$) of layout cost and computational time for the 30 random problems created in Section 4.3 are shown in Table 20. Because each random problem was accomplished 5 times using meta-heuristic algorithms, the relative percentage difference (RPD) is calculated for the cost and computational time criteria. Then, the average values or ($\overline{\text{RPD}}$) of the performances were computed and applied for comparison among the three proposed algorithms. The results are presented in Table 20. The RPD index was acquired using the following equation:

$$\text{RPD}_{ij} = \frac{\text{Best}_{ij} - \min_j \text{Best}_{ij}}{\min_j \text{Best}_{ij}} \times 100, \tag{27}$$

where i is the random problem number, and j represents the algorithm used ($j = 1$ is ICA, $j = 2$ is PSO, and $j = 3$ is GA). Besides, Best_{ij} is the best value achieved from the implementation of algorithm number j for random problem i, and $\min_j \text{Best}_{ij}$ is the best result obtained from implementing the algorithms on random problem i.

Figures 13 and 14 show the ($\overline{\text{RPD}}$) of implementation of three meta-heuristic algorithms in terms of layout cost and computational time criteria, respectively. Figure 13 shows the relative difference of the layout cost of ICA, PSO, and GA with the symbols COICA, COPSO, and COGA, respectively. Figure 14 denotes the RPD values of ICA, PSO, and GA with the symbols TOICA, TOPSO, and TOGA, respectively. The *mean* symbol represents the RPD of the layout cost, and *NP* symbol represents the number of random problems in Figures 13 and 14.

4.3.2. Normality Test of Three Meta-Heuristic Algorithms. The results of performing the normality test for the three proposed algorithms are displayed in Table 21. The results related to the significant value show that the layout cost of PSO and the computational time of PSO and GA are normal. Regarding the central limit theorem, since the number of samples is 30, the setup cost of ICA and GA and the computational time of ICA are also normal.

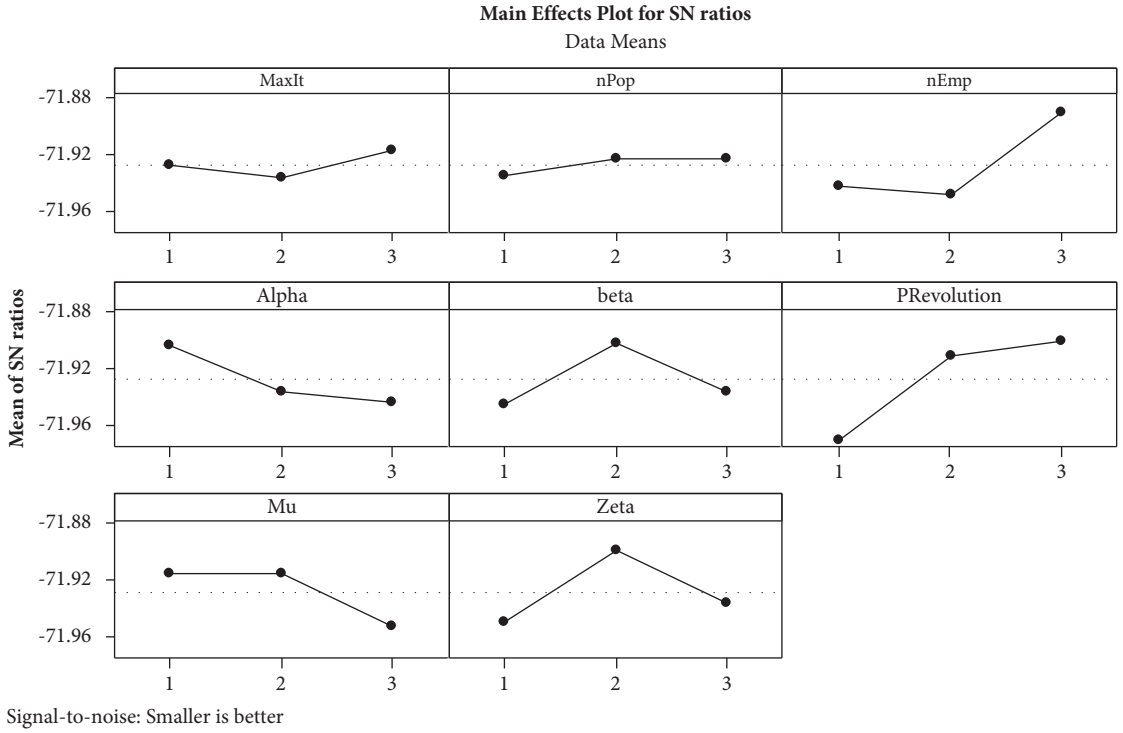

Figure 7: Diagram of the main effects plot for signal-to-noise ratios for ICA.

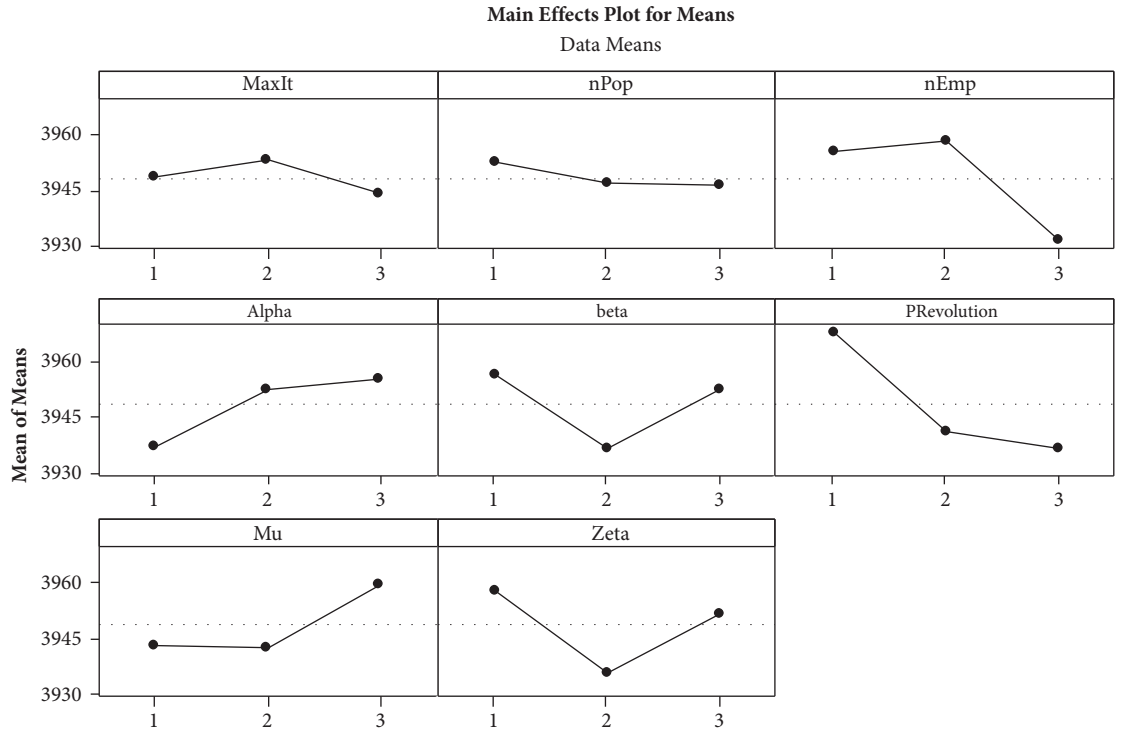

Figure 8: Diagram of the main effects plot for means for ICA.

4.4. Analysis of Variance Test for Assuming Equality of Means of Layout Cost and Computational Time of Three Meta-Heuristic Algorithms (ICA, PSO, and GA). To compare the mean layout costs of three proposed meta-heuristic algorithms using the analysis of variance (ANOVA) test, four conditions must be met: samples from each group or community should have a normal distribution, samples from each group or community should be random, the three

Table 11: Parameter setting results for (ICA).

Factor name	MaxIt	nPop	nEmp	Alpha	Beta	PRevolution	Mu	Zeta
Factor description	Maximum iteration	Population size	Number of empires	Selection pressure	Similarity coefficient	Probability of revolution operator	Revolution operator rates	Average cost ratio of the colony
Optimal value	500	100	10	1	2	0.1	0.05	0.1
Optimal level	Third	Second	Third	First	Second	Third	Second	Second

Table 12: Parameter setting results for (PSO).

Factor name	MaxIt	nPop	C_1	C_2	W
Factor description	Maximum iteration	Number of particles	Acceleration coefficient of the best personal solution	Acceleration coefficient of the best overall solution	Inertia weight coefficient
Optimal value	200	300	0.5	1.2	0.4
Optimal level	First	Second	First	Third	Second

Table 13: Parameter setting results for (GA).

Factor name	MaxIt	nPop	Pc	P_m	Mu
Factor description	Maximum iteration	Number of population	Percentage of cross-over operator	Percentage of mutation operator	Mutation rate
Optimal value	400	200	0.8	0.3	0.01
Optimal level	Third	Second	Third	First	Second

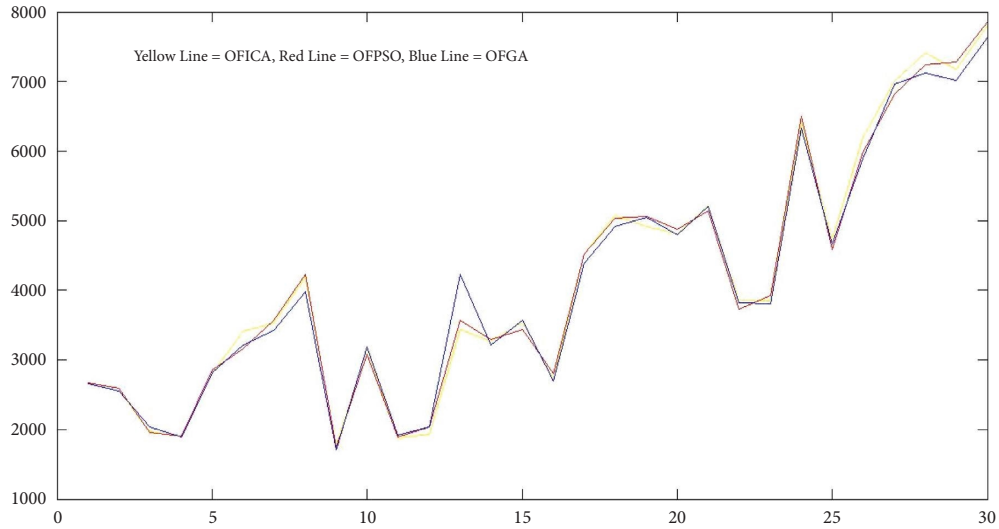

Figure 9: Mean values of the objective function of meta-heuristic algorithms according to sample size.

communities should be independent of each other, and the variances of the three communities should be homogeneous. Since the first three conditions were met, we used Levene's statistic to test the fourth condition, and its results are shown in Table 22. Because of the high performance of 95% confidence level, the tests were performed at this confidence level.

According to Table 22, because the significance level is greater than 0.05, there is no significant difference between the variances of the three communities; in other words, the variances of these communities are homogeneous. Therefore, to test the equality of the means of the three communities in terms of layout cost, the ANOVA test can be used at a 95% confidence level. The analysis of variance compares the mean of multiple populations. The null hypothesis in the analysis of variance states that $\overline{\text{RPD}}$ values of the three algorithms are equal according to the layout cost criterion, and there is no significant difference between the mean layout costs of the three algorithms. Hypothesis one states that the mean $\overline{\text{RPD}}$ value of the three algorithms differs in terms of the layout cost criterion.

ANOVA results for assuming equality of the mean layout cost of three meta-heuristic algorithms are provided in Table 23. As shown, because the value of the significance level is greater than 0.05, there is no significant difference between the mean layout cost of the three communities, and the assumption of equality of means at 95% confidence level is accepted.

To suppose the equality of the mean computational time of the three communities, the above three conditions are met; to test the fourth condition, we used Levene's statistic (Table 24).

Because the significance level is less than 0.05, the null hypothesis is rejected; so, the variances of three communities or three meta-heuristic algorithms are not equal. The results of the corresponding ANOVA are given in Table 25. As shown, since the significance level is less than 0.05, the null hypothesis is rejected (i.e., a significant difference exists between the mean computational times of the three communities). Therefore, the Tukey test should be executed to check the possible inter-group differences. The results of the Tukey test in Table 26 confirm that the mean computational time of all the three communities is different.

Since the variances are not homogeneous, the validity of the ANOVA test may be questioned. Therefore, Tamhane's T2 test was used and the results are displayed in Table 27. Fortunately, Tamhane's T2 test results manifested the previous results; i.e. the mean computational time of the three meta-heuristic algorithms is different significantly.

A comparison of the mean computational time of the three proposed meta-heuristic algorithms is shown in Figure 15. Numbers 1, 2, and 3 on the x-axis represent ICA, PSO, and GA, respectively. The mean computational time of ICA is much less than that of the other two algorithms. Therefore, based on the numerical results achieved from the ANOVA, it is obvious that ICA has much better results in terms of computational time comparing to the other two algorithms.

4.5. Discussion. In this paper, we first solved a small-scale problem with GAMS software to evaluate the model validity. Then, we compared the results of GAMS software with the results acquired from ICA. Numerical results presented the validity of the model as well as the efficiency of the proposed algorithm. Next, parameter settings for meta-heuristic algorithms were executed using the Taguchi method. In the next step, 30 random problems were created using MATLAB R2015 and performed by three meta-heuristic algorithms. After designing and implementing random problems with ICA, PSO, and GA, the center coordinates of the cells and machines were determined. To demonstrate a more accurate approximation of the criterion for meta-heuristic algorithms, we determined the ($\overline{\text{RPD}}$) values of layout cost and computational time. Also, the ($\overline{\text{RPD}}$) results of the three meta-heuristic algorithms in terms of layout cost and computational time criterion were

Table 14: Mean values of the objective function obtained from three meta-heuristic algorithms.

Problem number	$N \times M$	ICA		PSO		GA	
		Objective function	Computational times	Objective function	Computational times	Objective function	Computational times
1	3×12	2849.80	76.23	2768.62	221.14	2750.32	132.40
2	3×12	2659.08	74.98	2679.66	216.98	2632.20	130.13
3	3×10	2037.72	72.68	1996.7	205.33	2072.60	123.96
4	3×10	1917.26	73.56	1923.55	205.78	1933.93	124.43
5	3×15	2942.28	79.31	2971.85	243.38	3060.59	149.71
6	3×15	3451.31	79.45	3407.67	238.22	3388.70	146.38
7	3×16	3699.79	81.80	3658.51	257.32	3725.47	152.69
8	3×16	4325.25	80.89	4313.03	249.24	4133.24	155.19
9	3×13	1781.41	78.24	1795.53	227.47	1835.23	135.48
10	3×13	3327.71	77.63	3204.45	225.67	3284.96	136.20
11	4×12	1959.2	92.70	1969.3	257.33	2061.4	154.37
12	4×12	1991.82	92.64	2143.08	263.26	2166.94	154.68
13	4×14	3595.10	94.09	3618.97	273.61	4311.67	162.90
14	4×14	3308.36	94.76	3352.13	276.02	3386.49	160.54
15	4×16	3598.38	95.68	3656.24	279.74	3648.26	169.95
16	4×16	2778.13	96.37	2814.83	280.85	2791.70	170.07
17	4×18	4586.97	103.69	4631.98	295.27	4540.73	181.61
18	4×18	5171.15	104.47	5136.73	299.21	5169.58	179.99
19	4×20	5041.08	101.46	5190.46	306.47	5163.96	190.46
20	4×20	4877.92	103.95	4984.84	316.46	4877.04	195.01
21	5×15	5439.84	115.35	5398.24	313.87	5399	190.78
22	5×16	3920.98	114.36	3874.34	319.43	3871.86	192.94
23	5×18	3942.04	115.89	4139.03	334.21	3913.54	199.91
24	5×18	6779.99	116.76	6889.71	339.50	6581.08	199.85
25	5×20	4863.41	117.81	4776.85	343.90	4797.79	202.24
26	5×20	6449.17	129.546	6212.09	346.20	6160.17	206.52
27	3×12	2849.80	76.23	2768.62	221.14	2750.32	132.40
28	3×12	2659.08	74.98	2679.66	216.98	2632.20	130.13
29	3×10	2037.72	72.68	1996.7	205.33	2072.60	123.96
30	3×10	1917.26	73.56	1923.55	205.78	1933.93	124.43

Table 15: Center coordinates of cells in the workshop and center coordinates of machines inside each cell for the 30th random problem using ICA.

Workshop	Cells	1	2	3	4	5	
	Center coordinates of cells along the x-axis	79.30	114.30	114.32	146.80	84.32	
	Center coordinates of cells along the y-axis	132.60	132.60	100.10	132.60	102.60	
	Orientation of cells comparing to the main direction	0	1	0	0	0	
Cell	Machines	1	2	3	4	5	
	Center coordinates of machines along the x-axis	20.45	11.45	16.45	8.95	14.45	
1	Center coordinates of machines along the y-axis	8.79	8.79	8.79	8.79	8.79	
	Orientation of machines comparing to the main direction	0	1	0	1	0	
Cell	Machines	6	7	8	9	10	11
	Center coordinates of machines along the x-axis	10.55	7.49	3.55	4.49	6.05	7.55
2	Center coordinates of machines along the y-axis	21.95	28.95	21.95	29.45	21.95	21.95
	Orientation of machines comparing to the main direction	0	1	0	0	1	0
Cell	Machines	12	13	14	15		
	Center coordinates of machines along the x-axis	10.68	10.68	6.18	5.18		
3	Center coordinates of machines along the y-axis	23.33	17.83	18.33	23.33		
	Orientation of machines comparing to the main direction	0	0	0	1		
Cell	Machines	16	17	18	19	20	
	Center coordinates of machines along the x-axis	11.48	11.48	10.48	14.98	6.48	
4	Center coordinates of machines along the y-axis	11.15	9.65	11.15	11.15	11.15	
	Orientation of machines comparing to the main direction	0	1	1	0	0	
Cell	Machines	21	22	23	24	25	
	Center coordinates of machines along the x-axis	21.19	21.19	21.19	26.19	21.19	
5	Center coordinates of machines along the y-axis	18.51	23.01	21.51	18.51	14.51	
	Orientation of machines comparing to the main direction	1	0	0	1	0	

Table 16: Center coordinates of cells in the workshop and center coordinates of machines inside each cell for the 30th random problem using PSO.

Workshop	Cells	1	2	3	4	5	
	Center coordinates of cells along the x-axis	108.24	110.33	140.33	80.33	140.74	
	Center coordinates of cells along the y-axis	117.56	82.56	82.56	82.56	115.06	
	Orientation of cells comparing to the main direction	0	0	0	0	0	
Cell	Machines	1	2	3	4	5	
	Center coordinates of machines along the x-axis	11.08	17.08	15.08	15.08	20.08	
1	Center coordinates of machines along the y-axis	12.76	12.76	12.76	11.26	12.76	
	Orientation of machines comparing to the main direction	0	1	0	0	0	
Cell	Machines	6	7	8	9	10	11
	Center coordinates of machines along the x-axis	18.49	19.04	18.49	18.49	13.98	18.49
2	Center coordinates of machines along the y-axis	22.46	18.34	15.32	9.32	15.32	12.32
	Orientation of machines comparing to the main direction	0	0	1	1	1	1
Cell	Machines	12	13	14	15		
	Center coordinates of machines along the x-axis	10.57	14.07	15.07	10.07		
3	Center coordinates of machines along the y-axis	9.24	9.24	13.74	16.74		
	Orientation of machines comparing to the main direction	0	1	0	0		
Cell	Machines	16	17	18	19	20	
	Center coordinates of machines along the x-axis	8.94	7.94	9.94	13.44	8.94	
4	Center coordinates of machines along the y-axis	12.21	12.21	13.01	13.01	7.01	
	Orientation of machines comparing to the main direction	0	0	1	0	0	
Cell	Machines	21	22	23	24	25	
	Center coordinates of machines along the x-axis	18.84	15.34	13.84	22.84	17.81	
5	Center coordinates of machines along the y-axis	10.63	11.19	11.19	11.19	15.63	
	Orientation of machines comparing to the main direction	0	1	1	1	0	

Table 17: Center coordinates of cells in the workshop and center coordinates of machines inside each cell for the 30th random problem using GA.

Workshop	Cells	1	2	3	4	5	
	Center coordinates of cells along the x-axis	153.50	118.50	118.50	86	118.50	
	Center coordinates of cells along the y-axis	141.41	141.41	111.41	141.41	171.41	
	Orientation of cells comparing to the main direction	0	1	1	0	0	
Cell	Machines	1	2	3	4	5	
	Center coordinates of machines along the x-axis	24.81	19.81	14.81	28.81	16.81	
1	Center coordinates of machines along the y-axis	18.85	18.85	18.85	18.85	18.85	
	Orientation of machines comparing to the main direction	0	1	0	0	0	
Cell	Machines	6	7	8	9	10	11
	Center coordinates of machines along the x-axis	24.43	24.43	24.43	18.33	24.33	24.33
2	Center coordinates of machines along the y-axis	9.37	13.37	17.38	17.37	14.87	20.38
	Orientation of machines comparing to the main direction	0	0	1	0	0	1
Cell	Machines	12	13	14	15		
	Center coordinates of machines along the x-axis	9.48	9.48	9.48	15.48		
3	Center coordinates of machines along the y-axis	22.78	26.28	18.28	18.28		
	Orientation of machines comparing to the main direction	1	0	0	1		
Cell	Machines	16	17	18	19	20	
	Center coordinates of machines along the x-axis	10.86	10.86	9.86	6.36	14.86	
4	Center coordinates of machines along the y-axis	16.20	17.70	16.20	16.20	16.20	
	Orientation of machines comparing to the main direction	0	0	1	0	0	
Cell	Machines	21	22	23	24	25	
	Center coordinates of machines along the x-axis	17.31	17.31	15.81	22.81	19.81	
5	Center coordinates of machines along the y-axis	15.94	10.44	10.44	10.44	10.44	
	Orientation of machines comparing to the main direction	1	1	1	1	1	

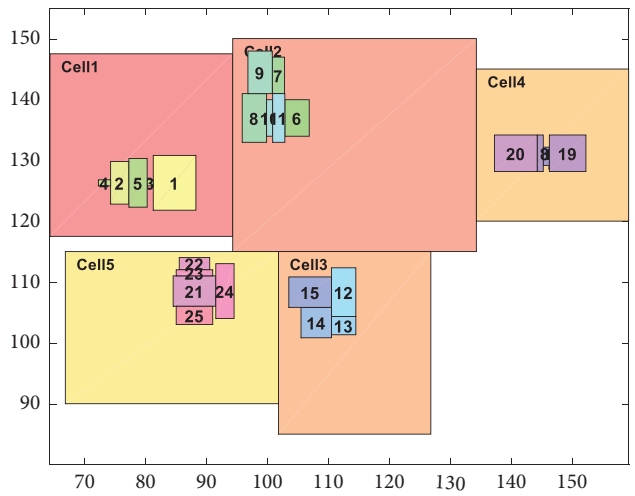

Figure 10: Layout of cells in the workshop and layout of machines inside each cell using ICA.

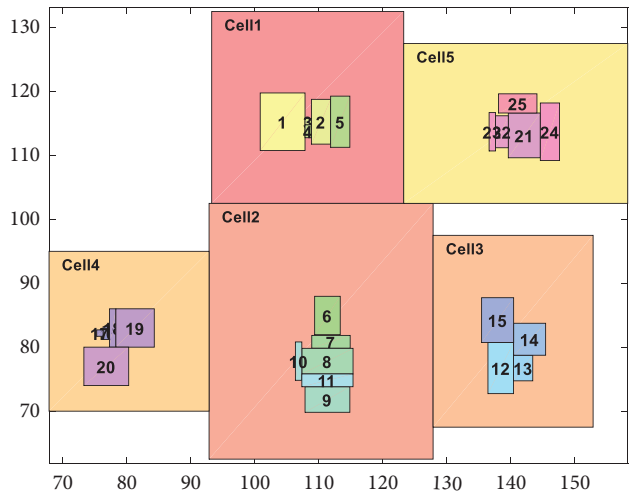

Figure 11: Layout of cells in the workshop and layout of machines inside each cell using PSO.

obtained. Then the ANOVA was executed for assuming the equality of means of layout cost and computational time of three meta-heuristic algorithms aiming to compare their mean layout costs. The results denoted the equality of means of layout cost of the three proposed meta-heuristic algorithms. However, the computational time results showed the inequality of the means of computational time of all the three meta-heuristic algorithms. Therefore, the Tukey test was used to investigate the possible inter-group differences. According to the results, the mean computational time of all algorithms was different. Finally, the comparison of the mean computational time of the mentioned algorithms indicated that the mean computational time of ICA was much less than the other two algorithms; in other words, it demonstrated much better results in terms of computational time.

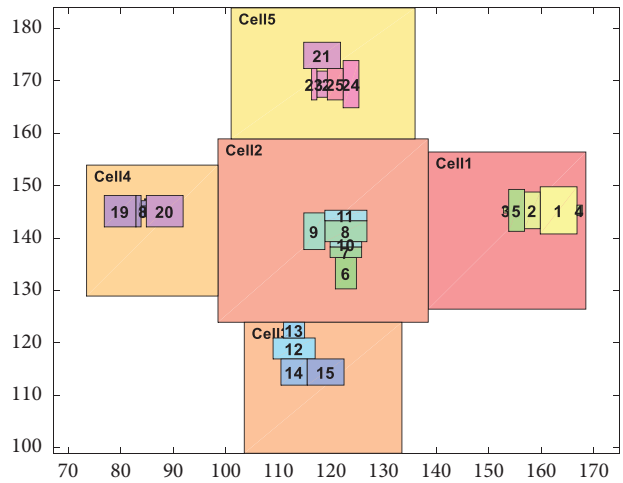

Figure 12: Layout of cells in the workshop and layout of machines inside each cell using GA.

Table 18: Length and width of cells and number of machines inside cells for problems 26 to 30.

Cells	Length of cell	Width of cell	Machines inside each cell
P26-cell1	30	20	{1, 2, 3, 4, 5}
P26-cell2	25	30	{6, 7, 8, 9}
P26-cell3	25	30	{10, 11, 12}
P26-cell4	30	40	{13, 14, 15, 16}
P26-cell5	40	45	{17, 18, 19, 20}
P27-cell1	40	35	{1, 2, 3, 4, 5}
P27-cell2	35	35	{6, 7, 8, 9, 10}
P27-cell3	25	30	{11, 12, 13, 14}
P27-cell4	35	45	{15, 16, 17, 18}
P27-cell5	40	30	{19, 20, 21, 22}
P28-cell1	30	25	{1, 2, 3, 4}
P28-cell2	35	40	{5, 6, 7, 8}
P28-cell3	35	30	{9, 10, 11, 12, 13}
P28-cell4	20	30	{14, 15, 16, 17, 18}
P28-cell5	25	35	{19, 20, 21, 22}
P29-cell1	35	40	{1, 2, 3, 4, 5}
P29-cell2	45	40	{6, 7, 8, 9, 10}
P29-cell3	30	35	{11, 12, 13, 14, 15}
P29-cell4	45	40	{16, 17, 18, 19, 20}
P29-cell5	45	50	{21, 22, 23, 24, 25}
P30-cell1	30	30	{1, 2, 3, 4, 5}
P30-cell2	35	40	{6, 7, 8, 9, 10, 11}
P30-cell3	25	30	{12, 13, 14, 15}
P30-cell4	25	25	{16, 17, 18, 19, 20}
P30-cell5	35	25	{21, 22, 23, 24, 25}

5. Managerial Insights and Practical Implications

Based on the research findings, a cellular layout that assumes unequal dimensions of cells and machines can be used for batch production of products. Such products have a wide variety and low to medium demand. In addition, cell layout can be used in CMSs for moving from traditional job shop layout to cellular layout. Likewise, cellular layout is used in noncontinuous industries that have a job shop layout. In continuous layout, for example, one may consider a factory that produces four parts by machines 1, 2, 3, and 4 using the same fixed procedure. In job shop layout, there is no need for the production procedure of all parts to be the same.

Other managerial insights are presented as follows:

(i) The flow of materials as an influencing factor in the links between machines in different cells must be determined suitably because the incorrect input of

Table 19: Length and width of machines inside cells for problems 26 to 30.

Machines	1	2	3	4	5	6	7	8	9	10	11	12	13	14	15	16	17	18	19	20	21	22	23	24	25
P26-length	9	1	8	1	3	9	3	3	1	7	1	6	4	3	9	3	8	3	4	3					
P26-width	3	1	1	4	2	8	4	2	8	3	7	7	2	8	8	7	1	4	9	9					
P27-length	8	8	6	8	3	4	2	2	8	2	5	2	4	4	9	6	7	1	1	6	5	7			
P27-width	6	2	2	7	8	5	7	3	9	5	4	3	5	1	5	6	4	6	4	1	4	2			
P28-length	5	3	8	4	6	9	7	3	8	5	3	1	8	4	1	1	2	4	2	4	6	1			
P28-width	1	8	1	3	9	7	9	8	5	1	3	7	8	2	4	6	8	3	8	9	8	1			
P29-length	2	1	6	7	9	3	7	6	5	7	7	2	2	4	9	5	3	5	5	5	1	6	3	7	6
P29-width	3	5	1	6	8	9	2	6	8	5	2	1	8	8	4	1	6	7	2	4	7	4	8	8	9
P30-length	7	7	1	1	3	4	6	4	4	6	2	4	4	5	5	1	1	6	6	7	5	5	6	9	6
P30-width	9	3	1	2	8	6	2	8	7	1	8	8	3	5	7	2	1	1	6	6	7	2	1	3	3

Table 20: Mean values ($\overline{\mathbf{RPD}}$) of the criteria obtained from implementation of three meta-heuristic algorithms on 30 random problems.

Problem number	Problem size	ICA		PSO		GA	
		Cost	Time	Cost	Time	Cost	Time
1	3 × 12	7.29	1.38	4.24	194.08	3.55	76.07
2	3 × 12	4.13	0.90	4.94	192.01	3.08	75.12
3	3 × 10	3.75	0.57	1.66	184.11	5.52	71.52
4	3 × 10	1.38	0.44	1.72	180.97	2.27	69.89
5	3 × 15	4.83	0.06	5.88	208.53	9.05	89.79
6	3 × 15	21.05	1.24	7.69	203.54	7.09	86.52
7	3 × 16	8.23	2.74	7.02	223.17	8.98	91.76
8	3 × 16	8.77	1.27	8.46	212.03	3.94	94.29
9	3 × 13	4.17	3.07	4.99	199.66	7.32	78.15
10	3 × 13	8.20	1.36	4.19	194.64	6.81	77.83
11	4 × 12	4.04	0.75	4.58	179.69	9.47	67.78
12	4 × 12	3.09	0.57	10.92	185.76	12.16	67.91
13	4 × 14	4.78	2.006	5.47	196.62	25.66	76.60
14	4 × 14	3.16	1.43	4.52	195.50	5.59	71.87
15	4 × 16	4.70	1.35	6.39	196.31	6.15	80.02
16	4 × 16	3.96	0.90	5.34	194.05	4.47	78.06
17	4 × 18	4.61	4.89	5.63	198.68	3.55	83.71
18	4 × 18	5.18	5.24	4.48	201.41	5.15	81.31
19	4 × 20	2.64	1.73	5.69	207.26	5.13	90.95
20	4 × 20	3.42	1.23	3.83	210.43	1.59	91.29
21	5 × 15	5.80	2.74	4.99	179.57	5.01	69.93
22	5 × 16	5.25	1.25	4.003	182.81	3.93	70.83
23	5 × 18	3.40	0.35	8.57	189.39	2.65	73.11
24	5 × 18	7.07	0.70	8.80	192.81	3.72	72.37
25	5 × 20	5.97	1.76	4.09	197.05	4.55	74.69
26	5 × 20	9.32	10.60	5.30	195.59	4.42	76.34
27	5 × 22	3.24	0.68	1.75	203.29	11.36	103.01
28	5 × 22	3.45	0.58	5.16	204.43	4.22	79.71
29	5 × 25	3.72	1.94	5.38	216.79	2.76	88.68
30	5 × 25	4.23	1.44	5.32	152.66	4.56	86.64
Average		5.42	1.84	5.37	195.76	6.12	79.85

this parameter has a tremendous negative effect on the formation of cells and increases the layout cost.

(ii) The use of a meta-heuristic algorithm compared to exact solution methods is much better in terms of the speed of determining the layout, and managers are suggested to measure the efficiency of these algorithms in high-risk layouts while using multiple algorithms.

(iii) Cell layout technology can reduce the layout cost for many production units with continuous material flow and increase the speed of material flow.

(iv) Because CLPs that assume unequal dimensions for cells and machines are very difficult, entry and exit points of cells should be in their center to solve such problems.

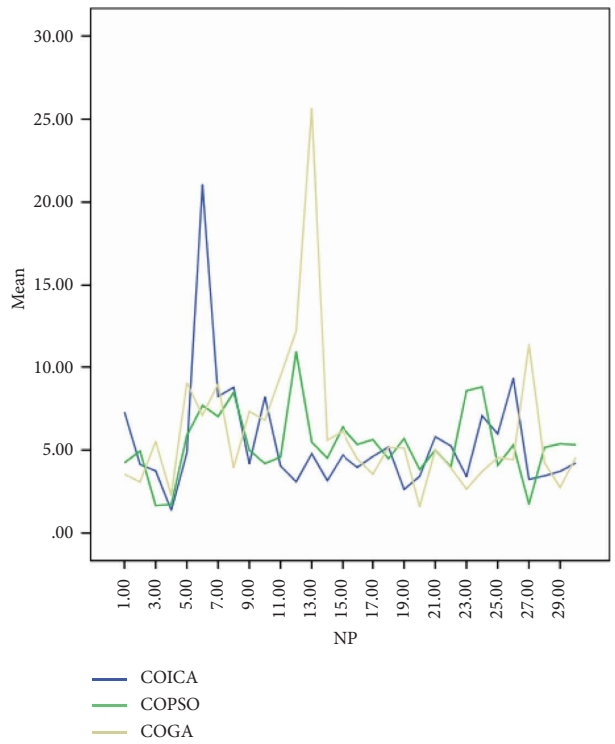

Figure 13: RPD values of the layout cost of meta-heuristic algorithms for stochastic problems.

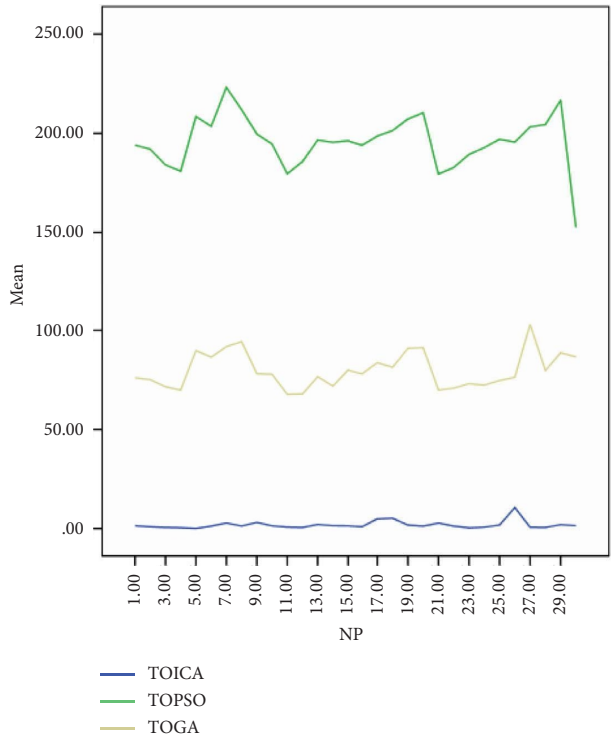

Figure 14: RPD values of the computational time of meta-heuristic algorithms for stochastic problems.

Table 21: Normality results of data related to the three proposed algorithms.

Criterion type	Kolmogorov–Smirnov's test[a]			Shapiro–Wilk's test		
	Statistic	Df	Sig	Statistic	Df	Sig
COICA	0.220	30	0.001	0.679	30	0.000
COPSO	0.171	30	0.025	0.932	30	0.055
COGA	0.214	30	0.001	0.697	30	0.000
TOICA	0.267	30	0.000	0.649	30	0.000
TOPSO	0.124	30	0.200*	0.947	30	0.144
TOGA	0.142	30	0.124	0.937	30	0.076

*Lower limit significance value. [a]Lilifores significance correction.

Table 22: Homogeneity results of variances of three independent communities in terms of layout cost.

Leven statistic	Intercellular degree of freedom (Df_1)	Intracellular degree of freedom (Df_2)	significant level (sig.)
2.111	2	87	0.127

Table 23: ANOVA results related to the equality of means of the three communities in terms of layout cost.

Source of changes	Sum of squares	Degree of freedom	Mean of squares	Statistic F	Significant level (sig.)
Intercells	10.610	2	5.305		
Intracells	1074.984	87	12.356	0.429	0.652
Total	1085.594	89			

Table 24: Homogeneity results of variances of three independent communities in terms of computational time.

Leven statistic	Intercellular degree of freedom (Df^1)	Intracellular degree of freedom (Df^2)	Significant level (sig.)
14.267	2	87	0.000

Table 25: Results of ANOVA related to the equality of means of the three communities in terms of computational time.

Source of changes	Sum of squares	Degree of freedom	Mean of squares	Statistic F	Significant (sig.)
Intercells	571265.895	2	285632.985	3212.937	0.000
Intracells	7734.377	87	88.901		
Total	579000.273	89			

Table 26: Tukey test results related to pairwise comparisons of computational time of three meta-heuristic algorithms.

F (I)	F (J)	Mean difference (I-J)	Standard deviation	Significant level	95% confidence level	
					Low level	High level
1	2	−193.92267	2.43449	0.000	−199.7277	−188.1177
	3	−78.01947	2.43449	0.000	−83.8245	−72.2145
2	1	193.92267	2.43449	0.000	188.1177	199.7277
	3	115.90320	2.43449	0.000	110.0982	121.7082
3	1	78.01947	2.43449	0.000	72.2145	83.8245
	2	−115.90320	2.43449	0.000	−121.7082	−110.0982

(v) Consequently and in order to solve CLPs, entry and exit points of machines should be considered in their center.

(vi) The flow of materials between cells and machines can be nondeterministic; in other words, it can be probabilistic and dynamic.

Table 27: Tamhane's T2 test results related to pairwise comparisons of computational time of three meta-heuristic algorithms.

F (I)	95% confidence level	Mean difference* (I-J)	Standard deviation	Significant level	95% confidence level	
					Low level	High level
1	2	−193.92267	2.43449	0.000	−200.2245	−187.6208
	3	−78.01947	1.67615	0.000	−82.2420	−73.7969
2	1	193.92267	2.49392	0.000	187.6208	200.2245
	3	115.90320	2.95822	0.000	108.5971	123.2093
3	1	78.01947	1.67615	0.000	73.7969	82.2420
	2	−115.90320	2.95822	0.000	−123.2093	−108.5971

*The values related to the mean difference are significant at 0.05.

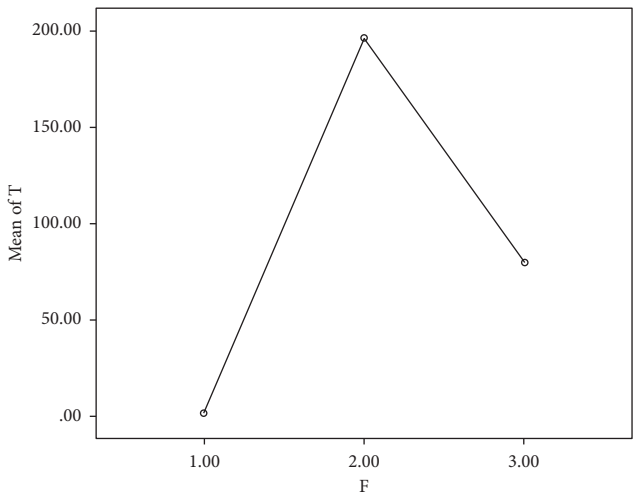

Figure 15: Mean computational time of three meta-heuristic algorithms.

These points can be determined in future works.

6. Conclusions

In this paper, a new mixed nonlinear programming model was presented for CLPs under the condition of unequal dimensions of cells and machines. Furthermore, it was assumed the cells' location in the workshop and the machines' location inside the cells are not predetermined, and the cells and machines can rotate. Based on the research findings, a cellular layout that assumes unequal dimensions of cells and machines can be used for products with batch production, and cell layout can be applied to CMSs aiming to move from traditional job shop layout to cellular layout. In the same way, cellular layout can be used in noncontinuous industries that have a job shop layout.

In brief, the following conclusions were made.

Due to nonlinearity of the developed model and failure to reach an optimal solution, the model was linearized. Then in order to assess its validity, a small-scale problem was solved by GAMS software and the results approved the model's validity.

(i) Since the problems considered in this research were continuous, (ICA), an efficient and continuous algorithm, was used to solve the small-scale problem. Comparison of the ICA and GAMS software showed that the presented model was valid.

(ii) To evaluate the mixed nonlinear programming model and meta-heuristic algorithms, 30 random problems were designed and solved by three algorithms (ICA, PSO, and GA). Then statistical analysis was done on the results.

(iii) Similarly, the mean values of the objective function related to three meta-heuristic algorithms were determined.

(iv) The results related to the center coordinates of the cells in the workshop and the center coordinates of the machines within each cell were presented in Tables and Figures after implementation of ICA, PSO, and GA for the 30^{th} random problem.

(v) The ($\overline{\text{RPD}}$) values of the layout cost and computational time for all the three mentioned algorithms were determined.

(vi) Normality and variance homogeneity tests were performed before doing the ANOVA test on the results obtained from the three meta-heuristic algorithms.

(vii) Then ANOVA test results indicated no significant difference between the mean costs of the three meta-heuristic algorithms; however, there was a significant difference between the mean computational times among the three algorithms. Therefore, the Tukey test was used to test which two groups differed in terms of computational time. The Tukey test results also revealed that the mean computational times of all the three algorithms were different.

(viii) Finally, it was found that ICA had reached the optimal solution in a very short computational time compared to the other two meta-heuristic algorithms. Thus, the superiority of ICA over PSO and GA is evident.

6.1. Study Limitations. There are always limitations in any research, and the current study is no exception. The limitations of the current research are as follows:

(1) Considering rectangular shapes for the machines to solve cell layout problems.

(2) Considering the entry and exit points of machines in their center.

(3) Considering the entry and exit points of cells in their center.

(4) Not considering stochastic condition for cells and machines.

6.2. Future Works. For future investigations, other researchers can further develop this research in the following directions:

(1) The problems of cellular layout can be investigated in dynamic and probabilistic modes.

(2) ICA provides encouraging results for CLPs when the material flow is considered at the center of the cells and machines. In the future, ICA can be applied for CLPs while considering entry and exit points for cells and machines.

(3) ICA is an optimization method that can reach a globally optimal solution in less computational time. Some parts of this algorithm can be modified to reduce the total cost value.

(4) ICA can cope with different types of optimization problems. In the future, new constraints and multiobjective cases can be considered.

(5) The cells and machines in this research had a rectangular shape. In the future, irregular shapes can be considered for them.

Data Availability

The data used to support the findings of this study are available in the article.

Conflicts of Interest

The authors declare that they have no conflicts of interest.

References

[1] C. R. Shiyas and V. M. Pillai, "A mathematical programming model for manufacturing cell formation to develop multiple configurations," *Journal of Manufacturing Systems*, vol. 33, no. 1, pp. 149–158, 2014.

[2] X. Wu, C. H. Chu, Y. Wang, and D. Yue, "Genetic algorithms for integrating cell formation with machine layout and scheduling," *Computers & Industrial Engineering*, vol. 53, no. 2, pp. 277–289, 2007.

[3] M. J. Rosenblatt, "The dynamics of plant layout," *Management Science*, vol. 32, no. 1, pp. 76–86, 1986.

[4] A. J. Vakharia and U. Wemmerlov, "Designing a cellular manufacturing system: a materials flow approach based on operation sequences," *IIE Transactions*, vol. 22, no. 1, pp. 84–97, 1990.

[5] V. Venugopal and T. T. Narendran, "A genetic algorithm approach to the machine-component grouping problem with multiple objectives," *Computers & Industrial Engineering*, vol. 22, no. 4, pp. 469–480, 1992.

[6] S. Jajodia, I. Minis, G. Harhalakis, and J. M. Proth, "CLASS: computerized layout solutions using simulated annealing," *International Journal of Production Research*, vol. 30, no. 1, pp. 95–108, 1992.

[7] B. Arvindh and S. A. Irani, "Cell formation: the need for an integrated solution of the sub problems," *International Journal of Production Research*, vol. 32, no. 5, pp. 1197–1218, 1994.

[8] J. Y. Kim and Y. D. Kim, "Graph theoretic heuristics for unequal-sized facility layout problems," *Omega*, vol. 23, no. 4, pp. 391–401, 1995.

[9] A. J. Vakharia and Y. L. Chang, "Cell formation in group technology: a combinatorial search approach," *International Journal of Production Research*, vol. 35, no. 7, pp. 2025–2044, 1997.

[10] M. Liang and S. Zolfaghari, "Machine cell formation considering processing times and machine capacities: an orthosynapse Hopfield neural network approach," *Journal of Intelligent Manufacturing*, vol. 10, no. 5, pp. 437–447, 1999.

[11] T. Y. Wang, K. B. Wu, and Y. W. Liu, "A simulated annealing algorithm for facility layout problems under variable demand in cellular manufacturing systems," *Computers in Industry*, vol. 46, no. 2, pp. 181–188, 2001.

[12] S. Lozano, D. Dobado, J. Larrañeta, and L. Onieva, "Modified fuzzy C-means algorithm for cellular manufacturing," *Fuzzy Sets and Systems*, vol. 126, no. 1, pp. 23–32, 2002.

[13] M. Solimanpur, P. Vrat, and R. Shankar, "Ant colony optimization algorithm to the inter-cell layout problem in cellular manufacturing," *European Journal of Operational Research*, vol. 157, no. 3, pp. 592–606, 2004.

[14] C. Andres and S. Lozano, "A particle swarm optimization algorithm for part–machine grouping," *Robotics and Computer-Integrated Manufacturing*, vol. 22, no. 5-6, pp. 468–474, 2006.

[15] R. Tavakkoli-Moghaddam, N. Javadian, B. Javadi, and N. Safaei, "Design of a facility layout problem in cellular manufacturing systems with stochastic demands," *Applied Mathematics and Computation*, vol. 184, no. 2, pp. 721–728, 2007.

[16] G. H. Hu, Y. P. Chen, Z. D. Zhou, and H. C. Fang, "A genetic algorithm for the inter-cell layout and material handling system design," *The International Journal of Advanced Manufacturing Technology*, vol. 34, no. 11-12, pp. 1153–1163, 2007.

[17] F. T. S. Chan, K. W. Lau, L. Y. Chan, and V. H. Y. Lo, "Cell formation problem with consideration of both intracellular and intercellular movements," *International Journal of Production Research*, vol. 46, no. 10, pp. 2589–2620, 2008.

[18] R. Tavakkoli-Moghaddam, N. Safaei, and F. Sassani, "A new solution for a dynamic cell formation problem with alternative routing and machine costs using simulated annealing," *Journal of the Operational Research Society*, vol. 59, no. 4, pp. 443–454, 2008.

[19] I. Mahdavi, M. M. Paydar, M. Solimanpur, and M. Saidi-Mehrabad, "A mathematical model for integrating cell formation problem with machine layout," *International Journal of Industrial Engineering & Production Research*, vol. 21, no. 2, pp. 61–70, 2010.

[20] K. Rafiee, M. Rabbani, H. Rafiei, and A. Rahimi-Vahed, "A new approach towards integrated cell formation and inventory lot sizing in an unreliable cellular manufacturing system," *Applied Mathematical Modelling*, vol. 35, no. 4, pp. 1810–1819, 2011.

[21] S. Ariafar, N. Ismail, S. H. Tang, M. K. A. M. Ariffin, and Z. Firoozi, "Inter-cell and intra-cell layout design in a cellular manufacturing system," in *Proceedings of the 2011 IEEE*

Symposium on Business, Engineering and Industrial Applications (ISBEIA), pp. 28–33, IEEE, Langkawi, Malaysia, September 2011.

[22] I. Mahdavi, E. Teymourian, N. T. Baher, and V. Kayvanfar, "An integrated model for solving cell formation and cell layout problem simultaneously considering new situations," *Journal of Manufacturing Systems*, vol. 32, no. 4, pp. 655–663, 2013.

[23] A. D. Asl and K. Y. Wong, "Solving unequal area static facility layout problems by using a modified genetic algorithm," in *Proceedings of the 2015 IEEE 10th Conference on Industrial Electronics and Applications (ICIEA)*, pp. 302–305, IEEE, Auckland, New Zealand, June 2015.

[24] E. Mehdizadeh and V. Rahimi, "An integrated mathematical model for solving dynamic cell formation problem considering operator assignment and inter/intra cell layouts," *Applied Soft Computing*, vol. 42, pp. 325–341, 2016.

[25] T. Ghosh, B. Doloi, and P. K. Dan, "An Immune Genetic algorithm for inter-cell layout problem in cellular manufacturing system," *Production Engineering*, vol. 10, no. 2, pp. 157–174, 2016.

[26] A. Derakhshan Asl and K. Y. Wong, "Solving unequal-area static and dynamic facility layout problems using modified particle swarm optimization," *Journal of Intelligent Manufacturing*, vol. 28, no. 6, pp. 1317–1336, 2017.

[27] M. Rabbani, H. Farrokhi-Asl, H. Rafiei, and R. Khaleghi, "Using metaheuristic algorithms to solve a dynamic cell formation problem with consideration of intra-cell layout design," *Intelligent Decision Technologies*, vol. 11, no. 1, pp. 109–126, 2017.

[28] H. Feng, L. Xi, T. Xia, and E. Pan, "Concurrent cell formation and layout design based on hybrid approaches," *Applied Soft Computing*, vol. 66, pp. 346–359, 2018.

[29] A. M. Golmohammadi, M. Honarvar, G. Guangdong, and H. Hosseini-Nasab, "A new mathematical model for integration of cell formation with machine layout and cell layout by considering alternative process routing reliability; a novel hybrid metaheuristic," *International Journal of Industrial Engineering & Production Research*, vol. 30, no. 4, pp. 405–427, 2019.

[30] V. Mahmoodian, A. Jabbarzadeh, H. Rezazadeh, and F. Barzinpour, "A novel intelligent particle swarm optimization algorithm for solving cell formation problem," *Neural Computing & Applications*, vol. 31, no. S2, pp. 801–815, 2019.

[31] M. Danilovic and O. Ilic, "A novel hybrid algorithm for manufacturing cell formation problem," *Expert Systems with Applications*, vol. 135, pp. 327–350, 2019.

[32] S. Paramasamy, A. Manimaran, K. Vinayagar, and G. Nagaraj, "Cell formation in sheet metal processing industry using genetic algorithm," *Caribbean Journal of Science*, vol. 53, no. 2, pp. 2526–2532, 2019.

[33] V. Rahimi, J. Arkat, and H. Farughi, "A vibration damping optimization algorithm for the integrated problem of cell formation, cellular scheduling, and intercellular layout," *Computers & Industrial Engineering*, vol. 143, 2020.

[34] Y. Zhao, J. Lu, and W. Yi, "A new cellular manufacturing layout: multi-floor linear cellular manufacturing layout," *International Journal of Advanced Robotic Systems*, vol. 17, no. 3, p. 172988142092530, 2020.

[35] J. S. Neufeld, F. F. Teucher, and U. Buscher, "Scheduling flowline manufacturing cells with inter-cellular moves: non-permutation schedules and material flows in the cell scheduling problem," *International Journal of Production Research*, vol. 58, no. 21, pp. 6568–6584, 2020.

[36] A. M. Golmohammadi, M. Honarvar, H. Hosseini-Nasab, and R. Tavakkoli-Moghaddam, "A bi-objective optimization model for a dynamic cell formation integrated with machine and cell layouts in a fuzzy environment," *Fuzzy Information and Engineering*, vol. 12, no. 2, pp. 204–222, 2020.

[37] A. Rostami, M. M. Paydar, and E. Asadi-Gangraj, "A hybrid genetic algorithm for integrating virtual cellular manufacturing with supply chain management considering new product development," *Computers & Industrial Engineering*, vol. 145, 2020.

[38] A. Ayough, M. Zandieh, and F. Farhadi, "Balancing, sequencing, and job rotation scheduling of a U-shaped lean cell with dynamic operator performance," *Computers & Industrial Engineering*, vol. 143, 2020.

[39] A. Goli, E. B. Tirkolaee, and N. S. Aydın, "Fuzzy integrated cell formation and production scheduling considering automated guided vehicles and human factors," *IEEE Transactions on Fuzzy Systems*, vol. 29, no. 12, pp. 3686–3695, 2021.

[40] S. Salimpour, H. Pourvaziri, and A. Azab, "Semi-robust layout design for cellular manufacturing in a dynamic environment," *Computers & Operations Research*, vol. 133, 2021.

[41] A. M. Golmohammadi, H. Rasay, Z. Akhoundpour Amiri, M. Solgi, and N. Balajeh, "Soft computing methodology to optimize the integrated dynamic models of cellular manufacturing systems in a robust environment," *Mathematical Problems in Engineering*, vol. 2021, Article ID 3040391, pp. 1–13, 2021.

[42] P. K. Mondal, M. Rafiquzzaman, and Z. Rahman, "A constructive algorithm for cell formation in cellular manufacturing systems considering cell load variations," *Journal of Manufacturing Technology Research*, vol. 13, no. 3/4, pp. 145–161, 2021.

[43] V. Razmjoei, I. Mahdavi, and S. Gutmen, "A hybrid multi-objective algorithm to solve a cellular manufacturing scheduling problem with human resource allocation," *Journal of Applied Research on Industrial Engineering*, vol. 9, no. 2, pp. 272–287, 2021.

[44] M. Hazarika, "An improved genetic algorithm for the machine-part cell formation problem," *International Journal of System Assurance Engineering and Management*, vol. 14, pp. 206–219, 2022.

[45] H. Mansour, I. H. Afefy, and S. M. Taha, "Heuristic-based approach to solve layout design and workers' assignment problem in the cellular manufacturing system," *International Journal of Management Science and Engineering Management*, vol. 17, no. 1, pp. 49–65, 2022.

[46] M. B. Fakhrzad, F. Barkhordary, and A. J. Afari Nodoushan, "A mathematical model for dynamic cell formation problem based on scheduling, worker allocation, and financial resources constraint," *Industrial Management Journal*, vol. 13, no. 3, pp. 435–463, 2022.

[47] K. Forghani and S. Fatemi Ghomi, "Joint cell formation, cell scheduling, and group layout problem in virtual and classical cellular manufacturing systems," *Applied Soft Computing*, vol. 97, 2020.

[48] R. Tavakkoli-Moghaddam, M. B. Aryanezhad, N. Safaei, M. Vasei, and A. Azaron, "A new approach for the cellular manufacturing problem in fuzzy dynamic conditions by a genetic algorithm," *Journal of Intelligent and Fuzzy Systems*, vol. 18, no. 4, pp. 363–376, 2007.

[49] K. Forghani, S. M. T. Fatemi Ghomi, and R. Kia, "Group layout design of manufacturing cells incorporating assembly and energy aspects," *Engineering Optimization*, vol. 54, no. 5, pp. 770–785, 2022.

[50] A. Ballakur and H. J. Steudel, "A within-cell utilization based heuristic for designing cellular manufacturing systems," *International Journal of Production Research*, vol. 25, no. 5, pp. 639–665, 1987.

[51] E. Atashpaz-Gargari and C. Lucas, "Imperialist competitive algorithm: an algorithm for optimization inspired by imperialistic competition," in *Proceedings of the 2007 IEEE Congress on Evolutionary Computation*, pp. 4661–4667, IEEE, Singapore, September 2007.

[52] E. Atashpaz Gargari, F. Hashemzadeh, R. Rajabioun, and C. Lucas, "Colonial competitive algorithm: a novel approach for PID controller design in MIMO distillation column process," *International Journal of Intelligent Computing and Cybernetics*, vol. 1, no. 3, pp. 337–355, 2008.

[53] S. Nazari-Shirkouhi, H. Eivazy, R. Ghodsi, K. Rezaie, and E. Atashpaz-Gargari, "Solving the integrated product mix-outsourcing problem using the imperialist competitive algorithm," *Expert Systems with Applications*, vol. 37, no. 12, pp. 7615–7626, 2010.

[54] J. Behnamian and M. Zandieh, "A discrete colonial competitive algorithm for hybrid flowshop scheduling to minimize earliness and quadratic tardiness penalties," *Expert Systems with Applications*, vol. 38, no. 12, pp. 14490–14498, 2011.

[55] R. L. Haupt and S. E. Haupt, *Practical Genetic Algorithms*, A John Wiley & Sons. Inc., Publication, Hoboken, New Jersey, NJ, USA, 2004.

[56] G. Taguchi, "Introduction to quality engineering: designing quality into products and processes (No. 658.562 T3)," 1986, http://worldcat.org/isbn/9283310845.

Hindawi
Complexity
Volume 2023, Article ID 2140631, 9 pages
https://doi.org/10.1155/2023/2140631

Research Article

Complexity Model for Predicting Oil Displacement by Imbibition after Fracturing in Tight-Oil Reservoirs

Aijun Chen,[1] Yiqing Zhou,[2] Rulin Song,[3] Yangrong Song,[3] Hanlie Cheng,[4] and David Cadasse[5]

[1]*The No. 12 Oil Production Plant of Changqing Oilfield Company, PetroChina, Qingyang 745400, Gansu, China*
[2]*Downhole Operation Company, CNPC Bohai Drilling Engineering Co., Ltd., Renqiu, Hebei 062552, China*
[3]*Technical Center of the First Oil Production Plant of Qinghai Oilfield, Mangya, Qinghai 816400, China*
[4]*COSL-EXPRO Testing Services (Tianjin) Co., Ltd., Tianjin 300457, China*
[5]*The King's School, BP1560, Bujumbura, Burundi*

Correspondence should be addressed to David Cadasse; davidcadasse@ksu.edu.bi

Received 28 September 2022; Revised 16 December 2022; Accepted 5 April 2023; Published 5 May 2023

Academic Editor: Fuli Zhou

With the increasing difficulty of conventional oil and gas exploration and development, oil and gas resources have developed from conventional to unconventional, and the exploration and development of tight-oil reservoirs are highly valued. In view of the complexity of the influencing factors of oil-water spontaneous seepage after fracturing and the instability of reservoir recovery, this paper takes the tight sandstone reservoir of Yanchang Formation in the southern Ordos Basin as the research object. Based on the micro-nano pore throat characteristics of tight sandstone, the seepage experiment is carried out, and the theoretical model of seepage suction is constructed. The mechanism and influencing factors of suction and oil displacement after fracturing in tight reservoirs are analyzed. Based on the analysis of fluid buoyancy and gravity, a mathematical model of the oil-water spontaneous flow after fracturing was established, and its influencing factors were analyzed. The experimental results show that the pore throats of tight sandstone are mainly in micron- and submicron scale, and the reservoir permeability is related to the pore throat structure, oil-water interfacial tension, and wettability. After fracturing, with the increase of the fracture length, the seepage velocity gradually decreases. With the increase of fracture opening, the influence of buoyancy and gravity on seepage velocity increases. With the increase of the fracture number, seepage velocity also increases. The fracture helps to reduce the adsorption of oil droplets on the core surface and improve the efficiency of spontaneous imbibition and oil displacement of the core. The research results provide theoretical data support for enhancing oil recovery and have important application guiding significance for the operational reliability of manufacturing systems with complex topology and the complexity and operability of production operations in manufacturing systems.

1. Introduction

It is important to investigate the operational reliability of manufacturing systems with complex topology structures and complexity and operability of production jobs in manufacturing systems. As a typical application of operational reliability of manufacturing systems with complex topology structures and complexity and operability of production jobs in manufacturing systems, the economy developed rapidly, the external demand for oil is increasing year by year, and the current domestic self-developed oilfield has entered the middle and late stages, and crude oil production is decreasing year by year, which poses a serious threat to China's energy security [1–3]. In the case of energy shortage, it is of great strategic and practical significance to continuously improve the degree of exploitation of petroleum resources, and with the development of the petroleum industry, the exploration and development of traditional conventional oil and gas resources has gradually shifted to unconventional oil and gas exploration and development

[4–7]. In the face of the increasingly severe energy security situation, China has increased its efforts in oil and gas exploration and development, especially unconventional oil and gas. In recent years, with the rapid development of science and technology, unconventional oil and gas has become the main energy source to be developed. With the successful development and commercialization of shale oil and gas in North America, the world has set off a boom in the development of unconventional oil and gas [5, 8–10]. As the most important one of unconventional oil and gas reservoirs, tight-oil reservoirs have a permeability of less than 1 mD in air, a formation overlay permeability of less than 0.1 mD, and a porosity of less than 10% which is a typical low porosity and low permeability. Tight oil is an oil and gas resource existing in tight reservoirs, with broad development prospects, and it is widely distributed in the world. China tight oil is rich in resources, distributed in Songliao Basin, Junggar Basin, Ordos Basin and Sichuan Basin, with an oil-bearing area of about $5 \times 105\ km^2$ and recoverable reserves of about 25×109t. With the continuous development of tight reservoirs at home and abroad, the problem of productivity decline and production decline is inevitable. Therefore, it is necessary to study the methods of enhancing oil recovery in tight reservoirs. At the same time, due to the particularity of tight reservoirs, it is necessary to adjust and optimize the lifting methods of ordinary reservoirs when they are applied to tight reservoirs, establish an evaluation method for the applicability of the lifting methods of tight reservoirs, and give the restrictions of different lifting methods [11–14].

As an important unconventional oil reservoir, tight-oil reservoir has complex physical conditions, such as ultralow permeability and ultralow porosity, which makes the output of a single well of tight oil decline too fast and stay in a low efficiency state for a long time. There are two main reasons for the difficulty of tight reservoir development. On the one hand, it is difficult to supplement energy for reservoir development, and it is even more difficult for tight reservoirs to be recovered by supplementing external energy. Therefore, depletion recovery is the main production mode of tight reservoirs. On the other hand, tight reservoirs generally have high water saturation, which makes oil encounter high resistance in the process of percolation; so, it is difficult to produce oil, which also leads to the low recovery factor of tight oil in China. The size, distribution, and distribution type of pore throat are all important factors affecting the imbibition capacity of tight oil, especially tight reservoirs are characterized by poor physical properties, strong heterogeneity, and obvious microscale effect. Therefore, it is more important to correctly understand the micropore structure of tight-oil reservoirs. However, the rapid flowback after high displacement volume fracturing and refracturing can achieve the desired effect of increasing production. The imbibition replacement technology for ultralow permeability tight oil is that fracturing fluid gel breaking fluid or displacement fluid enters capillary channels through capillary force to occupy the capillary space and drives crude oil into larger roaring channels or fractures, thus improving the recovery of tight crude oil. In view of the complex influencing factors of oil-water spontaneous seepage after fracturing and the difficulty in predicting oil recovery, this paper conducts seepage suction experiments on the micro/nano-pore throat characteristics of tight sandstone, analyzes the oil displacement mechanism and influencing factors of tight reservoir after fracturing, analyzes the mechanical characteristics of oil and water phases in fractures, establishes the mathematical model of spontaneous oil and water seepage after fracturing, and analyzes its influencing factors. The research results can be used to improve the recovery of tight crude oil and can provide theoretical support for improving reservoir recovery.

2. Literature Review

Tight-oil reservoirs have the characteristics of low porosity, low permeability, and many micro- and nanopores, and conventional mining methods cannot meet the exploitation of tight-oil reservoirs [15–17]. At present, the exploitation of tight oil is mainly through hydraulic fracturing and other methods to transform the reservoir, open up the internal cracks of the reservoir, and enhance the fluidity of the reservoir fluid to reduce the seepage resistance of the formation fluid to improve the seepage recovery rate. The foreign tight oil and gas production technologies mainly include the following: (1) horizontal well drilling and completion technology: tight reservoir has low production and generally long production cycle, and the application of horizontal drilling technology just solves these problems; so, it is the main method of exploiting tight oil abroad at present. The main completion methods include intelligent completion, perforation completion after casing cementing, open hole perforation completion, and combined bridge plug completion; (2) multistage fracturing technology for horizontal wells: the technology consists of several parts, including horizontal well drilling and completion, staged fracturing, and micro seismic detection technology; and (3) other fracturing technologies including refracturing and synchronous fracturing technology and channel fracturing technology developed in the recent years.

At the present stage, most tight reservoirs are exploited by water drive. Due to the huge difference in the permeability between fractures and matrix, there is still a large amount of remaining oil enriched in matrix rock blocks at the later stage of water injection development. Oilfield development practice has proved that capillary pressure imbibition is the key to improve oil recovery in tight reservoirs. Therefore, it is of great significance to study the capillary imbibition law on the basis of considering the characteristics of tight reservoirs to understand the oil displacement mechanism of tight reservoirs. Some researchers have carried out spontaneous aspiration studies when the dense reservoir contains a large number of natural or artificial cracks under the action of capillary force to wet the phase flow into the matrix. The imbibition displacement of crude oil mainly occurs in the dual medium area. In porous media, the process of replacing the nonwetting phase fluid by the wetting phase fluid relying on the capillary force is called imbibition. When the fluid suction rate in the fracture is slow, the inflow direction of the wetted phase fluid in the

reservoir and the outflow direction of the nonwetting phase are the same to achieve codirectional seepage. When the seepage rate of fractured fluid is relatively fast, the reservoir matrix is surrounded by cracks, and the wetting phase fluid flows into the matrix pores from all directions, and the opposite direction of the outflow direction of the nonwetting phase and the inflow direction of the wetting phase is reverse seepage. Some researchers have studied capillary pressure, pore development, phase osmotic curves, matrix, fracture permeability, and in a static and dynamic manner. The influence of matrix oil saturation on reservoir suction velocity is linearly related to capillary pressure, matrix permeability and residual oil saturation, exponential relationship with bound water saturation, and viscosity of crude oil under static conditions power index relationship [18–21]. Some researchers have studied the seepage suction and flooding oil of the core of the fractured reservoir with low permeability under different permeability through spontaneous crack seepage experiments and concluded that the higher the capillary force in the oil reservoir suction system, the higher the suction process. Reverse fracture seepage has a high oil production at the initial stage of oil absorption, and the oil production will decrease obviously after 50 hours until no oil is produced. When the permeability is less than 2 mD, the degree of spontaneous suction and extraction increases with the increase of permeability, and the better the pore and throat structure, the more conducive to spontaneous suction effect. Some researchers have simulated the geological characteristics and fluid properties of tight sandstone reservoirs and carried out dynamic seepage suction experiments, indicating that with the increase of liquid injection pressure, the oil exhalation rate of core seepage and drainage accelerated [22–24]. After the injection rate was accelerated, the suction recovery rate showed a change of first increase and then decreased, and the size of the plug of the infiltration injection section was increased, the holding time was prolonged, and the number of alternate injections was increased. It can effectively improve the seepage recovery of the reservoir. Some researchers have studied the influencing factors of seepage in tight reservoirs and when the sorption method is different, the permeability rate will affect the suction rate. To produce a certain effect, the fracture of the dense reservoir has effectively increased the contact area of the dense matrix, and the suction solution effectively reduced the seepage resistance to improve the seepage recovery rate; when the water injection throughput increases the suction distance, the large-scale volume fracturing changes [25–27]. The wettability of the reservoir and the water injection throughput are conducive to improving the oil recovery of the reservoir. Some researchers have carried out research on the factors affecting the seepage of the core, mainly the influence of the physical properties of the core itself, such as the permeability of the core, the structure of the pore throat and the surface wettability of the core, the influence of fluid properties, including the viscosity of crude oil, the mineralization of the leachate, and the interface tension of oil and water, and the influence of external conditions, including boundary conditions, temperature, and pressure.

In the existing literature, the research results of imbibition are mostly aimed at fractured reservoirs or low permeability and ultralow permeability reservoirs, while the research on tight reservoirs is still in its infancy. At home and in abroad, the existing spontaneous imbibition mechanism, influencing factors, models, and production experience are difficult to be transplanted into the production of tight oil, and the micro-nano pore throat characteristics have a great impact on it. Therefore, it is an effective method to build a theoretical model of seepage suction to characterize the irregularity of its microstructure to study the spontaneous imbibition mechanism of tight reservoirs.

3. The Geological Background and Research Methods of the Study Area

3.1. Geological Overview. Ordos Basin is located in the west-central region of China, and the basin is generally rectangular, north and south spread; the north extends Yin Mountain, Daqing Mountain is close to the border, the south is bounded by Qinling Mountains, the east is connected with Lüliang Mountain and Zhongtiao Mountain, and the west extends to Helan Mountain and Liupan Mountain. The research area is a dense sandstone reservoir of the Yanchang Formation in the southern Ordos Basin, with a total area of about 2600 km^2, located in the eastern part of Gansu province, and the surface is characterized by the gully area of the Loess Plateau in the middle reaches of the Yellow River, mostly mountainous. The terrain gradually rises northeast along the river valley, with an altitude of 900–1800 m, with an average altitude of 1400 m. The exploration and development of tight-sandstone reservoirs is mainly 8, 9, and 10 long reservoirs. The first set of oil reservoir systems developed after the formation of large inland depression lake basins in the Ordos Basin is a set of sedimentary systems caused by braided river deltas, meandering river deltas and turbidity fans, and the whole is dominated by medium-fine sandstone and mudstone and its local development of oil shale and coal-bearing sandwich layers. There are 6 reservoir formations in the Yanchang Formation from bottom to top, all of which have reservoir discoveries, of which the Yanchang Formation 8, 9, and 10 are the heyday of lake basin development, and the average permeability of the sandstone of the Reservoir Formation is less than 0.3×10^{-3} μm^2, which is the most typical tight-oil reservoir.

3.2. Specimen Preparation and Test Methods. At present, there are two main methods to recognize the pore throat structure of tight sandstone, namely, the image analysis method and the calculation of pore throat size and structural parameters through the change of fluid mass, volume, and pressure. In this paper, the micropore structure of tight-sandstone reservoir is further studied by high-pressure mercury injection and casting thin section experiment. Casting thin section can effectively analyze the reservoir space and the pore type of tight-sandstone reservoir, while the high-pressure mercury injection test is helpful to further determine the pore distribution characteristics of tight-

Table 1: Core parameters before and after fracturing.

Core numbers	Core lengths (cms)	Core diameters (cms)	Permeability (mD) before fracturing	Permeability (mD) after fracturing	Cracks open degree (μm)	Core crevice types
1	4.894	2.522	0.095	27.290	1.64	Single slit
2	5.477	2.49	0.079	0.137	0.09	Cross-seams
5	5.661	2.512	0.081	15.748	1.43	Cross-seams
7	5.234	2.511	0.041	18.523	1.82	Single slit
10	4.972	2.498	0.082	10.639	0.922	Cross-seams

sandstone reservoir. In order to better understand the micro pore structure of experimental cores, FE-SEM field scanning electron microscopy was used to conduct experimental analysis on several representative compact cores. The FE-SEM field scanning electron microscope further verified that the reservoir is dominated by micropore throat, and the main types are micro- and nanopore throat. For the conventional mining method of micron and nanometer sized pore throat, it is difficult to use, the development effect is not obvious, and the economic benefit is low. How to effectively improve the recovery efficiency of micron and nanometer sized tight reservoirs is the focus of the research.

This time, 10 compact sandstone cores were selected for matrix seepage experiments, with a core length of 5.01–5.71 cm and a diameter of about 2.5 cm. The permeability was 0.01 4–0.185 mD, the porosity is between 3.4% and 12%, and the core appears as weak hydrophilic. In this study, 5 of the tight cores were selected for physical fracturing and fracturing, and a certain amount was applied by bending the fine wire into a U-shaped clamping core pressure fracturing the core so that the core cracks, and then we used glue to paste the fractured core and measured the permeability before and after the cracking and other parameters. Due to the difference in the texture structure of the core, the fractures produced by fracturing may not be single penetration joints, but there are still certain horizontal fractures, which is followed in this article core fracture distribution, dividing the core into single and cross fractures after fracturing. Table 1 and Figure 1 show the comparison of the parameters of the core before and after fracturing, especially with regards to the change in permeability, and the core porosity is between 8% and 13.6%, the permeability range is 0.086 mD–0.105 mD, and the core permeability increases greatly after fracturing, of which the penetration rate of the core increased by 451 times.

Using the collected crude oil and kerosene 1 : 1 configuration simulation oil, the Physica MCR 301 rheometer was used to measure its density and viscosity to obtain a density of 0 8 g/cm^3 with a viscosity of 4.8 MPa·s. The formation water used in the test was 2 × 104 mg/L of NaCl solution, and the surfactant was dodecylbenzenesulfonate, which was obtained by the volumetric method. The degree of seepage extraction and the rate of seepage suction of the core are carried out by using a 0.01 ml suction flask. The SVT20 interface tensioner is used to perform tension measurements at the oil-water interface of different seeps by filling the sample tube with the seepage and injecting a drop of simulated oil at high centrifugal forces. Under

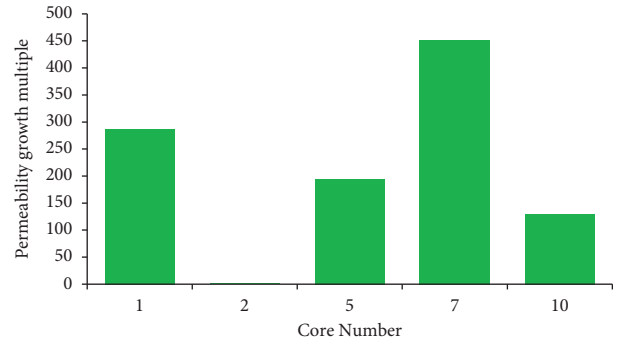

Figure 1: Multiple increase in core permeability before and after fracturing.

the action of a centrifugal velocity of 6000 r/min, the simulated oil is stretched and deformed, and the shooting capture is carried out by a high-precision camera, and its interfacial tension is calculated according to the curvature of the droplets. After that, the core sheet is cut from the core for the wettability test, and the core sheet is first polished and smoothed into the infiltration for 48 hours, and then the contact angle between the oil droplets and the core piece is measured by a high-power microscope. Place the core chip holder in the sample box, add oil droplets under the core slice and pour the seepage solution and observe the contact between the oil droplets and the core piece in the exudation by adjusting the sample box position and using high-power microscope irradiation. The high-powered microscope focal length ensures that the oil droplets and core pieces are in the center of the screen. Take photos and save them using a protractor to measure the angle between the core piece and the oil droplet, which is the wetting angle.

3.3. Test Procedure. Due to the difference of fluid properties and reservoir physical properties, tight reservoirs have different percolation laws and mechanisms from conventional high permeability reservoirs, usually showing low-speed nonlinear percolation characteristics. The narrow pore throat and complex environment in the tight reservoir make the oil-water channel fine and have great seepage resistance and liquid-solid interface interaction, and the reservoir permeability is low. The overlying effective stress has a great influence on the physical parameters of low permeability porous media, affects the seepage law, deviates from Darcy's law, and presents the phenomenon of low-speed nonlinear seepage.

The opening of the crack directly affects the seepage process of the crack, and the suction rate is faster when the crack is opened. As the surrounding pressure of the core increases, the cracks in the core begin to close under the action of pressure and the opening of the fractures gradually decreases. The core liquid permeability measurement step is to dry the core at 100°C for more than 12 h and measure the dry weight of the core. After the weight of the core is stabilized, the core is evacuated for 12 h; saturation of the core using stratigraphic water; place the core into the gripper, adjust the equipment, set the confining pressure, pump the formation water in through the constant-flux pump, and record at the same time the pressure and flow rate of the inlet and outlet of the lower gripper, and the permeability of the core is calculated after the flow is stabilized; by increasing the confining pressure, the permeability of the core under different confining pressures is calculated. Figure 2 shows the permeability of the core sample 5 at different confining pressures. The permeability of the core gradually increases with the increase of the confining pressure, and the two are essentially linear, which is consistent with Darcy's law; that is, the core permeability is proportional to the fracture opening, and the greater the core permeability, the greater the crack opening.

By performing a seepage test on the core after fracturing, Figure 3 shows the process of the seepage test of the core after fracturing, through a 35°C incubator. Simulate the reservoir temperature, take the time when the solution touches the bottom of the core as the starting point of the seepage time, record the seepage of the core at different times, and take pictures to record the changes of oil droplets on the surface of the core.

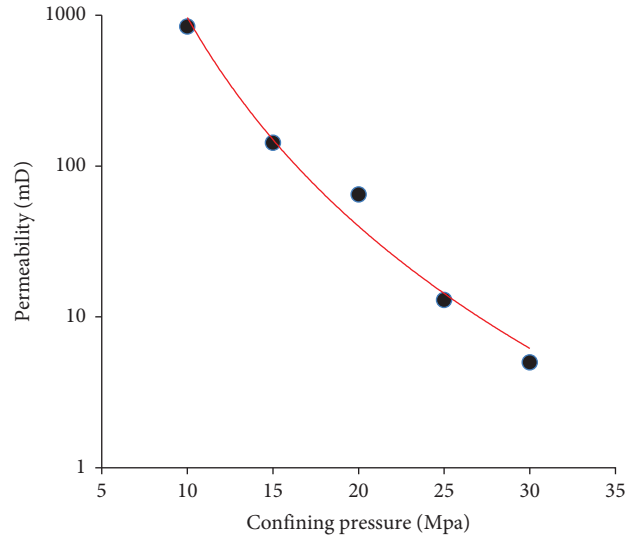

Figure 2: Permeability of the core sample 5 under different confining pressures.

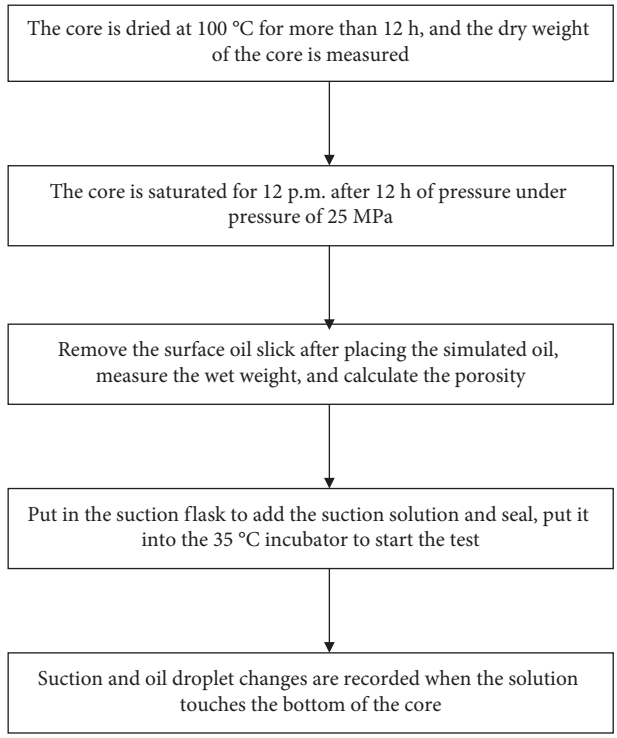

Figure 3: Core seepage test process after fracturing.

4. Results

4.1. Test Results. Hagen–Poiseuille's law (H-P law) describes the steady laminar flow of incompressible fluid in a horizontal pipe. In 1927, Kozeny J applied the H–P law to the capillary flow and established an ideal capillary bundle model for the reservoir flow, that is, the flow path of fluid in the pores was equivalent to a group of parallel capillary bundles with different radii. When there is a crack in the core, the crack will seep due to capillary force. When the crack is completely immersed in water, the crack is mainly affected by gravity, viscosity, capillary force, buoyancy force, crack end pressure, crack seepage and crack opening, length, and inclination. The oil-water interface tension is related to the wetting angle. In order to analyze the influence of different factors on crack seepage, this paper simulates using MATLAB based on the control variable method, and Table 2 gives the parameters required for crack seepage simulation.

(1) *Effect of Fracture Length on Crack Seepage.* Set the opening degree and the inclination angle of the fracture according to Table 2, and select the core of different fracture length to carry out the infiltration test. The test shows that the seepage rate of the core is gradually increased with the suctioning test, but the oil and water suction rate decrease with the increase of the fracture length. In the process of seepage and suction, due to the constant crack opening, the capillary force of the crack remains unchanged, and the pressure difference between the two ends of the crack is the main driving force for the suction of the crack. As the infiltration continues, the oil in the crack is driven out by water, the height of the oil-water interface increases, and the internal flow weight of the fracture increases, resulting in a decrease in the buoyancy and viscosity of the fluid. At the same time, the combined force of the fluid in the

Table 2: Parameters required for fracture seepage simulation.

Names	Numeric values
Crack length (cm)	12
Crack width (cm)	2.525
Crack opening (μm)	1.2
Crack inclination (°)	62
Oil phase viscosity (MPa·s)	5
Aquatic phase viscosity (MPa·s)	1.1
Oil-water interface tension (mN/m)	14.19
Contact angle (°)	48

crack increases, and the seepage rate of the fracture increases. Therefore, when the crack opening degree is fixed, the viscosity is the main factor affecting the seepage rate.

(2) *Effect of Crack Opening on Crack Seepage*. Crack opening is an important parameter to describe the characteristics of cracks, and different crack opening degrees are set, which are 100 μm, 10 μm, 1 μm, 0.1 μm, 0.01 μm, etc., to simulate crack penetration. The test shows that with the increase of crack opening, the crack seepage rate continues to increase, and when the crack opening degree is 100 μm, the crack seepage rate decreases with the increase of the height of the oil-water interface, and when the crack opening is ≤10 μm, the crack seepage rate increases with the increase of the height of the oil-water interface. At the same time, as the crack opening increases, the capillary force gradually decreases, but the gravity, buoyancy, and viscosity of the fluid are subjected as the pressure increases at both ends of the crack. Therefore, when the crack opening degree is certain, the viscosity is the main factor affecting the fracture seepage, and increasing the crack opening can effectively improve the crack penetration rate.

(3) *Effect of Crack Inclination on Crack Seepage*. Different crack inclination angles are set, which are 0°, 45°, 60°, 75°, and 90°, to simulate the fracture suction process. When the crack opening is small (crack opening is 1 μm), the fracture penetration rate does not change significantly with the increase of the crack inclination. With the increase of crack opening, the gravity and buoyancy of the fluid in the crack also increase, the capillary force of the crack decreases the seepage suction, and the seepage rate increases with the increase of the crack inclination, and at the same time, with the increase of the inclination angle of the crack, the fluid viscosity of the crack increases slightly, which is mainly due to the increase of the inclination angle of the crack, resulting in the increase of pressure difference, buoyancy, and gravity components at both ends of the crack so that the fluid viscosity in the crack increases.

(4) *Influence of Interface Tension on Crack Seepage*. The fracture length, crack opening, and crack inclination angle are set according to Table 2 and passed. The fracture infiltration was simulated by changing the oil-water interface tension, and the oil-water interface was set to 14.91 mN/m, 10.62 mN/m, 7.23 mN/m, 4.67 mN/m, and 3.63 mN/m, respectively. Since each group of samples is taken from the same full diameter core, the basic physical properties, pore structure, and wettability are roughly the same. The role of interfacial tension in fracture seepage can be simply investigated without the influence of other factors. When the oil-water interface tension is greater, the greater the seepage rate of the crack. This is due to the increase of the oil-water interface tension, in which the capillary force of the crack also increases, and at the same time, under the action of crack seepage, the viscosity of the water is less than the oil viscosity in the crack. The combined force of the fluid increases so that the fracture seepage rate increases. Due to the small crack opening of the setting, the influence of gravity and buoyancy on the fracture seepage is small, and with the increase of the height of the oil-water interface, the viscous resistance of the fluid gradually decreases, which accelerates the fracture suction rate.

(5) *The Influence of the Wetting Angle on Crack Seepage*. At present, researchers at home and abroad have proposed a variety of methods to analyze the wettability. The Amott self-priming oil drainage method has the advantages of a large test range, clear numerical definition, and small impact on oil and gas exploration and development and is widely used in the quantitative evaluation of core wettability. The wetting angle of the crack surface is set to 0°, 30°, 50°, 70°, 80°, and 89°, respectively. The test shows that with the increase of the wetting angle of the crack, the seepage rate of the crack is significantly reduced, and in the process of suction and suction, when the length, opening, inclination angle, and oil-water interface tension of the crack remain unchanged, the gravity of the fluid in the crack, both buoyancy and pressure difference, remain constant, and the viscosity of the fluid in the crack decreases as the rate of seepage decreases. This is due to the fact that the hydrophilicity of the fracture surface decreases with the increase of the wetting angle and the capillary force of the fracture decreases, resulting in a decrease in the seepage rate of the fracture. The relative wettability index has a positive correlation with the imbibition recovery. The imbibition process is a process in which the wetting phase spontaneously inhales into the porous medium by capillary pressure to displace the nonwetting phase. For water wet reservoirs, water is the wetting phase and capillary pressure is the imbibition power. Therefore, the higher the degree of water wetness is, the stronger the role of capillary pressure is. The higher the proportion of pores that water can enter in the total pores, the more the oil expelled, and therefore, the higher the imbibition recovery factor.

Table 3: Summary of core aspiration results.

Core numbers	Degrees of extraction	Core numbers after fracturing	Degrees of extraction
1	0.184	2	0.254
3	0.201	5	0.266
14	0.154	11	0.215
19	0.104	16	0.184
20	0.112	19	0.177

4.2. Comparison of Oil Drainage before and after Fracturing. In order to study the effect of fractures on core aspiration, a comparative analysis of seepage suction tests of fractured cores and matrix cores was carried out, as shown in Table 3 and Figure 4. The seepage results of each core are given, and the degree of core extraction and the seepage rate are analyzed.

First, dry and weigh the core, vacuumize, saturate the test water, and weigh the wet weight; then, oil displacement is carried out at room temperature to saturate the core with experimental oil; finally, without external pressure, the core is completely immersed in the experimental water. At this time, the core will self-absorb water and drain oil under the action of capillary force. In the process of absorbing water and draining oil, the core quality will continue to increase due to the poor density of oil and water. Use the electronic balance to continuously weigh the core and record the change of core quality.

It can be seen from Figure 4 that after core fracturing, due to the development of fractures, the degree of core extraction and the seepage rate are significantly improved, and the degree of core extraction after fracturing increases at least 10%; this is due to the presence of cracks to increase the contact area between the suction and the core, providing an infiltration channel for the flow of fluid inside the core.

The degree of crack opening obtained from the seepage specimen has a certain influence on the seepage of the crack, and with the increase of the crack opening, the fracture seepage rate also increases. In this experiment, the fractures of core 11 and core 16 are the same, but the fracture opening of the two is very different, and the seepage rate of core 16 is much higher than that of core 11, which is consistent with the model results.

According to the seepage of each core, the relationship between the degree of extraction and the seepage rate of each core and the number of fractures in the core is compared. Core 5 is a single fracture, and its recovery degree and seepage rate are high; Core 16 is a cross fracture, although the number of fractures is large, but the degree of extraction is between core 20 and core 5, and the seepage rate is much higher than that of the other two tight cores. The seepage rate is about 2 times that of core 5. Therefore, it can be concluded that the number of core fractures has a certain influence on the seepage rate of the core and the greater the core seepage rate is with the increase of the number of fractures. At the same time, by comparing the seepage rate curve of the three cores, it can be found that each core has a high seepage rate in the early stage of seepage, but the seepage rate decreases rapidly, and with the increase of the number of core fractures, the seepage rate decreases significantly.

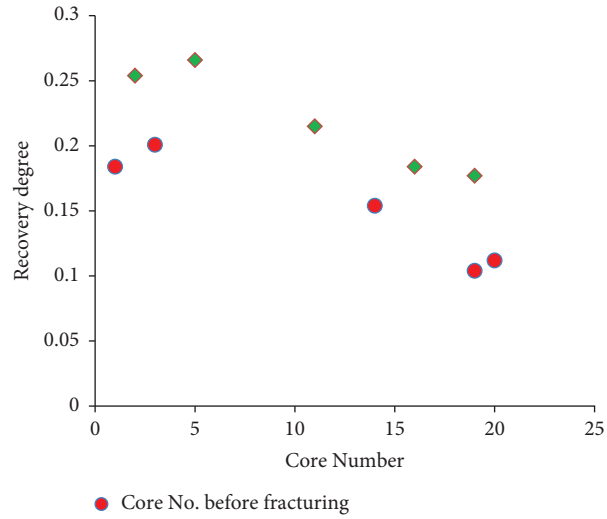

Figure 4: Different degrees of core extraction.

By observing the oil droplets on the surface of the core during the seepage process, it can be found from Figure 4 that when the infiltration begins, oil droplets appear at the fractures of the core, but with the growth of time, the oil droplets will gradually become larger and eventually leave the core. Core 5 and 16 seepages are the same, but from the distribution of oil droplets on the core surface, the number of oil droplets adsorbed on the surface of the core 16 is small. This is mainly due to the different distribution of fractures in the core 5 and 16; the core 16 is a cross-fractured core and the number of fractures is more. In the process of seepage suction, the oil produced by the seepage of the matrix is discharged through the fracture of the core Therefore, there are fewer oil droplets on the surface of the core. The radius of the oil droplets adsorbed on the surface of the core 5 is very large, which is due to the large interfacial tension between the formation water and the simulated oil, resulting in small oil droplets on the surface of the core that cannot be separated from the core; so, with the increase of the infiltration time, the oil droplets on the surface of the core accumulate to form large oil droplets. The core 16 oil droplets are mainly concentrated and produced at the cracks, and more cracks in the core make the oil droplets in the core more likely to gather, which is also the main reason for the rapid output and the large seepage rate at the beginning of the core 16 seepage.

5. Conclusion

This paper takes the tight sandstone reservoir of Yanchang Formation in the south of Ordos Basin as the research object, conducts core seepage pumping experiments before and after fracturing, builds a seepage theoretical model, analyzes the seepage drainage mechanism of tight reservoirs after fracturing and its influencing factors, and establishes a mathematical model of oil and water spontaneous seepage after fracturing and analyzes its influencing factors, which provides theoretical data support for improving oil recovery. (1) The porous throat of tight sandstone is mainly at the micron- and submicron scales, and the infiltration rate of the reservoir is related to the pore throat structure, oil-water interface tension, and wettability. The oil-water infiltration rate decreased with the increase of fracture length. With the increase of crack opening, the suction rate of crack seepage increases; with the increase of crack inclination, the seepage rate of the crack increases; with the greater the tension at the oil-water interface, the greater the seepage rate of the crack; with the increase of the wetting angle of the crack, the suction rate of the crack is significantly reduced. (2) The crack is the main seepage channel of the fractured core, which can effectively reduce the adsorption of oil droplets on the outer surface of the core. At the beginning of the seepage, the oil droplets first appear at the fractures of the core, and as time increases, the oil droplets gradually become larger and eventually leave the core. With the increase of cracks in the core, the number of adsorbed oil droplets on the core surface decreases and the radius of adsorbed oil droplets decreases. This work serves as an important reference to operational reliability of manufacturing systems with complex topology structures and complexity and operability of production jobs in manufacturing systems.

Data Availability

Data used to support the findings of this study are included within the article.

Conflicts of Interest

The authors declare that they have no conflicts of interest.

Acknowledgments

The authors would like to show sincere thanks to those technicians who have contributed to this research.

References

[1] J. Yao, X. Deng, Y. Zhao, T. Han, M. Chu, and J. Pang, "Characteristics of tight oil in triassic Yanchang Formation, Ordos Basin," *Petroleum Exploration and Development*, vol. 40, no. 2, pp. 161–169, 2013.

[2] P. Kathel and K. K. Mohanty, "Wettability alteration in a tight oil reservoir," *Energy and Fuels*, vol. 27, no. 11, pp. 6460–6468, 2013.

[3] X. Zhou, Q. Yuan, Y. Zhang, H. Wang, F. Zeng, and L. Zhang, "Performance evaluation of CO2 flooding process in tight oil reservoir via experimental and numerical simulation studies," *Fuel*, vol. 236, pp. 730–746, 2019.

[4] Y. Braverman, A. Chizov-Ginzburg, and B. A. Mullens, "Mosquito repellent attracts Culicoides imicola (Diptera: Ceratopogonidae)," *Journal of Medical Entomology*, vol. 36, no. 1, pp. 113–115, 1999.

[5] J. Fic and P. K. Pedersen, "Reservoir characterization of a "tight" oil reservoir, the middle jurassic upper shaunavon member in the whitemud and eastbrook pools, SW saskatchewan," *Marine and Petroleum Geology*, vol. 44, pp. 41–59, 2013.

[6] X. Zhou, Y. Wang, L. Zhang et al., "Evaluation of enhanced oil recovery potential using gas/water flooding in a tight oil reservoir," *Fuel*, vol. 272, Article ID 117706, 2020.

[7] Y. Zhang, Y. Di, W. Yu, and K. Sepehrnoori, "A comprehensive model for investigation of carbon dioxide enhanced oil recovery with nanopore confinement in the Bakken tight oil reservoir," *SPE Reservoir Evaluation and Engineering*, vol. 22, no. 01, pp. 122–136, 2019.

[8] B. Ren, S. Ren, L. Zhang, G. Chen, and H. Zhang, "Monitoring on CO2 migration in a tight oil reservoir during CCS-EOR in Jilin Oilfield China," *Energy*, vol. 98, pp. 108–121, 2016.

[9] G. J. Venter, K. Labuschagne, S. N. Boikanyo, L. Morey, and M. G. Snyman, "The repellent effect of organic fatty acids on Culicoides midges as determined with suction light traps in South Africa," *Veterinary Parasitology*, vol. 181, no. 2-4, pp. 365–369, 2011.

[10] X. Wang, X. Peng, S. Zhang, Z. Du, and F. Zeng, "Characteristics of oil distributions in forced and spontaneous imbibition of tight oil reservoir," *Fuel*, vol. 224, pp. 280–288, 2018.

[11] F. Wang, K. Yang, and J. Cai, "Fractal characterization of tight oil reservoir pore structure using nuclear magnetic resonance and mercury intrusion porosimetry," *Fractals*, vol. 26, no. 2, Article ID 1840017, 2018.

[12] C. N. Zou, R. K. Zhu, B. Bai et al., "Significance, geologic characteristics, resource potential and future challenges of tight oil and shale oil," *Bulletin of Mineralogy, Petrology and Geochemistry*, vol. 34, no. 1, pp. 3–17, 2015.

[13] H. Cheng, D. Yang, C. Lu, Q. Qin, and D. Cadasse, "Intelligent oil production stratified water injection technology," *Wireless Communications and Mobile Computing*, vol. 2022, Article ID 3954446, 7 pages, 2022.

[14] H. Wang, X. Liao, N. Lu, Z. Cai, C. Liao, and X. Dou, "A study on development effect of horizontal well with SRV in unconventional tight oil reservoir," *Journal of the Energy Institute*, vol. 87, no. 2, pp. 114–120, 2014.

[15] H. Cheng, P. Ma, G. Dong, S. Zhang, J. Wei, and Q. Qin, "Characteristics of carboniferous volcanic reservoirs in beisantai oilfield, Junggar Basin," *Mathematical Problems in Engineering*, vol. 2022, Article ID 7800630, 10 pages, 2022.

[16] Z. C. Songtao and Y. Z. Xuanjun, "Types, characteristics, genesis and prospects of conventional and unconventional hydrocarbon accumulations: taking tight oil and tight gas in China as an instance," *Acta Petrolei Sinica*, vol. 33, no. 2, p. 173, 2012.

[17] H. Cheng, J. Wei, and Z. Cheng, "Study on sedimentary facies and reservoir characteristics of Paleogene sandstone in Yingmaili block, Tarim basin," *Geofluids*, vol. 2022, Article ID 1445395, 14 pages, 2022.

[18] X. S. Zhang, H. J. Wang, F. Ma, X. C. Sun, Y. Zhang, and Z. H. Song, "Classification and characteristics of tight oil plays," *Petroleum Science*, vol. 13, no. 1, pp. 18–33, 2016.

[19] W. Zhang, Z. Cheng, H. Cheng, Q. Qin, and M. Wang, "Research of tight gas reservoir simulation technology," *IOP Conference Series: Earth and Environmental Science*, vol. 804, no. 2, Article ID 22046, 2021.

[20] L. Sun, C. Zou, A. Jia et al., "Development characteristics and orientation of tight oil and gas in China," *Petroleum Exploration and Development*, vol. 46, no. 6, pp. 1073–1087, 2019.

[21] B. Ren, L. Zhang, H. Huang, S. Ren, G. Chen, and H. Zhang, "Performance evaluation and mechanisms study of near-miscible CO2 flooding in a tight oil reservoir of Jilin Oilfield China," *Journal of Natural Gas Science and Engineering*, vol. 27, pp. 1796–1805, 2015.

[22] J. Du, H. Liu, D. Ma, J. Fu, Y. Wang, and T. Zhou, "Discussion on effective development techniques for continental tight oil in China," *Petroleum Exploration and Development*, vol. 41, no. 2, pp. 217–224, 2014.

[23] R. Aguilera, "Flow units: from conventional to tight-gas to shale-gas to tight-oil to shale-oil reservoirs," *SPE Reservoir Evaluation and Engineering*, vol. 17, no. 2, pp. 190–208, 2014.

[24] S. Li, C. Qiao, C. Zhang, and Z. Li, "Determination of diffusion coefficients of supercritical CO2 under tight oil reservoir conditions with pressure-decay method," *Journal of CO_2 Utilization*, vol. 24, pp. 430–443, 2018.

[25] J. Zhang, H. X. Zhang, L. Y. Ma, Y. Liu, and L. Zhang, "Performance evaluation and mechanism with different CO2 flooding modes in tight oil reservoir with fractures," *Journal of Petroleum Science and Engineering*, vol. 188, Article ID 106950, 2020.

[26] Z. Cao, G. Liu, B. Xiang et al., "Geochemical characteristics of crude oil from a tight oil reservoir in the Lucaogou Formation, Jimusar sag, Junggar Basin," *AAPG Bulletin*, vol. 101, no. 01, pp. 39–72, 2017.

[27] X. Zhao, X. Liu, Z. Yang et al., "Experimental study on physical modeling of flow mechanism in volumetric fracturing of tight oil reservoir," *Physics of Fluids*, vol. 33, no. 10, Article ID 107118, 2021.

Hindawi
Complexity
Volume 2023, Article ID 6751849, 10 pages
https://doi.org/10.1155/2023/6751849

Research Article

Protocol-Based Reliable Control for Power Systems with Communication Constraints

Yong Chen, Meng Li, Song Li, Yunhui Wang, Min Xie, and Yongkun Yang

Infrastructure Department of Yunnan Power Grid Company Limited, China Southern Power Grid, LTD., Kunming, Yunnan 650000, China

Correspondence should be addressed to Yong Chen; 1033687453@qq.com

Received 8 November 2022; Revised 20 December 2022; Accepted 5 April 2023; Published 22 April 2023

Academic Editor: Fuli Zhou

This study focuses on the protocol-based control for single-area power systems subject to actuator failures and deception attacks. Specifically, actuator failures, network attacks, unreliability, and bandwidth restrictions that emerge in power systems are taken into consideration at the same time. To cut down on the number of broadcast packets, a novel memory-adaptive event-triggered protocol is developed, where the trigger threshold parameter is adaptively changed in accordance with numerous historical sampled signals. Then, in virtue of the proposed algorithm, sufficient stabilization conditions are acquired to ensure the asymptotically stable of power systems with H_∞ performance. Finally, the efficiency of the proposed control strategy is demonstrated by using a simulation example.

1. Introduction

Due to its potent capacity to change the system frequency to a predetermined value in the presence of load fluctuations, load frequency control (LFC) has been utilized successfully in power systems for several decades [1–3]. Modern LFC in power systems transmits control signals and measured values across open communication networks (OCNs) as opposed to classic LFC, which transfers data over specialized communication channels. As the size of the power system grows, data transmission over a dedicated communication channel in traditional LFC will increase maintenance costs and reduce flexibility; hence, modern LFC with OCNs is becoming more popular [4]. However, as OCNs are prone to data loss, network attacks, and communication delay, data transfer through them might present considerable difficulties. Consequently, there has been a lot of interest in the study and development of LFC schemes for power systems with OCNs (see, for more details, [5–7]).

Actuators are crucial components of networked control systems, and it is a common phenomenon that a variety of malfunctions occur, which may affect the system performance [8]. In this regard, for the purpose of guaranteeing the desired performance, a seemingly natural ideal is to introduce reliable control schemes. As discussed in [9], benefiting from the reliable control schemes, actuator failures can be compensated and avoided. As a consequence, a lot of focus has been placed on the research of actuator failures in an effort to address these shortcomings and boost dependability, and several findings have been published [10, 11]. The finite-time tracking control problem for nonlinear systems with faults has been studied in [10]. Besides, the fault-tolerant control problem for multiagent systems subject to DoS attacks has been exploited in [11]. However, reliable control schemes have not gained sufficient interest in power systems probably due to dynamic complexities including unknown perturbations. To date, despite considerable accomplishments, power systems subject to reliable control schemes are still in their infancies, which remain the first motivation for this study.

It is essential to mention that communication networks are large-scale and decentralized and that the links between each part of a networked power system might make them vulnerable to cyberattacks [12]. According to [13], cyberattacks can have significant negative effects on system performance, such as information leaks, system failures, and

financial losses. Additionally, control methods might be used as a compensating strategy since cyber security approaches are insufficient to secure power systems [14]. Among some control methods, denial-of-service (DoS) attacks and deception attacks have generated a lot of research attention [11, 15–18]. Some common concepts or solutions have been carried out for DoS attacks. From the point of adversary, DoS attacks have been described by stochastic models, i.e., the Bernoulli method [19] and Markov method [20]. Additionally, from the standpoint of the attacker, deception attack can alter data to compromise its integrity, and the time-varying attack behavior cannot be detected [21]. As a result, the study of deception attacks becomes more challenging ([14, 18, 22]). Following this trend, a seemingly natural research topic is established for security control of networked power systems, which gives rise to deception attacks.

In light of the limited communication capacity, a range of networked phenomena emerged. In response to communication networks with constrained network resources, two transmission strategies are most adopted: the time-triggered protocol [23–25] and the event-triggered protocol [26, 27]. Note that conventional TTPs may result in wasted network resources; the event-triggered protocol has been developed in recent years to address these issues. Because trigger conditions are carried out after the event as opposed to before it, ETPs typically use fewer system resources than TTP. In general, the existing ETPs can be classified into static event-triggered protocols (SETPs) [15, 28], dynamic event-triggered protocols (DETPs) [29–31], and adaptive event-triggered protocols (AETPs) [32, 33]. For AETPs, threshold functions, based on the evolution of system states, are updated adaptively. Although there are several AETPs with dynamically changed threshold functions, there is still significant potential for development. For instance, in [32, 33], the threshold function is built using a quantitative relationship with the error between the latest transmitted data and the currently sampled data. Inspired by the work of the authors of [34], the aforementioned approach can be improved by containing the historically transmitted packets in the threshold function. Furthermore, memory-based AETPs have not gained proper research interest in power systems, which prompts us to the current study.

In light of the description above, this study examines the based-protocol LFC problem for single-area power systems (SAPSs) that are vulnerable to deception attacks and actuator failures. The following is a summary of our paper's main points: (1) A memory-adaptive event-triggered protocol (MAETP) is presented for operating SAPSs across communication networks with constrained bandwidth. Meanwhile, the MAETP accomplishes the goal of memory by dynamically altering the adaptive parameters using historical trigger data while preserving the intended control performance. (2) The proposed SAPS results account for a common framework together with the effects of deception attacks, actuator faults, and memory-based event-triggered protocols. (3) For the established power system model, according to the Lyapunov stability method, the asymptotic stability (AS) with preset performance is ensured.

2. Problem Formulations

2.1. System Model. Throughout the study, the dynamic model of a single-area power system is described as follows [35]:

$$\left\{\dot{\tilde{x}}(t) = \tilde{A}\tilde{x}(t) + \tilde{B}u^F(t) + \tilde{H}v(t), \tilde{y}(t) = \tilde{C}\tilde{x}(t),\right. \tag{1}$$

where

$$\begin{aligned}
\tilde{x}(t) &= \left[\Delta f \;\; \Delta P_v \;\; \Delta P_m\right]^\top,\\
\tilde{y}(t) &= ACE,\\
v(t) &= \Delta P_d,\\
\tilde{A} &= \begin{bmatrix} -\dfrac{D}{M} & 0 & \dfrac{1}{M} \\ -\dfrac{1}{RT_g} & -\dfrac{1}{T_g} & 0 \\ 0 & \dfrac{1}{T_t} & -\dfrac{1}{T_t} \end{bmatrix},\\
\tilde{B} &= \begin{bmatrix} 0 \\ \dfrac{1}{T_g} \\ 0 \end{bmatrix},\\
\tilde{H} &= \begin{bmatrix} -\dfrac{1}{M} \\ 0 \\ 0 \end{bmatrix},\\
\tilde{C} &= \left[\beta \;\; 0 \;\; 0\right].
\end{aligned} \tag{2}$$

Table 1 provides a list of parameters' physical meanings.

Note that, for a single-area power system without power exchange, the ACE signal is written as $ACE = \beta\Delta f$, where β is frequency bias. In actual fact, actuator failures cannot be ignored, so the failure model between the controller and the actuator is represented as follows:

$$u^F(t) = \rho u(t), \tag{3}$$

where $\rho = \mathrm{diag}\{\rho_1, \rho_2, \cdots, \rho_{n_u}\}$ and $0 \le \underline{\varrho}_m \le \varrho_m \le \overline{\varrho}_m \le 1$ $(m = 1, 2, \cdots, n_u)$, in which ρ_m is unknown, and we assume

Table 1: The physical meaning of parameters.

Parameters	Physical meaning
Δf	The deviation of frequency
ΔP_m	The deviation of governor mechanical output increment
ΔP_v	The valve position deviation
ΔP_d	Load disturbance
ACE	Area control error
D	Governor damping coefficient
M	Rotational inertia
T_t	Turbine time constant
T_g	Governor time constant
R	Droop property

that ϱ and $\overline{\varrho}_m$ are known. We define $\varrho = \min\left\{\varrho_m^m, m = 1, 2, \cdots, n_u\right\}$ and $\overline{\varrho} = \max\{\overline{\varrho}_m, m = 1, 2, \cdots, n_u\}$.

As a consequence, a PI controller is inferred as

$$u(t) = -K_P ACE - K_I \int ACE. \tag{4}$$

Furthermore, we define state vectors as $x(t) = \left[\Delta f \ \ \Delta P_v \ \ \Delta P_m \ \ \int ACE\right]^\top$ and measured output as $y(t) = [ACE \int ACE]$; the dynamic model of the single-area power system is redescribed as

$$\begin{cases} \dot{x}(t) = Ax(t) + B\rho u(t) + Hv(t), \\ y(t) = Cx(t), \end{cases} \tag{5}$$

where

$$A = \begin{bmatrix} -\frac{D}{M} & 0 & \frac{1}{M} & 0 \\ -\frac{1}{RT_g} & -\frac{1}{T_g} & 0 & 0 \\ 0 & \frac{1}{T_t} & -\frac{1}{T_t} & 0 \\ \beta & 0 & 0 & 0 \end{bmatrix},$$

$$B = \begin{bmatrix} 0 \\ \frac{1}{T_g} \\ 0 \\ 0 \end{bmatrix}, \tag{6}$$

$$H = \begin{bmatrix} -\frac{1}{M} \\ 0 \\ 0 \\ 0 \end{bmatrix},$$

$$C = \begin{bmatrix} \beta & 0 & 0 & 0 \\ 0 & 0 & 0 & 1 \end{bmatrix}.$$

2.2. Memory-Adaptive Event-Triggered Protocol. By using some historical data, a sampling-based MAETP is proposed in [34]:

$$t_{k+1}h = t_k h + \inf_{l\in\mathbb{N}^+}\left\{lh \,\middle|\, e^{\top}(t)\Omega e(t) - \sigma(t)y^{\top}(t_k h)\Omega y(t_k h) \geq 0\right\}, \tag{7}$$

and $e(t) = y(t_k h + lh) - y(t_k h)$. h, kh, and $t_k h$ describe the sampling interval, instant, and latest broadcast instant, respectively. The matrix $\Omega > 0$. Meanwhile, $\{t_k h, k \in \mathbb{N}^+\} \subseteq \{kh, k \in \mathbb{N}^+\}$. In the sequel, the adaptive parameter $\sigma(t)$ yields

$$\sigma(t) = \sigma + \left(\overline{\sigma} - \sigma\right)e^{-\epsilon\left\| y(t_k h + lh) - \frac{1}{\mathcal{S}}\sum_{s=1}^{\mathcal{S}} y(t_{k-s}h)\right\|^2}, \tag{8}$$

where σ and $\overline{\sigma}$ indicate two bounds of the adaptive threshold parameters, $\epsilon > 0$, and $\mathcal{S}$ is the number of recent released packets.

Remark 1. Note that the adaptive threshold function of MAETP (7) taken into consideration in this study, which substitutes the latest trigger sample with the arithmetic mean of $\mathcal{S}$ historically trigger data, can lessen the sensitivity of $\sigma(t)$ to the most latest transmitted data $y(t_k h)$. As in [18], the proposed controller gain number is $\mathcal{S}$, which increases the computing cost if the amount of historical data is too large. To avoid this situation, the MAETM proposed in this research adds the memory feature to the adaptive rule.

Remark 2. In addition to providing flexibility in modifying the trigger threshold, the MAETP (7) also improves control performance. Nevertheless, the MAETP (5) provided in this research is more inclusive and covers the majority of the current protocols. When $\mathcal{S} = 1$, MAETPs (7) reduce to AETPs [32]. When $\mathcal{S} = 1$ and $\sigma(t)$ is a constant, the MAETP (7) degenerates to SETPs [15]. Following this fact, the designed DMETP is more appropriate than the current SETP/AETP to describe the actual scenario.

Considering the delay in transmitting data, we define the transmission interval as $\bigcup_{l=0}^{n}\mathcal{I}_l = [t_k h + d_k, t_{k+1}h + d_{k+1}]$, and one gets $\mathcal{I}_l = [t_k h + lh + d_{k+l}, t_{k+1}h + lh + h + d_{k+l+1}]$ and $(l = 0, 1, \cdots, n, n = t_{k+1} - t_k - 1)$. We set $d(t) = t - t_k h - lh$, which yields

$$0 \leq d(t) \leq h + \overline{d} \triangleq d_M, \tag{9}$$

where $\overline{d}$ is the upper bound of $\{d_k\}$.

Summarizing the aforementioned analysis, we let $K = \begin{bmatrix} -K_P & -K_I \end{bmatrix}$. Under the MAETP, the PI controller is rewritten as

$$u(t) = Ky(t_k h). \tag{10}$$

As a follow-up, the measurement output is assumed to be attacked by random deception attacks. In this regard, the load frequency controller is remodelled as

$$u(t) = (1 - \alpha(t))Ky(t_k h) + \alpha(t)Kf(t_k h), \tag{11}$$

where the nonlinear function $f(t_k h)$ indicates the deception signal. $\alpha(t) \in \{0, 1\}$ is a Bernoulli random variable, from which one has

$$\begin{aligned} \Pr\{\alpha(t) = 1\} &= \mathbb{E}\{\alpha(t)\} \\ &= \overline{\alpha}, \\ \Pr\{\alpha(t) = 0\} &= 1 - \overline{\alpha}. \end{aligned} \tag{12}$$

Assumption 1 (see [15]). It is assumed that the nonlinear function can be characterized by the following condition:

$$\|f(y(t))\| \leq \|F(y(t))\|, \tag{13}$$

where F is a known matrix.

Substituting (11) into (5), the closed-loop power system can be established as

$$\begin{cases} \dot{x}(t) = Ax(t) + \rho(1 - \alpha(t))BK(Cx(t - d(t)) - e(t)) + \rho\alpha(t)BKf(y(t_k h)) + Hv(t), \\ y(t) = Cx(t). \end{cases} \tag{14}$$

In order to solve static output-feedback control questions, we let $\mathscr{B} = \begin{bmatrix} B & \overline{B} \end{bmatrix}$, in which $\overline{B}$ has $4 - p$ [36]. Then, we introduce a new variable $\chi(t) = (\widehat{B})^{-1}x(t)$; system (15) is reformulated as

$$\begin{cases} \dot{\chi}(t) = \mathscr{A}\chi(t) + \rho(1 - \alpha(t))\mathscr{K}(\mathscr{C}\chi(t - d(t)) - e(t)) + \rho\alpha(t)\mathscr{K}f(y(t_k h)) + \mathscr{H}v(t), \\ y(t) = \mathscr{C}\chi(t), \end{cases} \tag{15}$$

where $\mathscr{A} = (\mathscr{B})^{-1}A\mathscr{B}$, $\mathscr{K} = [K^{\top}0]^{\top}$, $\mathscr{C} = C\mathscr{B}$, and $\mathscr{H} = \mathscr{B}^{-1}H$.

The goal of this paper is to construct the controller (11) in such a way that it satisfies asymptotically stable subjects to preset performance for the closed-loop power system (16) under MAETPs (7). In particular, the following requirements are met:

1) The closed-loop power system (16) with $v(t) = 0$ is AS.

2) Under zero initial conditions, it holds that $\mathscr{E}\{\int_0^\infty \|y(t)\|^2 \mathrm{dt}\} < \gamma^2 \mathscr{E}\{\int_0^\infty \|v(t)\|^2 \mathrm{dt}\}$ for all $v(t) \neq 0$ and prescribed $\gamma > 0$.

Lemma 1 (see [37]). *For any matrices $\mathscr{R} \in \mathbb{R}^{n\times n}$ and $\mathscr{U} \in \mathbb{R}^{n\times n}$, we satisfy $\begin{bmatrix} \mathscr{R} & * \\ \mathscr{U} & \mathscr{R} \end{bmatrix} > 0$, $d(t) \in [0, d_M]$, with $d_M \geq 0$, and the vector function $\dot{x}$: $[0, d_M] \longrightarrow \mathbb{R}^n$; the following condition holds*

$$-d_M \int_{t-d_M}^{t} \dot{x}^\top(s)\mathscr{R}\dot{x}(s)\mathrm{ds} \leq -\zeta^\top(t)\Lambda\zeta(t), \tag{16}$$

where $\zeta(t) = col[x(t), x(t-d(t)), x(t-d_M)]$ *and* $\Lambda = \begin{bmatrix} \mathscr{R} & * & * \\ \mathscr{U}-\mathscr{R} & 2\mathscr{R} - \mathbf{He}\{\mathscr{U}\} & * \\ -\mathscr{U} & \mathscr{U}-\mathscr{R} & \mathscr{R} \end{bmatrix}$.

3. Main Results

Theorem 1. *For given scalars $d_M \geq 0$, $\bar{\sigma} \in (0,1)$, $\iota > 0$, $\epsilon > 0$, $\bar{\rho}$, and $\rho \in [0,1]$, the closed-loop power system (16) is AS in the sense of the H_∞ performance index γ if there exist matrices $P > 0$, $Q > 0$, $R > 0$, and $\Omega > 0$ and matrices U and $\mathscr{M}$ such that*

$$\begin{bmatrix} R & U^\top \\ U & R \end{bmatrix} > 0, \tag{17}$$

$$\begin{bmatrix} \Xi^1 & \Xi^2 & \Xi^3 & \Xi^4 \\ * & -\gamma^2 I & 0 & 0 \\ * & * & -\bar{\alpha} I & 0 \\ * & * & * & -I \end{bmatrix} < 0, \tag{18}$$

where

$$\begin{aligned}
\Xi^1 &= \begin{bmatrix} \Xi^{1,1} & \Xi^{1,2} \\ * & \Xi^{2,2} \end{bmatrix}, \\
\Xi^2 &= \begin{bmatrix} \mathscr{H}^\top\mathscr{M}^\top & 0 & 0 & \iota\mathscr{H}^\top\mathscr{M}^\top & 0 & 0 \end{bmatrix}^\top, \\
\Xi^3 &= \begin{bmatrix} 0 & \bar{\alpha}\mathscr{F}\mathscr{C} & 0 & 0 & \bar{\alpha}\mathscr{F}\mathscr{C} & 0 \end{bmatrix}^\top, \\
\Xi^4 &= \begin{bmatrix} \mathscr{C} & 0 & 0 & 0 & 0 & 0 \end{bmatrix}^\top, \\
\Xi^{1,1} &= \begin{bmatrix} \Upsilon^{11} & \Upsilon^{12} & U^\top \\ * & -2R + U^\top + U + \bar{\sigma}\mathscr{C}^\top\Omega\mathscr{C} & R - U^\top \\ * & * & -R - Q \end{bmatrix}, \\
\Xi^{1,2} &= \begin{bmatrix} \Upsilon^{14} - \rho(1-\bar{\alpha})\mathscr{M}\mathscr{K} & \bar{\rho}\bar{\alpha}\mathscr{M}\mathscr{K} \\ \iota\bar{\rho}(1-\bar{\alpha})(\mathscr{M}\mathscr{K}\mathscr{C})^\top & -\bar{\sigma}\mathscr{C}^\top\Omega \quad 0 \\ 0 & 0 \quad 0 \end{bmatrix}, \\
\Xi^{2,2} &= \begin{bmatrix} d_M^2 R - \mathbf{He}\{\iota\mathscr{M}\} - \iota\rho(1-\bar{\alpha})\mathscr{M}\mathscr{K} & \iota\bar{\rho}\bar{\alpha}\mathscr{M}\mathscr{K} \\ * & (\bar{\sigma}-1)\Omega \quad 0 \\ * & * \quad -\bar{\alpha} I \end{bmatrix}, \\
\Upsilon^{11} &= \mathbf{He}\{\mathscr{M}\mathscr{A}\} + Q - R, \\
\Upsilon^{12} &= \bar{\rho}(1-\bar{\alpha})\mathscr{M}\mathscr{K}C - U^\top + R, \\
\Upsilon^{14} &= P - \mathscr{M}^\top + \iota\mathscr{A}^\top\mathscr{M}^\top.
\end{aligned} \tag{19}$$

Proof. Considering the following Lyapunov function,

$$V(t) = \sum_{l=1}^{3} V_l(t), \tag{20}$$

where

$$\begin{aligned}
V_1(t) &= \chi^\top(t)P\chi(t), \\
V_2(t) &= \int_{t-d_M}^{t} \chi^\top(s)Q\chi(s)ds, \\
&= d_M \int_{-d_M}^{0}\int_{t+s}^{t} \dot{\chi}^\top(v)R\dot{\chi}(v)dv\,ds.
\end{aligned} \tag{21}$$

Taking the derivative of $V(t)$, one has

$$\begin{aligned}
\mathscr{L}V_1(t) &= 2\dot{\chi}^\top(t)P\chi(t), \\
\mathscr{L}V_2(t) &= \chi^\top(t)Q\chi(t) - \chi^\top(t-d_M)Q\chi(t-d_M), \\
\mathscr{L}V_3(t) &= d_M^2\dot{\chi}^\top(t)R\dot{\chi}(t) - d_M\int_{t-d_M}^{t}\dot{\chi}^\top(s)R\dot{\chi}(s)\mathrm{ds}.
\end{aligned} \tag{22}$$

Based on Lemma 1, it follows

$$-d_M\int_{t-d_M}^{t}\dot{\chi}^\top(s)R\dot{\chi}(s)\mathrm{ds} \leq -\zeta^\top(t)\mathscr{R}\zeta(t), \tag{23}$$

where

$$\mathscr{R} = \begin{bmatrix} R & * & * \\ U-R & 2R-\mathbf{He}\{U\} & * \\ -U & U-R & R \end{bmatrix}, \quad \zeta(t) = \begin{bmatrix} \chi(t) \\ \chi(t-d(t)) \\ \chi(t-d_M) \end{bmatrix}. \tag{24}$$

Reviewing the established MAETP in (7), it holds that

$$\begin{aligned} 0 &< \sigma(t) y^{\top}(t_k h)\Omega y(t_k h) - e^{\top}(t)\Omega e(t), \\ &< \overline{\sigma} y^{\top}(t_k h)\Omega y(t_k h) - e^{\top}(t)\Omega e(t). \end{aligned} \tag{25}$$

Recalling (15), for any proper matrix Z, it holds that

$$0 = 2\left[\chi^{\top}(t)\mathscr{M} + \iota\dot{\chi}^{\top}(t)\mathscr{M}\right] \times \left[-\dot{x}(t) + \mathscr{A}\chi(t) + (1-\alpha(t))\mathscr{K}(\mathscr{C}\chi(t-d(t)) - e(t)) + \alpha(t)\mathscr{K} f(y(t_k h)) + \mathscr{H} v(t)\right]. \tag{26}$$

Then, based on Assumption 1, one has

$$\overline{\alpha}\left[f^{\top}(y(t_k h)) f(y(t_k h)) - y^{\top}(t_k h)\mathscr{F}^{\top}\mathscr{F} y(t_k h)\right] \le 0. \tag{27}$$

Taking (20)–(27) into account, we have that

$$\mathscr{L}V(t) \le \zeta^{\top}(t)\widetilde{\Xi}\zeta(t) - y^{\top}(t)y(t) + \gamma^2\omega^{\top}(t)v(t), \tag{28}$$

where $\zeta^{\top}(t) = [\chi^{\top}(t)\chi^{\top}(t-d(t))\chi^{\top}\ (t-d_M)\dot{\chi}^{\top}(t)e^{\top}(t)f^{\top}(y(t_k h))\omega^{\top}(t)]$, $\widetilde{\Xi} = \begin{bmatrix} \Xi^1 + (1/\alpha)\Xi^3\Xi^{3,\top} + \Xi^4\Xi^{4,\top} & \Xi^2 \\ * & -\gamma^2 I \end{bmatrix}$.

Applying the Schur complement to (19), one has

$$\mathscr{L}V(t) + \|y(t)\|^2 - \gamma^2\|v(t)\|^2 \le 0. \tag{29}$$

Integrating (29) from $t = 0$ to ∞ yields

$$V(\infty) - V(0) + \mathscr{E}\left\{\int_0^{\infty}\left(\|y(t)\|^2 - \gamma^2\|v(t)\|^2\right)\mathrm{d}t\right\} \le 0. \tag{30}$$

Under zero initial conditions, the following inequality holds:

$$\mathscr{E}\left\{\int_0^{\infty}\left(\|y(t)\|^2 - \gamma^2\|v(t)\|^2\right)\mathrm{d}t\right\} \le 0. \tag{31}$$

Furthermore, we get $\mathscr{E}\{\int_0^{\infty}\|y(t)\|^2\mathrm{d}t\} \le \gamma^2\mathscr{E}\{\int_0^{\infty}\|v(t)\|^2\mathrm{d}t\}$. When $\omega(t) = 0$, we can deduce the closed loop power system (16) AS by applying condition (19). This ends the proof.

Next, Theorem 2 presents essential conditions for designing the controller gain based on the conclusion of Theorem 1. □

Theorem 2. *For given scalars $d_M \ge 0$, $\overline{\sigma} \in (0,1)$, $\iota > 0$, $\epsilon > 0$, $\overline{\rho}$, and $\rho \in [0,1]$, the closed-loop power system (16) is AS in the sense of the H_∞ performance index γ if there exist matrices $P > 0$, $Q > 0$, $R > 0$, and $\Omega > 0$ and matrices U and Z with compatible dimensions such that (18) holds and*

$$\begin{bmatrix} \overline{\Xi}^1 & \Xi^2 & \Xi^3 & \Xi^4 \\ * & -\gamma^2 I & 0 & 0 \\ * & * & -\alpha I & 0 \\ * & * & * & -I \end{bmatrix} < 0, \tag{32}$$

where

$$\begin{aligned} \overline{\Xi}^1 &= \begin{bmatrix} \overline{\Xi}^{1,1} & \overline{\Xi}^{1,2} \\ * & \overline{\Xi}^{2,2} \end{bmatrix}, \\ \Xi^{1,1} &= \begin{bmatrix} \Upsilon^{11} & \overline{\Upsilon}^{12} & U^{\top} \\ * & -2R + U^{\top} + U + \overline{\sigma}\mathscr{C}^{\top}\Omega\mathscr{C} & U^{\top} - R \\ * & * & -R - Q \end{bmatrix}, \\ \overline{\Xi}^{1,2} &= \begin{bmatrix} \Upsilon^{14} - \rho(1-\overline{\alpha})\mathscr{Y}\mathscr{K} & \overline{\rho\alpha}\mathscr{Y}\mathscr{K} \\ \iota\overline{\rho}(1-\overline{\alpha})(\mathscr{Y}\mathscr{K}\mathscr{C})^{\top} & -\overline{\sigma}\mathscr{C}^{\top}\Omega\ 0 \\ 0 & 0\ \ 0 \end{bmatrix}, \\ \overline{\Xi}^{2,2} &= \begin{bmatrix} d_M^2 R - \mathbf{He}\{\iota\mathscr{M}\vdash \iota\rho(1-\overline{\alpha})\mathscr{Y}\mathscr{K} & \iota\overline{\rho\alpha}\mathscr{Y}\mathscr{K} \\ * & (\overline{\sigma}-1)\Omega\ \ 0 \\ * & *\ \ -\overline{\alpha}I \end{bmatrix}, \\ \Upsilon^{12} &= \overline{\rho}(1-\overline{\alpha})\mathscr{Y}\mathscr{K}\mathscr{C} - U^{\top} + R, \\ \mathscr{Y} &= \mathrm{diag}\{I_p, 0\}. \end{aligned} \tag{33}$$

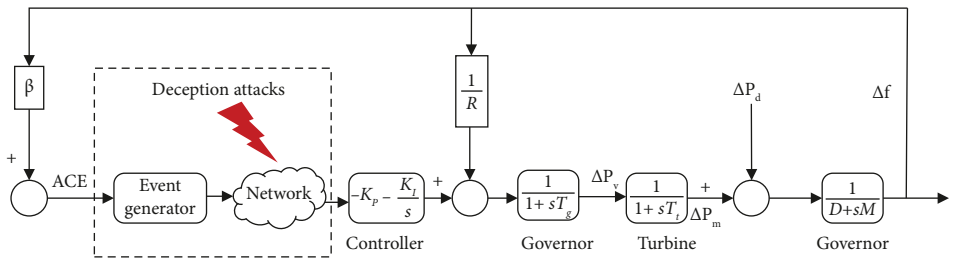

Figure 1: Dynamic mode of the single-area power system under deception attacks.

Table 2: Parameters of the power system.

M	D	T_t	T_g	β	R
10	1	0.3	0.1	21	0.05

Furthermore, the gains can be computed as

$$\mathcal{K} = \mathcal{M}^{-1}\mathcal{Y}\mathcal{K}. \tag{34}$$

Proof. Let $\mathcal{Y}\mathcal{K} = \mathcal{M}\mathcal{K}$, and it is clear that

$$\begin{aligned}\mathcal{K} &= \mathcal{M}^{-1}\mathcal{Y}\mathcal{K} \\ &= \begin{bmatrix} \mathcal{M}_1^{-1} & 0 \\ 0 & \mathcal{M}_2^{-1} \end{bmatrix} \begin{bmatrix} I_p & 0 \\ 0 & 0 \end{bmatrix} \mathcal{K},\end{aligned} \tag{35}$$

where $\mathcal{M}$ is a diagonal matrix. On account of the Schur complement, (32) is ensured in virtue of (16). □

4. Numerical Examples

This section exhibits a simulation example in order to evaluate the effectiveness of the given methodology, Figure 1 describes dynamic modes of the single-area power system. Note that the parameters are explained in Table 2 [35], and the matrix $\overline{B}$ is presupposed to be $\overline{B} = [0\ 0\ 1; 1\ 0\ 0; 0\ 1\ 0; 0\ 1\ 0]$.

We set the deception attack as $f(y(t)) = -\tanh(Fy(t))$, which $\mathcal{F} = \mathrm{diag}\{0.1, 0.1\}$. The actuator failure is supposed to be $\rho \in [0.8, 0.9]$ with $\rho = 0.8$ and $\overline{\rho} = 0.9$. Other parameters are chosen as $\mathcal{S} = 3$, $\overline{\alpha} = 0.2$, $\overline{\sigma} = 0.1$, $\sigma = 0.015$, $\epsilon = 2$, $\iota = 0.1$, $d_M = 0.05$, and the sampling period $h = 0.02$.

In light of Theorem 2, the controller gain and the event-triggered matrix can be calculated:

$$\begin{aligned} K &= [1.8220\ \ -1.0658], \\ \Omega &= \begin{bmatrix} 13.9953 & -0.9412 \\ -0.9412 & 8.7407 \end{bmatrix}. \end{aligned} \tag{36}$$

Specifically, we select the load disturbance as

$$\omega(t) = \begin{cases} 0.05\sin(t), \text{if } t \in [0, 8], \\ 0, \text{if } t \in [8, \infty], \end{cases} \tag{37}$$

and the initial value is set as $\chi_0 = [-0.9\ -0.1\ -0.01\ -0.01]^\top$.

The numerical simulations of the system (16) are presented in Figures 2–6 using the aforementioned parameters

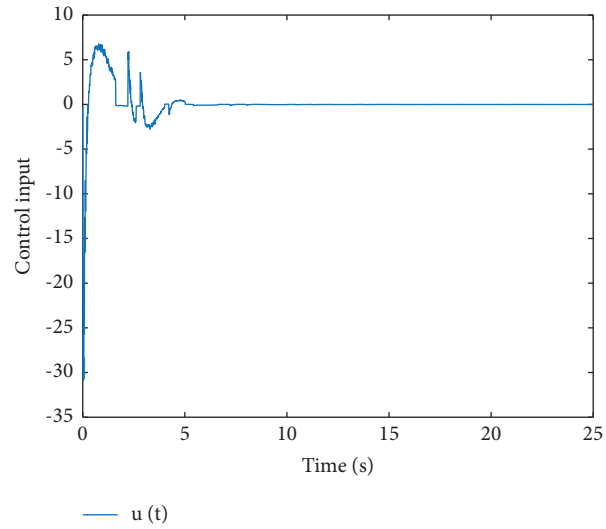

Figure 2: The control input $u(t)$.

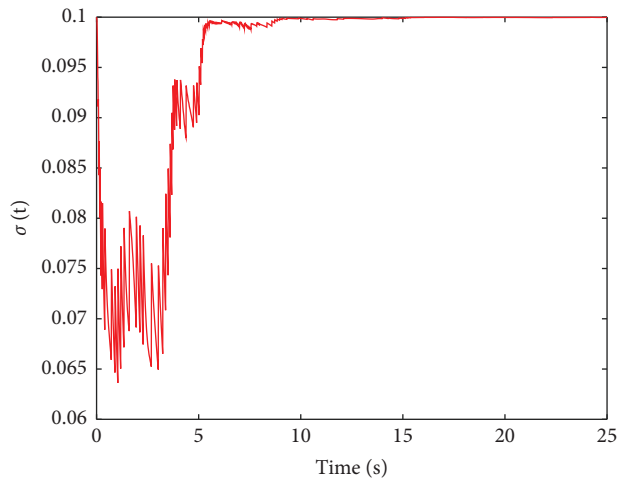

Figure 3: The evolution of the adaptive parameter $\sigma(t)$.

and assumptions. Figures 2 and 3 depict the control input $u(t)$ and the trend of the adaptive parameter (t). Figure 4 illustrates the deception attacks signals $\alpha(t)$ with the expectation $\overline{\alpha} = 0.2$. Additionally, to demonstrate the superiority of the proposed MAETP, we compared it with the METP of literature [18], as shown in Figures 5–7, where Figures 5 and 8 depict the power system state trajectory curves under different ETPs, respectively, and Figures 6 and

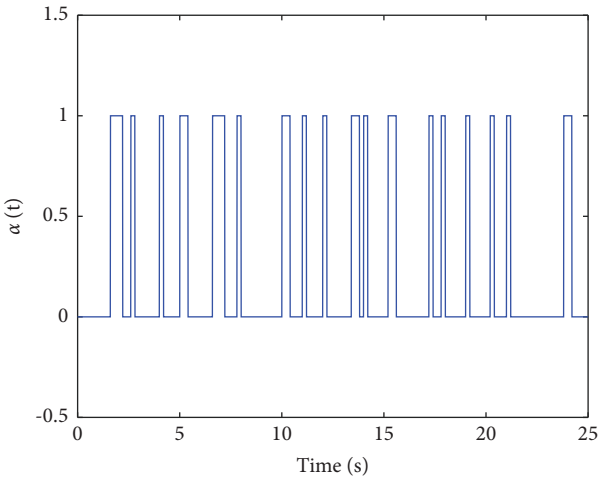

Figure 4: $\alpha(t)$ of deception attacks with $\overline{\alpha} = 0.2$.

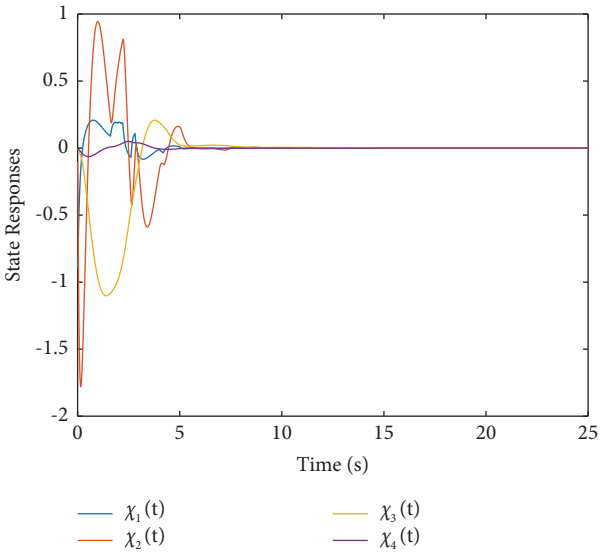

Figure 5: The state trajectories $\chi(t)$ for MAETP.

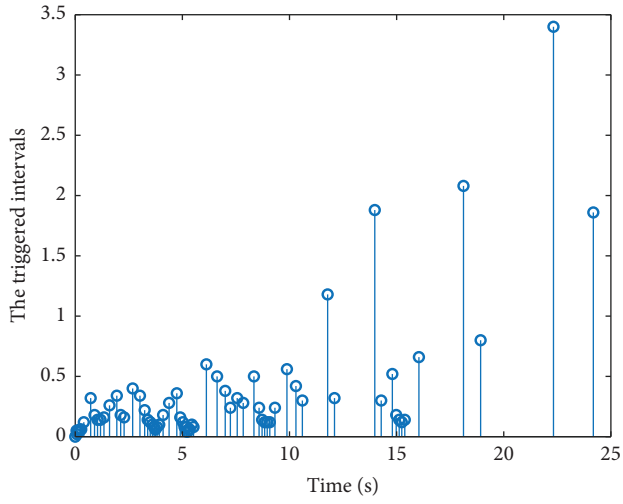

Figure 6: The triggering instants for MAETP.

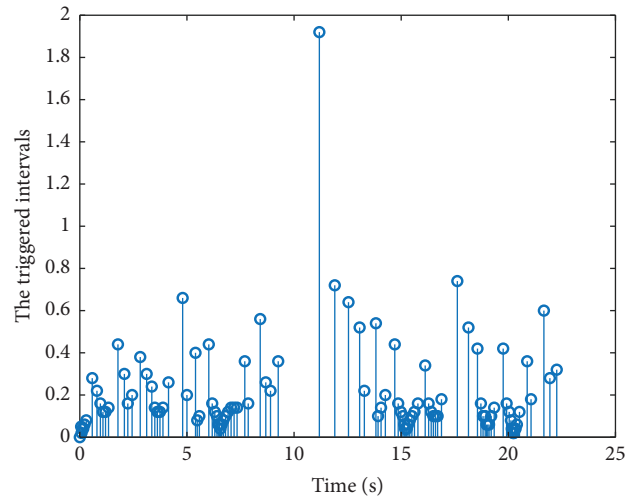

Figure 7: The triggering instants for METP.

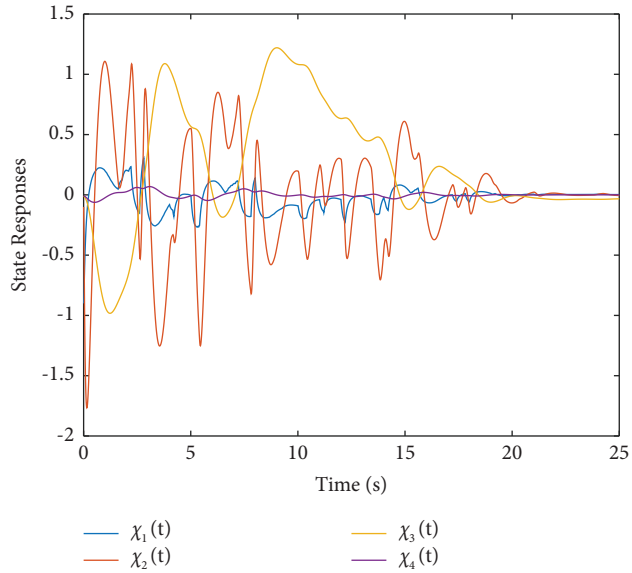

Figure 8: The state trajectories $\chi(t)$ for METP.

7 correspond to their triggering instants. In Figures 5 and 8, it can be seen that the system curve takes less time to reach stability with the proposed MAETP. Furthermore, 108 packets have been transmitted under METS, while 68 packets have been transmitted under MAETS. Therefore, by comparison, it can be found that the proposed MAETP not only achieves good control performance but also saves transmission resources to a certain extent.

5. Conclusions

In this paper, a protocol-based LFC issue for SAPSs has been discussed. In light of the network's actual state, the networked power system is expanded to include actuator failures and deception attacks. Furthermore, by adaptively modifying the trigger thresholds based on historical sample data, MAETPs are developed to conserve network resources. By using Lyapunov function theory, sufficient criteria have

been forwarded to guarantee the AS of SAPSs. In the end, an example has been applied to demonstrate the viability of the presented control scheme.

Data Availability

The data used to support the findings of this study are available from the corresponding author upon request.

Conflicts of Interest

The authors declare that they have no conflicts of interest.

References

[1] K. Lim, Y. Wang, and R. Zhou, "Robust decentralised load–frequency control of multi-area power systems," *IEE Proceedings - Generation, Transmission and Distribution*, vol. 143, no. 5, pp. 377–386, 1996.

[2] H. A. Yousef, K. Al-Kharusi, M. H. Albadi, and N. Hosseinzadeh, "Load frequency control of a multi-area power system: an adaptive fuzzy logic approach," *IEEE Transactions on Power Systems*, vol. 29, no. 4, pp. 1822–1830, 2014.

[3] L. Xie, J. Cheng, Y. Zou, Z.-G. Wu, and H. Yan, "A dynamic-memory event-triggered protocol to multiarea power systems with semi-markov jumping parameter," *IEEE Transactions on Cybernetics*, pp. 1–11, 2022.

[4] C. Peng, J. Zhang, and H. Yan, "Adaptive event-triggering $$\{H\}$ \_ $\{$$\backslash$infty$\}$ $ load frequency control for network-based power systems," *IEEE Transactions on Industrial Electronics*, vol. 65, no. 2, pp. 1685–1694, 2018.

[5] C.-K. Zhang, L. Jiang, Q. H. Wu, Y. He, and M. Wu, "Delay-dependent robust load frequency control for time delay power systems," *IEEE Transactions on Power Systems*, vol. 28, no. 3, pp. 2192–2201, 2013.

[6] S. Wen, X. Yu, Z. Zeng, and J. Wang, "Event-triggering load frequency control for multiarea power systems with communication delays," *IEEE Transactions on Industrial Electronics*, vol. 63, no. 2, pp. 1308–1317, 2016.

[7] Y. Zhang and T. Yang, "Decentralized switching control strategy for load frequency control in multi-area power systems with time delay and packet losses," *IEEE Access*, vol. 8, Article ID 15838, 15850 pages, 2020.

[8] Q. Zhao and J. Jiang, "Reliable state feedback control system design against actuator failures," *Automatica*, vol. 34, no. 10, pp. 1267–1272, 1998.

[9] W. Zhou, Y. Wang, C. K. Ahn, J. Cheng, and C. Chen, "Adaptive fuzzy backstepping-based formation control of unmanned surface vehicles with unknown model nonlinearity and actuator saturation," *IEEE Transactions on Vehicular Technology*, vol. 69, no. 12, Article ID 14749, 14764 pages, 2020.

[10] H. Wang, P. X. Liu, X. Zhao, and X. Liu, "Adaptive fuzzy finite-time control of nonlinear systems with actuator faults," *IEEE Transactions on Cybernetics*, vol. 50, no. 5, pp. 1786–1797, 2020.

[11] C. Deng and C. Wen, "Distributed resilient observer-based fault-tolerant control for heterogeneous multiagent systems under actuator faults and dos attacks," *IEEE Transactions on Control of Network Systems*, vol. 50, no. 5, pp. 1786–1797, 2019.

[12] A. Humayed, J. Lin, F. Li, and B. Luo, "Cyber-physical systems security-a survey," *IEEE Internet of Things Journal*, vol. 4, no. 6, pp. 1802–1831, 2017.

[13] Z. Guo, D. Shi, K. H. Johansson, and L. Shi, "Optimal linear cyber-attack on remote state estimation," *IEEE Transactions on Control of Network Systems*, vol. 4, no. 1, pp. 4–13, 2017.

[14] F. Yang, Z. Gu, and S. Yan, "Switched event-based control for nonlinear cyber-physical systems under deception attacks," *Nonlinear Dynamics*, vol. 106, no. 3, pp. 2245–2257, 2021.

[15] J. Liu, Y. Gu, L. Zha, Y. Liu, and J. Cao, "Event-Triggered $H_ \infty$ Load Frequency Control for Multiarea Power Systems under Hybrid Cyber Attackshoload frequency control for multiarea power systems under hybrid cyber attacks," *IEEE Transactions on Systems, Man, and Cybernetics: Systems*, vol. 49, no. 8, pp. 1665–1678, 2019.

[16] Y. Zhu and W. X. Zheng, "Observer-based control for cyber-physical systems with periodic dos attacks via a cyclic switching strategy," *IEEE Transactions on Automatic Control*, vol. 65, no. 8, pp. 3714–3721, 2020.

[17] Q. Sun, K. Zhang, and Y. Shi, "Resilient model predictive control of cyber-physical systems under dos attacks," *IEEE Transactions on Industrial Informatics*, vol. 16, no. 7, pp. 4920–4927, 2020.

[18] E. Tian and C. Peng, "Memory-based event-triggering H ∞ load frequency control for power systems under deception attacksHoload frequency control for power systems under deception attacks," *IEEE Transactions on Cybernetics*, vol. 50, no. 11, pp. 4610–4618, 2020.

[19] L. Guo, H. Yu, and F. Hao, "Event-triggered control for stochastic networked control systems against denial-of-service attacks," *Information Sciences*, vol. 527, pp. 51–69, 2020.

[20] H. Sun, C. Peng, T. Yang, H. Zhang, and W. He, "Resilient control of networked control systems with stochastic denial of service attacks," *Neurocomputing*, vol. 270, pp. 170–177, 2017.

[21] F. Qu, E. Tian, and X. Zhao, "Chance-constrained state estimation for recursive neural networks under deception attacks and energy constraints: the finite-horizon casehstate estimation for recursive neural networks under deception attacks and energy constraints: the finite-horizon case," *IEEE Transactions on Neural Networks and Learning Systems*, pp. 1–12, 2022.

[22] Y. Cui, Y. Liu, W. Zhang, and F. E. Alsaadi, "Sampled-based consensus for nonlinear multiagent systems with deception attacks: the decoupled method," *IEEE Transactions on Systems, Man, and Cybernetics: Systems*, vol. 51, no. 1, pp. 561–573, 2021.

[23] J. Cheng, J. H. Park, X. Zhao, J. Cao, and W. Qi, "Static output feedback control of switched systems with quantization: a nonhomogeneous sojourn probability approach," *International Journal of Robust and Nonlinear Control*, vol. 29, no. 17, pp. 5992–6005, 2019.

[24] J. Cheng, W. Huang, H.-K. Lam, J. Cao, and Y. Zhang, "Fuzzy-model-based control for singularly perturbed systems with nonhomogeneous Markov switching: a dropout compensation strategy," *IEEE Transactions on Fuzzy Systems*, vol. 30, no. 2, pp. 530–541, 2022.

[25] J. Cheng, Y. Shan, J. Cao, and J. H. Park, "Nonstationary control for t–s fuzzy Markovian switching systems with variable quantization density," *IEEE Transactions on Fuzzy Systems*, vol. 29, no. 6, pp. 1375–1385, 2021.

[26] C. Peng and T. C. Yang, "Event-triggered communication and hocontrol co-design for networked control systems," *Automatica*, vol. 49, no. 5, pp. 1326–1332, 2013.

[27] J. Cheng, L. Liang, J. H. Park, H. Yan, and K. Li, "A dynamic event-triggered approach to state estimation for switched memristive neural networks with nonhomogeneous sojourn

probabilities," *IEEE Transactions on Circuits and Systems I: Regular Papers*, vol. 68, no. 12, pp. 4924–4934, 2021.

[28] P. Shi, H. Wang, and C.-C. Lim, "Network-based event-triggered control for singular systems with quantizations," *IEEE Transactions on Industrial Electronics*, vol. 63, no. 2, pp. 1230–1238, 2016.

[29] J. Cheng, Y. Wu, Z. Wu, and K. Li, "Fuzzy filter design for affine systems with sensor faults: a dynamic event-triggered approach," *Journal of Systems Science and Complexity*, vol. 35, no. 5, pp. 1761–1784, 2022.

[30] S. Zhu, E. Tian, D. Xu, and J. Liu, "An adaptive torus-event-based controller design for networked t-s fuzzy systems under deception attacks," *International Journal of Robust and Nonlinear Control*, vol. 32, no. 6, pp. 3425–3441, 2022.

[31] L. Zha, R. Liao, J. Liu, X. Xie, E. Tian, and J. Cao, "Dynamic event-triggered output feedback control for networked systems subject to multiple cyber attacks," *IEEE Transactions on Cybernetics*, vol. 52, no. 12, pp. 13800–13808, 2022.

[32] Z. Gu, P. Shi, and D. Yue, "An adaptive event-triggering scheme for networked interconnected control system with stochastic uncertainty," *International Journal of Robust and Nonlinear Control*, vol. 27, no. 2, pp. 236–251, 2017.

[33] X. Xie, S. Li, and B. Xu, "Adaptive event-triggered H∞ fuzzy filtering for interval type-2 T–S fuzzy-model-based networked control systems with asynchronously and imperfectly matched membership functions," *Journal of the Franklin Institute*, vol. 356, no. 18, pp. 11760–11791, 2019.

[34] X.-G. Guo, X. Fan, J.-L. Wang, and J. H. Park, "Event-triggered switching-type fault detection and isolation for fuzzy control systems under dos attacks," *IEEE Transactions on Fuzzy Systems*, vol. 29, no. 11, pp. 3401–3414, 2021.

[35] H. Zhang, J. Liu, and S. Xu, "H-infinity load frequency control of networked power systems via an event-triggered scheme," *IEEE Transactions on Industrial Electronics*, vol. 67, no. 8, pp. 7104–7113, 2020.

[36] Y. Tian, H. Yan, H. Zhang, J. Cheng, and H. Shen, "Asynchronous output feedback control of hidden semi-markov jump systems with random mode-dependent delays," *IEEE Transactions on Automatic Control*, vol. 67, no. 8, pp. 4107–4114, 2022.

[37] P. Park, J. W. Ko, and C. Jeong, "Reciprocally convex approach to stability of systems with time-varying delays," *Automatica*, vol. 47, no. 1, pp. 235–238, 2011.

Hindawi
Complexity
Volume 2023, Article ID 1337928, 24 pages
https://doi.org/10.1155/2023/1337928

WILEY | Hindawi

Research Article

Designing a Scenario-Based Fuzzy Model for Sustainable Closed-Loop Supply Chain Network considering Statistical Reliability: A New Hybrid Metaheuristic Algorithm

Peyman Bahrampour,[1] Seyyed Esmaeil Najafi ,[1] Farhad Hosseinzadeh lotfi,[2] and Ahmad Edalatpanah [3]

[1]*Department of Industrial Engineering, Tehran Science and Research Branch, Islamic Azad University, Tehran, Iran*
[2]*Department of Mathematics, Tehran Science and Research Branch, Islamic Azad University, Tehran, Iran*
[3]*Department of Applied Mathematics, Ayandegan Institute of Higher Education, Tonekabon, Iran*

Correspondence should be addressed to Seyyed Esmaeil Najafi; e.najafi@srbiau.ac.ir

Received 4 November 2022; Revised 17 December 2022; Accepted 22 March 2023; Published 21 April 2023

Academic Editor: Fuli Zhou

In this study, a new nonlinear mathematical programming model of mixed integer was presented to formulate the problem of designing a sustainable closed loop supply chain, in which the three aspects of sustainability, i.e., social effect such as job creation, customer satisfaction, and distributors, environmental effects such as reducing air pollution, and economic effects such as reducing supply chain costs, increasing supply chain reliability, quality of returned products by customers, and product routing were considered. In order to solve the proposed model, a new hybrid metaheuristic algorithm based on the distinctive features of gray wolf algorithm and genetic algorithm was proposed in addition to MOPSO and NSGA-II algorithms. After tuning their parameters by the Taguchi method, their performance in problems with different dimensions was tested and evaluated by MID, DM, and SM criteria. The results of statistical analysis of indices indicated that no significant difference between the performance of the three algorithms at 5% error level. In general, GW-NS, NSGA-II and MOPSO algorithms had better performance in terms of MID index, respectively. In addition, GW-NS, NSGA-II, and MOPSO algorithms performed better in terms of DM index. NSGA-II, MOPSO, and GW-NS algorithms performed better in terms of SM index, respectively. In addition, the variability of DM index in all three algorithms was almost the same, but in MID index, GW-NS algorithm, and in SM index, MOPSO algorithm had the highest change and less sustainability.

1. Introduction

Globalization, the increased regulations of governmental and nongovernmental organizations, and the pressure and requests from customers to comply with environmental issues have led organizations to regard the necessary steps to apply sustainable closed-loop supply chain (SCLSC) management aimed at improving their environmental and economic performance [1]. The SCLSC management integrates the SCM with environmental requirements in all stages of product design, selection and supply of raw materials, production and manufacturing, distribution and transfer processes, delivery to the customer, and ultimately after consumption, recycling and reuse management aimed at maximizing the efficiency of energy, and resources consumption associated with improving the performance of the entire supply chain [2, 3]. The problem of vehicle routing in the supply chain distribution network is recognized as one of the subproblems of SCM, which involves selecting and allocating possible routes to available vehicles for distribution and delivery of goods to distribution centers or customers designated to minimize the relevant costs. The optimal solving of this problem will lead to timely delivery of goods, reduce the

need for warehousing and maintenance of goods, and increase customer satisfaction meanwhile reducing the distribution costs [4]. One may also claim that vehicle routing is one of the most challenging issues in the context of transportation and support of the supply chain [5]. A variety of products have to be made available to the customers at their request in today's global competitions. The customers' demand for high quality and fast service-providing has led to enhanced pressures that have not faced before [6]. In today's economic and industrial environment and given the growing trend of industries followed by the rise in environmental pollution in contrast, and most importantly, the use of limited resources, the need to recycle resources from manufactured products as well as informing the consumers about the need for a change in attitude seem to be a priority not only in the production of goods but in all the stages of production [7]. Ensuring sustainable development in any country is nowadays subject to the conservation and optimal use of limited and irreplaceable resources in that country. Thus, many measures have been taken in this direction, including recycling waste in the production cycle, the reuse of consumer goods, returning the quality control returned goods to the production line, recycling, etc. The set of these activities accompanied by applying environmental and social considerations form the concept of the SCLSC [8, 9]. On the other hand, aimed at accurate management and preventing the waste of resources, the management units currently have no choice other than to adopt and employ new scientific approaches, models, processes, and techniques tailored to the current conditions to provide proper performance regarding the resources used [10]. It is usually assumed in supply chain network (SCN) design studies that active utilities (facilities) are able to provide service continuously for a long period of time without any breakdown and will continue to operate without interruption. However, supply chains face a high degree of uncertainty due to their complex nature, which can adversely affect the quality of their performance [11]. In the real world, utilities may suffer from disruptions and failures with possible causes of human error, natural disasters, etc. [12, 13]. Thus, the failure of one component of the SCN may disrupt the functioning of the entire supply chain, or in the best case, reduce the efficiency of the chain. Hence, it seems essential to consider the factor of reliability in the design of the closed-loop supply chain, especially in its direct components (forward logistic stage). However, this issue has been less addressed in recent studies. In this study, a multiobjective (MO), multiperiod, multicommodity, and scenario-based fuzzy mathematical model, a new hybrid metaheuristic algorithm was proposed for locating, routing, and distributing goods in a sustainable closed loop supply chain. The uncertainty considered in the mathematical model was fuzzy. In the proposed hybrid approach, the search mechanism and update of the solution in the basic gray wolf algorithm and the crowding distance index mechanism of the MO genetic algorithm were used to select and remove unsuccessful solutions in the external archive.

2. Literature Review

The relevant literature that contributes to identify the general framework of this article is reviewed in this section. Zhang et al. [14] provided a mathematical model for a SCLSC based on economic turnaround. The goals of this model encompass maximum profitability according to the income and costs of the entire chain, minimizing the environmental impacts due to the carbon index and maximizing the social effects according to the job opportunities created. They utilized the weighted sum technique to solve the model. The sensitivity analysis results revealed that the enhanced demand rate has a remarkable impact on the goals. Hassangaviar et al. [15] provided a biobjective mathematical model for the closed-loop chain under uncertainty in prices. The model objectives included maximizing transaction level satisfaction and the profit from the supply chain. They used the NSGA-II algorithm to solve the model, and the results indicated a good performance in terms of maximum expansion and distancing. Mogale et al. [16] provided a CLSCs network, in which, the demand was considered sensitive to the price, consumer motivation, and the quality level. The core goal of the proposed model is to reduce the total cost and carbon emissions produced by the activities resulting from production, distribution, transportation, and disposal. They employed an NSGA-II algorithm and a cokriging approach to solve the model. The study results revealed the positive effects of motivational pricing on the returned goods. Kazancoglu et al. [17] presented an MILP model for designing the green dual-channel and CLSCs. The core goal of the proposed model is to optimally select echelons and transportation alternatives between these echelons in a CLSC network based on economic and environmental considerations. The proposed model is supported by a case study in the home appliance industry in this study. Khalili Nasr et al. [18] provided a new integrated approach based on the best-worst method and MOMILP for designing an SCLSC network with the LIR problem; they applied a fuzzy method for solving their model using GP. Sadeghi Ahangar et al. [19] provided a SCLSC network to manage municipal solid waste using a MILP model based on an FPA. This model minimized the total cost, labor, and emission level. Goli et al. [20] examined a multiobjective, multiperiod, and multiproduct closed-loop supply chain (CLSC) model with uncertain parameters aimed at combining the financial cash flow as cash flow and debt constraints and employment under uncertainty. The objectives of the proposed mathematical model in their study included increasing the cash flow, maximizing the jobs created, and maximizing the reliability of raw materials consumed. They developed and used MO simulated annealing, MO invasive weed optimization, and MO gray wolf metaheuristic algorithms to solve

the model at a large scale. Ali et al. [21] provided a novel mathematical model for reverse supply chain management of air conditioning products. Their considered supply chain was sustainable with fuzzy demand uncertainty. Locating hub and recycling centers was among the most important goals of their research. The case study covered the industries of Saudi Arabia and India. In their study, identified places were prioritized with a hierarchical process analysis approach after solving the mathematical model. Yun et al. [22] mathematically modeled a MO supply chain by considering economic, environmental, and social criteria. The objectives regarded by them included minimizing total costs, minimizing the amount of carbon dioxide released, and maximizing social impacts. Their innovation involved considering three types of distribution channels, including normal delivery, direct delivery, and direct displacement. The proposed model was solved using the genetic algorithm, whose results indicated the proper performance of the proposed model. Reyhani et al. [23] provided an MO and multiperiod mathematical model for inventory management for the SCLSC. The most important decisions made in their model included determining the amount of flow at each level and locating the hubs. The main objectives of the study contained minimizing transportation costs and the costs of carbon dioxide emissions and maximizing social responsibility. The case study was focused on agricultural products. Rabbani et al. [1] presented a sustainable MO and multilevel mathematical model to locate distribution hubs and allocate warehouses to distribution centers. The proposed innovation included a variety of technologies for cars, which causes the release of different amounts of carbon dioxide from different vehicles. They used the Epsilon constraint approach to solve the model in small and medium dimensions. Wang et al. [24] provided a mathematical model for the green inverse supply chain. One of their innovations was to consider the pricing of goods using the game theory. They considered three different prices for different types of goods in this article to price goods. Minimizing costs in the supply chain, including manufacturers, distributors, customers, and collection centers were some of the objectives of this study. According to their results, the chain costs were minimized to the desired level. Mohtashami et al. [25] proposed a mathematical model for reverse and green supply chains to minimize energy consumption and environmental impacts. Considering the queuing system with limited resources in hubs in this research was recognized as an innovation. They used the genetic algorithm to solve the proposed model in large dimensions. Sadeghi Rad et al. [26] provided a multilayer, multiperiod, multiproduct mixed-integer programming model, which included four layers in the forward (direction) flow (suppliers, production and regeneration centers, distribution center, and customers) and three layers in (backward) reverse (direction) flow (customers, inspection and collection centers, and disposal centers). The production and inspection centers were integrated into the proposed model to reduce transportation costs. Besides economic goals, environmental aspects such as green production, technology, and transportation modes were also considered in this model. Also, the amount of raw materials purchased and the volume of greenhouse gases produced in the production process were considered dependent on the level of technology. Hajiaghaei et al. [27] provided a nonlinear mixed-integer mathematical program model to formulate a SCLSC with consideration of discounts on shipping costs. They suggested three hybrid RDSA, KAGA, and ICTS algorithms to solve the model, which were compared by four evaluation criteria by Pareto analysis. The comparison result indicated that the proposed new hybrid KAGA algorithm brings better solutions compared to other algorithms but needs more time for solving. They finally introduced a real example in the glass industry to confirm the proposed model and the algorithms provided. Ghomi-Avili et al. [28] presented an MO model in the green closed-loop supply chain by considering the failure of downtime of centers. Pricing of products with a collaborative approach to game theory was one of the innovations of this research. The problem was fuzzily modeled due to the fuzzy nature of the data, whose most important goal was set to minimize the amount of pollutant gases released in the proposed chain. Rahimi and Ghezavati [29] presented an MO mathematical model for managing inventory and the flow of goods in a SCLSC. Considering discounts for customers associated with uncertainty in demand were among the innovations in their research. Their main goals were to minimize transportation costs and environmental costs. The results revealed an 11% reduction in costs after implementing the model. Wang and Gunasekaran [30] provided a closed-loop supply chain where three competitive scenarios implemented by the manufacturer were studied. They used Stackelberg's game theory for studying this model. According to their conclusion, a producer is more inclined to perform the recycling and reproduction processes by himself and refrains from outsourcing.

2.1. Research Gap. The research gap can be summarized as follows according to the subject literature and Table 1:

(1) Insufficient attention to the inherent uncertainty of supply chain issues together with their elements

(2) Lack of attention to statistical reliability and various errors in the proposed mathematical models

(3) Insufficient attention to the strengths of other metaheuristic algorithms aimed at utilizing them ogether in a new hybrid metaheuristic algorithm

2.2. Research Contributions

(1) In this model, increasing the supply chain reliability, the quality of the products returned by the customers, and the routing of the goods are also considered besides the three aspects of sustainability, namely, the social effect such as job creation, customer satisfaction, and distributors, the environmental effect such as reducing air pollution, and the economic effect such as reducing the supply chain costs.

Table 1: Literature review table.

Article	Network Type									Problem definition					Formulation			Objective											Network stage							Output		
					Continuous									Discrete									Forward logistic stage										Reverse logistic stage					
Author	Forward	Reverse	Closed loop	Multiproduct	Multiperiod	Capacity constraint	Reliability	Uncertainty	Discount	Continuous Approximation	Stochastic mixed integer programing	Fuzzy mixed integer programing	Mixed integer nonlinear programing	Mixed integer linear programing	Cost	Profit	Environment impact	Supply center	Production centers	Distribution centers	Hub	Warehouse	Customer zone	Recovering centers	Remanufacturing centers	Recycling centers	Disposal centers	Suppler/ Orders	Facility location	Facility capacity	Allocation	Discount	Production amount	Inventory	Transportation mode	Technology type	CO_2 emission amount	Solution method
Rahimi and Ghezavati [29]				*	*			*		*						*		*	*			*	*			*				*		*	*	*		*	*	Commercial solver
Ghomi et al. [28]					*		*			*									*				*	*								*				*		RDP algorithm
Hajiaghaei-Keshteli and Fathollahi Fard [27]	*	*			*	*				*	*	*	*	*	*			*	*	*	*	*	*		*				*			*			*			RDSA, KAGA و ICTS
Sadeghi Rad and Nahavandi [26]	*	*	*	*	*	*	*	*	*	**	*	*	*	*	*									*					*			*	*	*	*			Commercial solver
Mohtashami et al. [25]	*	*	*		*		*	*	*			*	*	*	*						*	*	*	*						*		*		*	*			Genetic
Wang et al. [24]					*			*			*	*	*	*				*	*	*		*	*	*					*			*	*	*	*			Commercial solver
Rabbani et al. [1]					*			*	*	*	*	*	*	*	*			*	*	*	*	*	*			*				*		*	*		*			HRPP-II
Reyhani et al. [23]					*	*		*	*		*	*	*	*	*			*	*	*	*	*			*				*	*			*		*			Commercial solver
Yun et al. [22]			*				*	*			*	*	*	*	*			*	*	*		*	*		*							*			*			Genetic algorithm
Ali et al. [21]					*						*							*	*	*	*		*	*									*			*		Commercial solver
Goli et al. [20]						*	*			*	*	*	*	*	*			*	*		*	*	*			*			*	*			*	*	*			MOSA, MOGWO, MOIWO
Sadeghi Ahangar et al. [19]	*	*			*	*				*	*	*	*	*	*			*	*	*		*	*	*					*			*	*	*	*			Commercial solver
Khalili Nasr et al. [18]	*	*	*		*		*	*	*			*	*	*	*						*	*	*	*				*	*			*		*	*			Commercial solver
Kazancoglu et al. [17]		*			*	*				*	*	*	*	*	*			*	*	*	*	*	*	*				*				*	*	*		*		Commercial solver
Mogale et al. [16]	*	*			*	*				*	*	*	*	*	*			*	*	*		*	*		*	*	*					*	*	*	*	*		NSGA-II, Cokriging
Hassangaviar et al. [15]	*				*	*	*			*	*	*	*	*	*			*	*	*	*		*							*		*	*	*	*	*	*	Commercial solver
Zhang et al. [14]			*		*	*	*			*	*	*	*	*	*			*	*	*	*			*						*		*	*	*	*	*	*	NSGA-II—NRGA
This study	*		*		*		*	*	*		*	*	*	*	*		*	*	*	*	*	*	*		*	*				*	*	*	*	*	*	*	*	NSGA-II,MOPSO,Epsilon-constraint, GW − NS

(2) In the real world, all the components of a closed-loop supply chain like production centers, etc., may not fully operate and are likely to stop working due to events such as human errors, weather conditions, terrorist attacks, etc., in period t. Thus, this limitation has been considered in the form of using statistical reliability to approach the real situation.

(3) Providing a hybrid metaheuristic algorithm to solve the model.

3. Problem Statement

The SCN provided in this study is a closed-loop, MO, and multiperiod scenario-based network, which encompasses suppliers, manufacturers, distributors, customers, hubs, repair, recycling, landfill, and demolition centers. It should be noted that the hubs, distribution centers, recycling centers, repair, and burial centers are equipped with the capability to be reopened. In the reopening process, some places are selected as candidate points and the model chooses the optimal place from them. In the supply chain functioning process, suppliers provide raw materials to manufacturers. The manufacturers and the warehouses under their supervision send the products to distributors. The breakdown and failure of raw materials supply centers, warehouses, and production centers are some of the issues and problems addressed in this study. This focus makes the issue closer and more similar to the real world. Distributors send products to customers. There are hubs, recycling, landfill, and repair centers in the backward direction. The important point is how to determine the flow of returned products is their quality. The hubs send the returned products to repair, landfill, or production centers depending on their quality. After repairing, the repair centers send the products to distributors. The recycling centers also send products to manufacturers. It should be noted that some of the returned goods from customers can be sent directly to the reproduction centers located in the production center and do not need recycling in the recycling centers. Figure 1 shows the proposed supply chain structure.

Maximizing the social responsibility dimension is one of the goals of the proposed model, in which, the employment rate, customer satisfaction, and distribution centers are maximized by sending maximum products from raw materials supply and production centers to them. Minimizing the economic and environmental costs of the supply chain is set to be another goal of this model. This parameter is considered to be fuzzy due to the inherent uncertainty of demand. Locating, examining the flow rate between components, and the routing of goods are other decisions that are supposed to be made in this research.

4. Formulating the Model

4.1. Model Assumptions

(1) The capacity of the centers is limited.

(2) The demand parameter is assumed to be fuzzy.

(3) The distances between centers is assumed to be fixed and definite.

(4) Every producer has a warehouse to store the produced goods.

(5) There is a reproduction center in each production center.

(6) The produced goods are sent both from production centers and from their warehouses to the distribution centers.

(7) The locations of supplier centers, producers, and their warehouses are fixed and predetermined and already known.

(8) Any production center and its warehouse and supply centers cannot be rehabilitated and reconstructed in the case of being destroyed by an accident.

4.2. Objective Functions. We know that the time it takes for the warehouse of the production center j to break down over a period of T_j follows an exponential distribution with a mean value of λ'_{jt}. Thus, the reliability of the warehouse of the production center j in sending products to the distribution center k in the period t is equal to:

$$R_j = p\left(T_j > \tau'_j\right) = \int_{\tau'_j}^{\infty} \lambda'_{jt} e^{-\lambda'_{jt}\tau'_j} dt = e^{-\lambda'_{jt}\tau'_j}. \tag{1}$$

Therefore, the mean value of the products sent from the warehouse of the production centers to distribution centers is equal to

$$\sum_{t\in T}\sum_{c\in C}\sum_{s\in S}\sum_{j\in J}\sum_{k\in K} Q^{ct}_{jks} e^{-\lambda'_{jt}\tau'_j}. \tag{2}$$

Therefore, the mean value of the products sent from production centers and their warehouses to distribution centers is equal to

$$\sum_{t\in T}\sum_{c\in C}\sum_{s\in S}\left(\sum_{j\in J}\sum_{k\in K} Q^{ct}_{jks} e^{-\lambda'_{jt}\tau'_j} + \sum_{j\in J}\sum_{k\in K} Z^{ct}_{jks} e^{-\lambda_{jt}\tau_j}\right). \tag{3}$$

Similarly, the average of raw materials sent from supplier centers to production centers is equal to

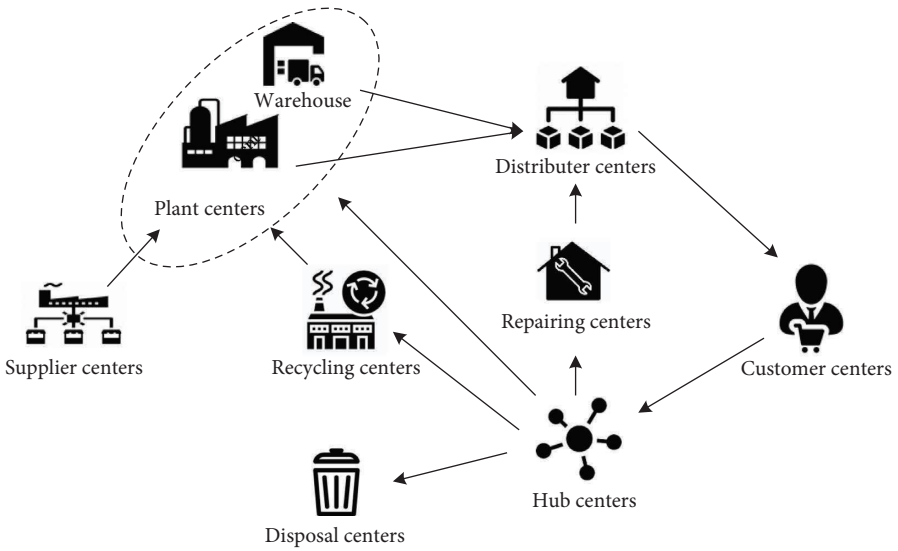

Figure 1: The structure of the proposed model.

$$\sum_{t\in T}\sum_{o\in O}\sum_{s\in S}\sum_{i\in I}\sum_{j\in J} Z_{ijs}^{ot} e^{-\lambda_{it}\tau_i''},$$

$$\max z_1 = J_1 + J_2 + R - \mathrm{In},$$

$$J_1 = \sum_{t\in T}\sum_{s\in S}\left(\sum_{m\in M}\alpha j_{m,s}x_m^t + \sum_{p\in P}\alpha j_{p,s}x_p^t + \sum_{w\in W}\alpha j_{w,s}x_w^t + \sum_{n\in N}\alpha j_{n,s}x_n^t + \sum_{k\in N}\alpha j_{k,s}x_k^t\right),$$

$$J_2 = \sum_{t\in T}\sum_{c\in C}\sum_{s\in S}\left(\sum_{k\in K}\sum_{l\in L}\frac{\beta j_k}{u_k^t} z_{kl,s}^{ct} + \sum_{l\in L}\sum_{m\in M}\sum_{q\in Q}\frac{\beta j_m}{u_m^t} z_{lmq,s}^{ct} + \sum_{m\in M}\sum_{n\in N}\sum_{q\in Q_4}\frac{\beta j_n}{u_n^t} z_{mnq,s}^{ct}\right. \tag{4}$$

$$\left. + \sum_{m\in M}\sum_{w\in W}\sum_{q\in Q_1}\frac{\beta j_w}{u_w^t} z_{mwq,s}^{ct} + \sum_{m\in M}\sum_{p\in P}\sum_{q\in Q_3}\frac{\beta j_p}{u_p^t} z_{mpq,s}^{ct}\right),$$

$$R = \sum_{t\in T}\sum_{c\in C}\sum_{s\in S}\left(\sum_{j\in J}\sum_{k\in K} Q_{jks}^{ct} e^{-\lambda_{jt}'\tau_j'} + \sum_{j\in J}\sum_{k\in K} Z_{jks}^{ct} e^{-\lambda_{jt}} + \sum_{t\in T}\sum_{o\in O}\sum_{s\in S}\sum_{i\in I}\sum_{j\in J} Z_{ijs}^{ot} e^{-\lambda_{it}}\right),$$

$$\mathrm{In} = \sum_{t\in T}\sum_{s\in S}\left(\sum_{j\in J}\sum_{c\in C}\left(dl_j^t\left(Q_{jj,s}^{ct} + \sum_{k\in K} z_{jk,s}^{ct}\right)\right)\right),$$

The first objective function represents the social responsibility dimension of the supply chain network, where

J_1: The number of fixed jobs created.

J_2: The number of variable jobs created.

R: The average amount of product flow sent from suppliers, production centers, and their warehouses (as the R value increases, the satisfaction level of distribution centers and customers will increase).

In: The work injury rate due to jobs created in the production centers and their warehouses.

$$
\begin{aligned}
&\text{Min } z_2 = C_1 + C_2 + C_3,\\
&C_1 = \sum_{t\in T}\left(\sum_{m\in M} E_m^t x_m^t + \sum_{n\in N} E_n^t x_n^t + \sum_{p\in P} E_p^t x_p^t + \sum_{w\in W} E_w^t x_w^t + \sum_{k\in K} E_k^t x_k^t\right),\\
&C_2 = \sum_{t\in T}\sum_{s\in S}\sum_{o\in O}\sum_{i\in I}\sum_{j\in J} h_{ij,s}^{o} z_{ij,s}^{ot} z_{vij,s}^{rt} + \sum_{t\in T}\sum_{s\in S}\sum_{c\in C}\left(\sum_{j\in J} cq_{jj,s}^{c} Q_{jj,s}^{ct} + \sum_{j\in J}\sum_{k\in K}\sum_{v\in V} h_{jk,s}^{c} z_{jk,s}^{ct} ro_{vjk,s}^{rt} + \sum_{j\in J}\sum_{k\in K}\sum_{v\in V} cq_{jk,s}^{c} Q_{jk,s}^{ct} Ro_{vjk,s}^{rt}\right.\\
&\quad \sum_{l\in L}\sum_{m\in M}\sum_{v\in V}\sum_{q\in Q} h_{lmq,s}^{c} z_{lmq,s}^{ct} ro_{vlm,s}^{rt} + \sum_{m\in M}\sum_{p\in P}\sum_{v\in V}\sum_{q\in Q_3} h_{mpq,s}^{c} z_{mpq,s}^{ct} ro_{vmp,s}^{rt}\\
&\quad + \sum_{k\in K}\sum_{l\in L}\sum_{v\in V} h_{kl,s}^{c} z_{kl,s}^{ct} ro_{vkl,s}^{rt} + \sum_{p\in P}\sum_{j\in J}\sum_{v\in V} h_{pj,s}^{c} z_{pj,s}^{ct} ro_{vpj,s}^{rt}\\
&\quad + \sum_{m\in M}\sum_{n\in N}\sum_{v\in V}\sum_{q\in Q_4} h_{mnq,s}^{c} z_{mnq,s}^{ct} ro_{vmn,s}^{rt} + \sum_{m\in M}\sum_{j\in J}\sum_{v\in V}\sum_{q\in Q_2} h_{mjq,s}^{c} z_{mjq,s}^{ct} ro_{vmj,s}^{rt}\\
&\quad \left. + \sum_{m\in M}\sum_{w\in W}\sum_{v\in V}\sum_{q\in Q_1} h_{mwq,s}^{c} z_{mwq,s}^{ct} ro_{vmw,s}^{rt} + \sum_{w\in W}\sum_{k\in K}\sum_{v\in V} h_{wk,s}^{c} z_{wk,s}^{ct} ro_{vwk,s}^{rt} + \sum_{c\in C}\sum_{j\in J} f_{j,s}^{ct} Inv_{j,s}^{ct}\right),\\
&C_3 = \sum_{t\in T}\sum_{s\in S}\sum_{c\in C}\left(\sum_{l\in L}\sum_{m\in M}\sum_{q\in Q} z_{lmq,s}^{ct} fp_{lmq,s}^{ct} + \sum_{m\in M}\sum_{p\in P}\sum_{q\in Q_3} z_{mpq,s}^{ct} cp_{ct,s} + \sum_{l\in L}\sum_{m\in M}\sum_{q\in Q} x_{lmq,s}^{ct} cm_{ct,s} + \sum_{k\in K}\sum_{l\in L} z_{kl,s}^{ct} ck_{ct,s}\right.\\
&\quad \left. + \sum_{m\in M}\sum_{n\in N}\sum_{q\in Q_4} z_{mnq,s}^{ct} cn_{ct,s} + \sum_{m\in M}\sum_{w\in W}\sum_{q\in Q_1} z_{mwq,s}^{ct} cw_{ct,s} + \sum_{m\in M}\sum_{j\in J}\sum_{q\in Q_2} z_{mjq,s}^{ct} rcj_{ct,s} + \sum_{j\in J}\left(cj_{ct,s}\left(Q_{jj,s}^{ct} + \sum_{k\in K} z_{jk,s}^{ct}\right)\right)\right).
\end{aligned}
\tag{5}
$$

The second objective function encompasses the supply chain costs as follows:

C_1: The costs of establishing hub, repair, distribution, demolition, landfill, and recycling centers.

C_2: The costs of production and maintenance of products in the production sector.

C_3: The costs of recycling, demolition, etc.

$$
\begin{aligned}
&\text{Min } z_3 = F_1 + F_2\\
&F_1 = \sum_{t\in T}\left(\sum_{n\in N} EM_n x_n^t + \sum_{m\in M} EM_m x_m^t + \sum_{p\in P} EM_p x_p^t + \sum_{w\in W} EM_w x_w^t + \sum_{k\in K} EM_M x_k^t\right),\\
&F_2 = \sum_{s\in S}\sum_{r\in R}\sum_{t\in T}\sum_{v\in V} EMS_v\left(\sum_{j\in J}\sum_{k\in K} a_{jk,s} z_{jk,s}^{ct} ro_{vjk,s}^{rt} + \sum_{j\in J}\sum_{k\in K} dq_{jk,s} Q_{jk,s}^{ct} Ro_{vjk,s}^{rt} + \sum_{k\in K}\sum_{l\in L} a_{kl,s} z_{kl,s}^{ct} ro_{vkl,s}^{rt}\right.\\
&\quad + \sum_{q\in Q}\sum_{l\in L}\sum_{m\in M} a_{lm,s}^{c} z_{lmq,s}^{ct} ro_{vlm,s}^{rt} + \sum_{q\in Q_3}\sum_{m\in M}\sum_{p\in P} a_{mp,s} z_{mpq,s}^{ct} ro_{vmp,s}^{rt} + \sum_{q\in Q_4}\sum_{m\in M}\sum_{n\in N} a_{mn,s} z_{mnq,s}^{ct} ro_{vmn,s}^{rt}\\
&\quad + \sum_{q\in Q_2}\sum_{m\in M}\sum_{j\in J} a_{mj,s} z_{mjq,s}^{ct} ro_{vmj,s}^{rt} + \sum_{q\in Q_1}\sum_{m\in M}\sum_{w\in W} a_{mw,s} z_{mwq,s}^{ct} ro_{vmw,s}^{rt} + \sum_{w\in W}\sum_{k\in K} a_{wk,s} z_{wk,s}^{ct} ro_{vwk,s}^{rt}\\
&\quad \left. + \sum_{p\in P}\sum_{j\in J} a_{pj,s} z_{pj,s}^{ct} ro_{vpj,s}^{rt} + \sum_{s\in S}\sum_{o\in O}\sum_{r\in R}\sum_{t\in T}\sum_{v\in V}\sum_{i}\sum_{j} EMS_v a_{ij,s} z_{ij,s}^{ot} ro_{vij,s}^{rt} + \sum_{t\in T}\sum_{s\in S}\sum_{c\in C}\sum_{j\in J} \gamma aq_{jj,s} Q_{jj,s}^{ct}\right)
\end{aligned}
\tag{6}
$$

The third objective function includes environmental effects and the amount of CO_2 emitted due to the establishment of potential centers (F_1), and transportation is in the supply chain (F_2).

$$\sum_{k\in K} x_k^t \geq 1 \forall t \in T, \tag{7}$$

$$\sum_{w\in W} x_w^t \geq 1 \forall t \in T, \tag{8}$$

$$\sum_{m\in M} x_m^t \geq 1 \forall t \in T, \tag{9}$$

$$\sum_{p\in P} x_p^t \geq 1 \forall t \in T, \tag{10}$$

$$\sum_{n\in N} x_n^t \geq 1 \forall t \in T, \tag{11}$$

$$\sum_{k\in K} ro_{vjk,s}^{rt} + \sum_{k\in K} Ro_{vjk,s}^{rt} \leq \sum_{k\in K} x_k^t \forall j \in J, r \in R, v \in V, t \in T, s \in S, \tag{12}$$

$$\sum_{m\in M} ro_{vlm,s}^{rt} \leq \sum_{m\in M} x_m^t \forall l \in L, r \in R, v \in V, t \in T, s \in S, \tag{13}$$

$$\sum_{p\in P} ro_{vmp,s}^{rt} \leq \sum_{p\in P} x_p^t \forall m \in M, r \in R, v \in V, t \in T, s \in S, \tag{14}$$

$$\sum_{n\in N} ro_{vmn,s}^{rt} \leq \sum_{n\in N} x_n^t \forall m \in M, r \in R, v \in V, t \in T, s \in S, \tag{15}$$

$$\sum_{w\in W} ro_{vmw,s}^{rt} \leq \sum_{w\in W} x_w^t \forall m \in M, r \in R, v \in V, t \in T, s \in S, \tag{16}$$

$$\sum_{k\in K} z_{kl,s}^{ct} = \widetilde{d_{l,s}^{ct}} \forall l \in L, c \in C, t \in T, s \in S, \tag{17}$$

$$\sum_{m\in M} z_{lmq,s}^{ct} = r_{lq,s}^{c} \left(\sum_{k\in K} \sum_{l\in L} z_{kl,s}^{ct} \right) \forall l \in L, c \in C, t \in T, q \in Q, s \in S, \tag{18}$$

$$\sum_{q\in Q_2} \sum_{j\in J} z_{mj,q,s}^{ct} = \sum_{j\in J} rb_{mj}^{ct} \sum_{q\in Q} \left(\sum_{l\in L} z_{lm,q,s}^{ct} \right) \forall m \in M, c \in C, t \in T, s \in S, \tag{19}$$

$$\sum_{q\in Q_3} \sum_{p\in P} z_{mpq,s}^{ct} = \sum_{p\in P} rb_{mp}^{ct} \sum_{q\in Q} \left(\sum_{l\in L} z_{lm,q,s}^{ct} \right) \forall m \in M, c \in C, t \in T, s \in S, \tag{20}$$

$$\sum_{q\in Q_4} \sum_{n\in N} z_{mnq,s}^{ct} = \sum_{n\in N} rb_{mn}^{ct} \sum_{q\in Q} \left(\sum_{l\in L} z_{lmq,s}^{ct} \right) \forall m \in M, c \in C, t \in T, s \in S, \tag{21}$$

$$\sum_{q\in Q_1} \sum_{w\in W} z_{mwq,s}^{ct} = \sum_{w\in W} rb_{mw}^{ct} \sum_{q\in Q} \left(\sum_{l\in L} z_{lmq,s}^{ct} \right) \forall m \in M, c \in C, t \in T, s \in S, \tag{22}$$

$$\sum_{w\in W} \sum_{k\in K} z_{wk,s}^{ct} + \sum_{j\in J} \left(z_{jk,s}^{ct} + Q_{jk,s}^{ct} \right) = \sum_{l\in L} z_{kl,s}^{ct} \forall k \in K, c \in C, t \in T, s \in S, \tag{23}$$

$$\sum_{q\in Q_3} \sum_{m\in M} z_{mpq,s}^{ct} = \sum_{j\in J} z_{pj,s}^{ct} \forall p \in P, c \in C, t \in T, s \in S, \tag{24}$$

$$\sum_{q\in Q_1} \sum_{m\in M} z_{mwq,s}^{ct} = \sum_{k\in K} z_{wk,s}^{ct} \forall w \in W, c \in C, t \in T, s \in S, \tag{25}$$

$$\sum_{i\in I} z_{ij,s}^{ot} + \sum_{q\in Q_2} \sum_{m\in M} z_{mjq,s}^{ct} + \sum_{p\in P} z_{pj,s}^{ct} = \sum_{k\in K} z_{jk,s}^{ct} + Inv_{j,s}^{ct} \forall j \in J, c \in C, o \in O, t \in T, s \in S, \tag{26}$$

$$\sum_{q\in Q_2}\sum_{j\in J} z_{mjq,s}^{ct} + \sum_{q\in Q_3}\sum_{p\in P} z_{mpq,s}^{ct} + \sum_{q\in Q_4}\sum_{n\in N} z_{mnq,s}^{ct} + \sum_{q\in Q_1}\sum_{w\in W} z_{mwq,s}^{ct} = \sum_{q\in Q}\sum_{l\in L} z_{lmq,s}^{ct} \forall m \in M, c \in C, t \in T, s \in S, \tag{27}$$

$$\sum_{r\in R} ro_{vjk,s}^{rt} + \sum_{r\in R} Ro_{vjk,s}^{rt} \geq 1 \forall j \in J, k \in K, v \in V, t \in T, s \in S, \tag{28}$$

$$\sum_{r\in R} ro_{vlm,s}^{rt} \geq 1 \forall m \in M, l \in L, v \in V, t \in T, s \in S, \tag{29}$$

$$\sum_{r\in R} ro_{vmp,s}^{rt} \geq 1 \forall m \in M, p \in P, v \in V, t \in T, s \in S, \tag{30}$$

$$\sum_{r\in R} ro_{vmn,s}^{rt} \geq 1 \forall m \in M, n \in N, v \in V, t \in T, s \in S, \tag{31}$$

$$\sum_{r\in R} ro_{vij,s}^{rt} \geq 1 \forall i \in I, j \in J, v \in V, t \in T, s \in S, \tag{32}$$

$$\sum_{r\in R} ro_{vkl,s}^{rt} \geq 1 \forall k \in K, l \in L, v \in V, t \in T, s \in S, \tag{33}$$

$$\sum_{r\in R} ro_{vpj,s}^{rt} \geq 1 \forall p \in P, j \in J, v \in V, t \in T, s \in S, \tag{34}$$

$$\sum_{r\in R} ro_{vmj,s}^{rt} \geq 1 \forall m \in M, j \in J, v \in V, t \in T, s \in S, \tag{35}$$

$$\sum_{r\in R} ro_{vwk,s}^{rt} \geq 1 \forall w \in W, k \in K, v \in V, t \in T, s \in S, \tag{36}$$

$$\sum_{r\in R} ro_{vmw,s}^{rt} \geq 1 \forall m \in M, w \in W, v \in V, t \in T, s \in S, \tag{37}$$

$$Inv_{j,s}^{ct} = Q_{jj,s}^{ct} - \sum_{k\in K} Q_{jk,s}^{ct} \forall j \in J, \forall c \in C, t \in T, \forall s \in S, \tag{38}$$

$$\sum_{c\in C} Inv_{j,s}^{ct} \leq u_{jj}^{t} \forall j \in J, t \in T, \forall s \in S, \tag{39}$$

$$\sum_{k\in K} Q_{jk,s}^{ct} \leq Q_{jj,s}^{ct} \forall j \in J, c \in C, t \in T, s \in S, \tag{40}$$

$$\sum_{o\in O}\sum_{j\in J} z_{ij,s}^{ot} \leq u_{i}^{t} \forall t \in T, i \in I, s \in S, \tag{41}$$

$$\sum_{c\in C}\sum_{k\in K} z_{jk,s}^{ct} + \sum_{c\in C} Q_{jj,s}^{ct} \leq u_{j}^{t} \forall j \in J, t \in T, s \in S, \tag{42}$$

$$\sum_{c\in C}\sum_{l\in L} z_{kl,s}^{ct} \leq u_{k}^{t} x_{k}^{t} \forall k \in K, t \in T, \forall s \in S, \tag{43}$$

$$\sum_{q\in Q_2}\sum_{c\in C}\sum_{j\in J} z_{mjq,s}^{ct} + \sum_{q\in Q_3}\sum_{c\in C}\sum_{p\in P} z_{mpq,s}^{ct} + \sum_{q\in Q_4}\sum_{c\in C}\sum_{n\in N} z_{mnq,s}^{ct} + \sum_{q\in Q_1}\sum_{c\in C}\sum_{w\in W} z_{mwq,s}^{ct} \leq u_{m}^{t} x_{m}^{t} \forall m \in M, t \in T, s \in S, \tag{44}$$

$$\sum_{c\in C}\left(\sum_{q\in Q_2}\sum_{m\in M} z_{mjq,s}^{ct} + \sum_{p\in P} z_{pj,s}^{ct}\right) + \sum_{i\in I}\sum_{o\in O} z_{ij,s}^{ot} \leq cr_{j}^{t} \forall j \in J, t \in T, s \in S, \tag{45}$$

$$\sum_{q\in Q_4}\sum_{c\in C}\sum_{m\in M} z^{ct}_{mnq,s} \le u^t_n x^t_n \forall n \in N, t \in T, \forall s \in S, \tag{46}$$

$$\sum_{q\in Q_3}\sum_{c\in C}\sum_{m\in M} z^{ct}_{mpq,s} \le u^t_p x^t_p \forall p \in P, t \in T, s \in S, \tag{47}$$

$$\sum_{q\in Q_1}\sum_{c\in C}\sum_{m\in M} z^{ct}_{mwq,s} \le u^t_w x^t_w \forall w \in W, t \in T, s \in S, \tag{48}$$

$$\sum_{r\in R} ro^{rt}_{vjk,s} + \sum_{r\in R} Ro^{rt}_{vjk,s} \le \sum_{r\in R} ro^{rt}_{vij,s} \forall j \in J, i \in I, k \in K, v \in V, t \in T, s \in S, \tag{49}$$

$$\sum_{r\in R} ro^{rt}_{vkl,s} \le \sum_{r\in R} ro^{rt}_{vjk,s} \forall j \in J, l \in L, k \in K, v \in V, t \in T, s \in S, \tag{50}$$

$$\sum_{r\in R} ro^{rt}_{vlm,s} \le \sum_{r\in R} ro^{rt}_{vkl,s} \forall m \in M, l \in L, k \in K, v \in V, t \in T, s \in S, \tag{51}$$

$$\sum_{r\in R} ro^{rt}_{vpj,s} \le \sum_{r\in R} ro^{rt}_{vmp,s} \forall j \in J, p \in P, m \in M, v \in V, t \in T, s \in S, \tag{52}$$

$$\sum_{r\in R} ro^{rt}_{vmw,s} \le \sum_{r\in R} ro^{rt}_{vwk,s} \forall w \in W, k \in K, m \in M, v \in V, t \in T, s \in S, \tag{53}$$

$$\sum_{r\in R}\left(ro^{rt}_{vmp,s} + ro^{rt}_{vmn,s} + ro^{rt}_{vmj,s} + ro^{rt}_{vmw,s}\right) \le \sum_{r\in R} ro^{rt}_{vlm,s} \forall m \in M, j \in J, w \in W, n \in N, l \in L, p \in P, v \in V, t \in T, s \in S, \tag{54}$$

$$\begin{aligned} &z^{ct}_{lmq,s}, z^{ct}_{mpq,s}, z^{ot}_{ij,s}, z^{ct}_{pj,s}, z^{ct}_{mnq,s}, z^{ct}_{mjq,s}, z^{ct}_{mwq,s}, z^{ct}_{wk,s}, z^{ct}_{jk,s}, z^{ct}_{kl,s}, Q^{ct}_{jk,s}, Q^{ct}_{jj,s}, Inv^{ct}_{j,s} \\ &\ge 0 x^t_k, x^t_p, x^t_m, x^t_n, x^t_w, Ro^{rt}_{vjk,s}, ro^{rt}_{vij,s}, ro^{rt}_{vjk,s}, ro^{rt}_{vkl,s}, ro^{rt}_{vlm,s}, ro^{rt}_{vmp,s}, ro^{rt}_{vpj,s}, ro^{rt}_{vmj,s}, ro^{rt}_{vmn,s}, ro^{rt}_{vmw,s}, ro^{rt}_{vwk,s} \in \{0, 1\}. \end{aligned} \tag{55}$$

4.3. Constraints. The constraints (7)–(11) suggest that at least one of the potential distribution, repair, hub, recycling, and disposal centers in the supply chain is established. The constraints (12)–(16) suggest that a potential center should first be established to subsequently create a route (path) to this potential center. The constraint (17) indicates the satisfaction of customers' demands. The constraint (18) shows the balance between distribution, customer, and hub centers. The constraint (29) indicates the balance between customer, hub, and production centers. The constraint (20) shows the balance between customer, hub, and recycling centers. The constraint (21) indicates the balance between customer, hub, and landfill and disposal centers. The constraint (22) shows the balance between customer, hub, and repair centers. The constraint (23) indicates the balance between manufacturer, distributor, customer, and repair centers. The constraint (24) shows the balance between hub, recycling, and manufacturing centers. The constraint (25) shows the balance between hub, repair, and distributor centers. The constraints (26) and (27) determine the product flows in terms of its quality. The constraints (28)–(37) suggest that there is at least one path between the supply chain elements. The constraints (38) and (39) indicate the amount of inventory and the final capacity of the manufacturer. The constraint (40) determines the amount of the producer's inventory in its warehouse. The constraints (41)–(48) indicate the capacity of the fixed and potential centers. The constraints (49)–(54) explain the limitations of vehicle routing. Finally, the constraint (55) represents the decision variables of the proposed model.

4.4. Converting the Indefinite Demand Constraint to Its Equivalent Definite Constraint. A fuzzy number is a generalization of ordinary and real numbers that refers not to a value but a connected set of values so that any possible value would have a weight between 0 and 1 [31]. This mentioned weight is called the membership function. Hence, a fuzzy number is a certain type of the normalized convex real line fuzzy set [32]. There are several patterns such as triangular, trapezoidal, bell-shaped patterns, etc. to describe fuzzy numbers. Triangular fuzzy numbers are the most popular type of fuzzy numbers and are widely used in representing uncertainty in applied sciences because of their ability to express the perception of experts [33]. We used the triangular fuzzy number in this article to represent the fuzzy demand parameter. Thus, we defined the demand fuzzy parameter as $((d^{ct}_{ls})^p, (d^{ct}_{ls})^m, (d^{ct}_{ls})^o)$, in which the upper indices o, m, and p represent the most pessimistic, most possible, and the most optimistic values for the parameter, respectively. Therefore, the demand membership function would be as follows:

$$\mu_{\tilde{d}_{ls}^{ct}}(x) = \begin{cases} \dfrac{x - \left(d_{ls}^{ct}\right)^{p}}{\left(d_{ls}^{ct}\right)^{m} - \left(d_{ls}^{ct}\right)^{p}} \left(d_{ls}^{ct}\right)^{p} \le x \le \left(d_{ls}^{ct}\right)^{m}, \\ \dfrac{\left(d_{ls}^{ct}\right)^{o} - x}{\left(d_{ls}^{ct}\right)^{o} - \left(d_{ls}^{ct}\right)^{m}} \left(d_{ls}^{ct}\right)^{m} \le x \le \left(d_{ls}^{ct}\right)^{o}. \end{cases} \tag{56}$$

We utilized the weighted-average method in this paper to convert the fuzzy demand parameter to the equivalent definite parameter. Therefore, the fuzzy constraint [5] is determined based on equation.

$$\sum_{k \in K} z_{kl,s}^{ct} = w_1 \left(d_{ls,\beta}^{ct}\right)^{p} + w_2 \left(d_{ls,\beta}^{ct}\right)^{m} + w_3 \left(d_{ls,\beta}^{ct}\right)^{o} \forall l \in L, c \in C, t \in T, s \in S. \tag{57}$$

In equation (57), $w_1 + w_2 + w_3 = 1$ and β are the minimum acceptable likelihood in converting the fuzzy parameter to an equivalent real number. The symbols w_3, w_2, w_1 show the most pessimistic, most possible, and the most optimistic weight of fuzzy demand values, respectively. Appropriate values for these weights are usually determined based on the experience and knowledge of the decision-maker. In this study, these weights were considered based on the proposed values of Lai and Hwang and other conducted studies [34, 35] as $\beta = 0.5, w_1 = w_3 = 1/6, w_2 = 4/6$.

5. Solving Approaches

5.1. Epsilon Constraint. This method is based on turning an MO optimization problem into a single-objective optimization problem. Thus, one of the objectives of the problem is optimized as the main objective regarding other objectives as a constraint in this method [36]. It is assumed that the decision to minimize the objective functions (58) is associated with the constraints (59).

$$\text{Min} \quad F(x) = \{f_1(x), ..., f_n(x)\}, \tag{58}$$

$$st: \begin{array}{l} g(\mathrm{x}) \le 0, \\ h(x) = 0. \end{array} \tag{59}$$

One of the objective functions is selected as the main objective function according to equation (60) based on this approach. Other objective functions are considered as the constraint (61), and each time, the problem is solved according to one of the objective functions, and optimal and corresponding values of each objective function are calculated. The range between two optimal and corresponding values of subobjective functions is subdivided into a predetermined number followed by specifying a table of values for ε_j. Finally, the Pareto solutions will be obtained [37].

$$\text{Min} \ F(x), \tag{60}$$

$$st: \begin{array}{l} f_j(x) \le \varepsilon_j \\ f_j^{\min}(x) \le \varepsilon_j \le f_j^{\max} \quad j = 1, \ldots, n, j \ne 1. \\ g(x) \le 0 \\ h(\mathrm{x}) = 0 \end{array} \tag{61}$$

5.2. MOPSO Algorithm. The MOPSO algorithm was introduced by Coello in 2004 [38], which is in fact a generalization of the PSO algorithm that is used to solve MO problems. An elitist policy is used in this algorithm to keep the superior and dominant results in the iterations of the algorithm. The dominant solutions are stored in an external archive. Selecting *P*best and *G*best is done by a special mechanism. *P*best is only updated when a new particle dominates its previous value; then, the new particle is replaced. If the new particle is defeated by the best previous particle, nothing occurs and the same previous particle is introduced as the solution. Otherwise, if neither of them defeats each other, one of them is randomly considered as the best particle [39]. *G*best is also selected from the nondominated solutions in the archive in each iteration. The proper selection of optimal solutions in the MO particle swarming algorithm is known as an important step since it is subject to the convergence of the algorithm and its ability to achieve a diverse set of nondominated solutions in the decision space. If the termination conditions for the algorithm are not met, the above steps are repeated. Otherwise, the set of solutions in the archive are presented as efficient front points and final solutions (Figure 2).

5.2.1. Tuning the Coefficients. The equations describing the behavior of the particles in the MOPSO algorithm are as follows. Equations (62) and (63) determine the velocity and location of the particle i at the moment $t+1$.

$$V_i[t+1] = wV_i[t] + c_1 r_1 \left(x_{i\text{best}}[t] - x_i[t]\right) + c_1 r_1 \left(x_{G\text{best}}[t] - x_i[t]\right), \tag{62}$$

$$x_i[t+1] = x_i[t] + V_i[t+1], \tag{63}$$

where $x_i[t]$: the location of the particle i at moment t. $V_i[t]$: the velocity of the particle i at moment t. $x_{G\text{best}}[t]$: the best location of the particle i at moment t. w: the coefficient of inertia r_1, r_2: Rand$(0, 1)$. c_1, c_2: individual and collective learning coefficients.

5.3. NSGA-II Algorithm. This algorithm was introduced by Deb in 2002. In this algorithm, first, the initial population of parents P_0 is randomly generated with the size N. The generated initial population is then sorted out by a nondominated approach and the solutions are categorized into different levels of degree of nondomination. Subsequently, each solution is assigned with a value or rank depending on its position on that front. Hence, the solutions of the first front, which are at the lowest level, are ranked first, the solutions of the second front are ranked second, and so are the rest. Then, the population of children Q_0 is generated by the size N using the binary tournament method based on the swarm comparison operator and the intersection and jump operators. Combining two populations of parents and children generates the $R_0 = P_0 \cup Q_0$ population with the size $2N$. The next generation is selected from the obtained R_0 population. Since this algorithm follows an elitist approach, the members of R_0 are categorized again by a nondominated sorting method. After creating different fronts of the

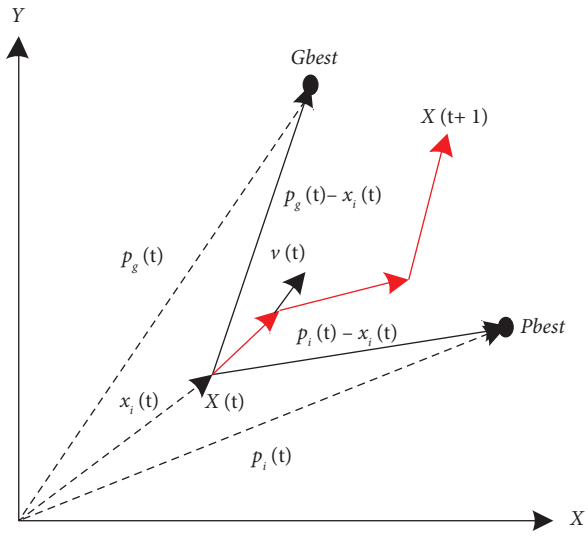

Figure 2: The mechanism of action of the particle swarm optimization algorithm.

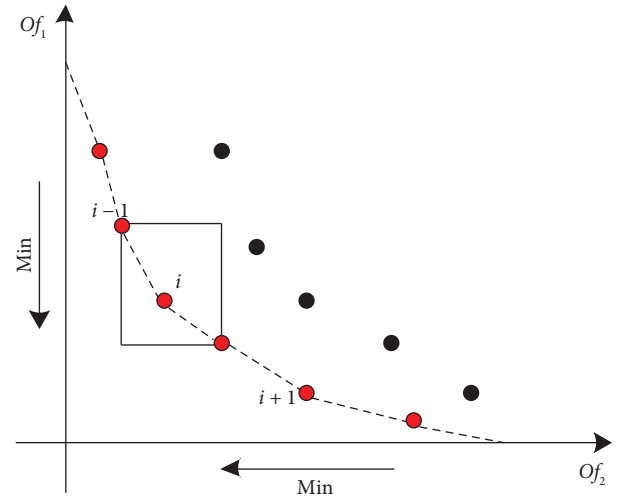

Figure 3: The concept of crowding distance.

nondomination degree, the next generation P_1 population with the size N will be filled in order from the first front onwards by in the following approach. By creating P_1, the same steps mentioned for the P_0 are performed and this loop continues until the algorithm is terminated. Ultimately, the first front achieved from the R_t sorting of the latest generation will be introduced as the set of Pareto solutions.

We assume that the R_t population resulting from combining the parents P_t and their children Q_t has been sorted by a nondominated approach the fronts F_i have been created for $i = 1, 2, \cdots$. Now, the solutions found on the first front F_1 are the first candidates to join the next generation as the best solutions available in the current generation. If the number of the F_1 members is lower than the N, all of them will be transferred to P_{t+1}. The rest of the P_{t+1} members are selected from the F_2 and then from the F_3, and so on. This procedure is continued until the F_1 would be considered as the last front from which the rest of the P_{t+1} members are supposed to be selected. At this time, since the total number of the F_1 members is higher than the required number of the remaining members, these members are sorted in order of decreasing the crowding distance, and then the remaining required number will be selected from the beginning of this list.

The most significant distinguishing feature of the MO genetic algorithm is the concept of crowding distance, as shown in Figure 3. This concept is used for determining the quality of a solution in a particular Pareto frontier. In fact, NSGA-II ensures the quality of the final unsuccessful solutions by using the crowding distance mechanism.

$$d_j(k) = \sum_{i=1}^{n} \frac{f_i(\mathrm{k}-1) - f_i(\mathrm{k}+1)}{f_i^{\max} - f_i^{\min}}. \tag{64}$$

In which n represents the number of objective functions. In addition, $f_i^{\max}, f_i^{\min}$ represent the highest and lowest values of the i-th and k objective functions of the current solution, respectively.

5.4. Gray Wolf Algorithm. The gray wolf optimization algorithm is one of the new metaheuristic algorithms proposed by Mirjalili et al. [40]; being inspired by the hunting behavior of gray wolves in the wild. In order to model the mathematical relations of the hierarchical structure of the wolf community for designing the GWO, the fittest solution is considered as alpha (α) wolf. Furthermore, the second and third optimal solutions are considered beta (β) and delta (δ), respectively. Other candidate solution are called omega (ω). In the GWO algorithm, hunting is guided by α, β, and δ. Wolves ω follow these three wolves in the hope of finding an optimal solution. In addition to leading the wolf community, the following relations state the simulation of the siege behavior of gray wolves while hunting prey.

$$\vec{D} = \left|\vec{C}.\vec{X}_p(t) - \vec{X}(t)\right| \vec{X}(t+1) = \vec{X}_p(t) - \vec{A}.\vec{D}, \tag{65}$$

where t represents iterations, $\vec{C}$. shows coefficient vectors, $\vec{X}_p$ represents prey position vectors, and $\vec{X}$ shows gray wolf position vectors. The vectors $\vec{C}$ and $\vec{A}$ are calculated as follows:

$$\vec{A} = \overrightarrow{2a}.\vec{r_1} - \vec{a}, \vec{C} = 2\vec{r_2}, \mathrm{Rand}(0,1). \tag{66}$$

In these relations, $\vec{a}$ decreases linearly from 2 to 0. The GWO algorithm uses community leadership simulation, as well as the siege mechanism to find the optimal solution to optimization problems. This algorithm selects the first three solutions from the desired solution and requires other search factors including omega wolves to improve their position over the top solutions. The following relations are applied to each factor during the optimization process to perform the hunting process and thus find the appropriate areas in the search space.

$$\vec{D}_{\alpha} = \left|\vec{C}_1.\vec{X}_{\alpha} - \vec{X}\right|,$$
$$\vec{D}_{\beta} = \left|\vec{C}_2.\vec{X}_{\beta} - \vec{X}\right|, \quad (67)$$
$$\vec{D}_{\delta} = \left|\vec{C}_2.\vec{X}_{\delta} - \vec{X}\right|,$$

$$\vec{X}_1 = \vec{X}_{\alpha} - \vec{A}_1.\vec{D}_{\alpha},$$
$$\vec{X}_2 = \vec{X}_{\beta} - \vec{A}_2.\vec{D}_{\beta}, \quad (68)$$
$$\vec{X}_3 = \vec{X}_{\delta} - \vec{A}_3.\vec{D}_{\delta},$$

$$\vec{X}(t+1) = \frac{\vec{x}_1 + \vec{x}_2 + \vec{x}_3}{3}. \quad (69)$$

The search in the problem space is guaranteed by the vector $\vec{A}$ with random values between [-1,1], necessitating the factors to distance themselves from the prey. Another GWO parameter which helps to search further is the vector $\vec{C}$. The vector $\vec{C}$ selects random values between [0, 2], leading to random weight values for the prey. These values show the effect of prey on the definition of distance in (64). The GWO algorithm begins the optimization process by generating a set of initial random solutions. During the optimization process, three of the best solutions are saved (α, β, δ). Then, the wolves' situation is updated through equations (67)–(69). Meanwhile, the values of A and a increase linearly with increasing repetitions. Thus, wolves will tend to distance from the prey and get closer to the prey. Ultimately, the position and value of the alpha solution are returned to the algorithm as the best solution found in terms of all constraints. A distinctive feature of the gray wolf algorithm is the use of several guides and the avoidance of falling into the optimal local trap.

Figure 4 shows the multisegment chromosome presented in this study. For example, the figure on the right shows the chromosome related to the $\mathrm{Inv}_{j,s}^{ct}$ variable. The value within each gene represents the amount of residual inventory of the product c in the warehouse of the production center j in the period t in scenario s. The figure on the left also shows the chromosome corresponding to the variable x_p^t. If the value within each gene is equal to 1, the recycling center at location p is established in period t.

Figure 5 illustrates the intersection operator. As seen in the figure, the single-point intersection has been used in this research. In this type of intersection, the two sides of the chromosome will be displaced together.

As shown in Figure 6, the mutation operator considered in this study is a reverse mutation type. In this type of mutation, a row of chromosomes is selected and will be then reversed.

5.5. Proposed Hybrid Metaheuristic Algorithm GW-NS. In order to implement the optimization process of the proposed method based on two algorithms NSGA-II and GWO, two ideas were hybridised with each other.

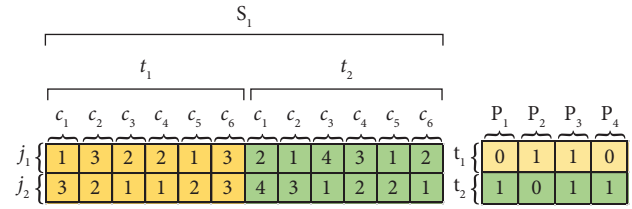

Figure 4: The proposed chromosome structure.

The first idea is the strategy of selecting a leader from the external archive of nondominated solutions.

In the proposed algorithm, the value of the crowding distance is calculated for each member in the external archive and using the roulette wheel mechanism, we select the three members alpha (α), beta (β), and delta (δ). Members of the external archive that have more crowding distance should have a more chance of being selected. In other words:

p_i: probability of selecting the i-th element

d_i: crowding distance of the i-th element in the external archive.

$$\forall i, j \in \text{Archive } d_i \geq d_j \Rightarrow p_i \geq p_j. \quad (70)$$

The second idea is the control process, when a nondominated solution aims to enter the external archive or when the number of archive members is higher than its capacity (it should be noted that there is always a certain number of members for the external archive).

In the proposed algorithm for deleting a nondominated solution, when the number of archive members exceeds its capacity, some members of the archive should be selected for deletion. The members with less crowding distance should have a more chance of being selected for deletion. The selection process is done by roulette wheel mechanism.

$$\forall i, j \in \text{Archive } d_i \geq d_j \Rightarrow p_i \leq p_j. \quad (71)$$

In general, the steps of the proposed algorithm are as follows (Figure 7):

(1) Defining a random primary population in the problem search space.

(2) Defining an external archive of nondominated members of the primary population.

(3) Selecting three members alpha (α), beta (β), and delta (δ) from the members in the external archive randomly, using the roulette wheel mechanism, based on the crowding distance

$$\forall i, j \in \text{Archive } d_i \geq d_j \Rightarrow p_i \geq p_j. \quad (72)$$

In which:

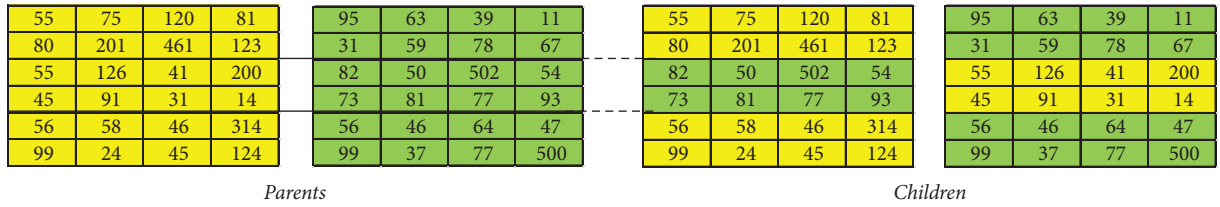

Figure 5: The intersection operator.

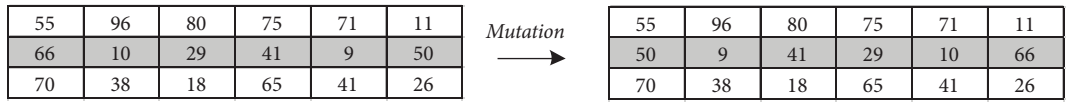

Figure 6: The mutation operator.

$$p_i = \frac{e^{\lambda d_i/d_{\max}}}{\sum_{j\in \text{Arcive}} e^{\lambda d_i/d_{\max}}},$$
$$\lambda = \sum_{i\in H} p_i, \tag{73}$$

H: A total of 50% better total external archive members based on crowding distance index.

(4) Updating the position of each current member based on equations (67)–(69) and forming a new population.

(5) Selecting a percentage of the new population of the previous stage (stage 4) for mutation and creation of a new population.

(6) Determining the nondominated members of the new population produced in the previous stage (stage 5).

(7) Adding the nondominated population created in the previous stage (stage 6) to the external archive and updating it.

(8) If the number of members of the external archive is higher than the determined capacity, extra members will be removed.

Note: Deletion is conducted by the roulette wheel mechanism and based on the crowding distance index, i.e., the smaller the crowding distance, the more likely it is to be eliminated.

$$\forall i, j \in \text{Archive } d_i \geq d_j \Rightarrow p_i \leq p_j. \tag{74}$$

In which:

$$p_i = \frac{e^{-\theta d_i/d_{\max}}}{\sum_{j\in \text{Arcive}} e^{-\theta d_i/d_{\max}}},$$
$$\theta = \sum_{i\in H} p_i, \tag{75}$$

H: A total of 50% better total external archive members based on crowding distance index.

(9) If the termination conditions are met, go to the next stage, otherwise return to stage 3.

(10) The End.

5.6. Tuning the Parameters. Since the output of the problems strongly depends on the parameters of the proposed algorithms, thus, we used the Taguchi method to tune their parameters. The advantage of the Taguchi method over other tests design methods in addition to cost is to obtain the optimal levels of parameters in less time [41]. Choosing an orthogonal array appears to be one of the most important steps, which estimates the effects of factors on the mean values of the solution and variations. The most appropriate test design in this research was found to be the three-level experiments at three low, moderate, and high levels. Then, the arrays L_9 and L_{27} were chosen as the suitable test design to tune the parameter of the proposed algorithms due to the Taguchi standard orthogonal arrays. The levels of the parameters of NSGA-II and MOPSO algorithms are given in Table 2 for their tuning.

A statistical measure of performance, known as the signal to noise ratio (S/N) is considered in the Taguchi method to tune the optimal parameters. This ratio encompasses mean values and variations, and it would be more desirable at higher levels. The solution variable considered in this study is the ratio of the two indices of the Mean Ideal Distance (MID, equation (77)) and the Diversification Metric (DM, equation (78)) for MO algorithms. Since this solution variable is of the type "the lower, the better", then, its corresponding S/N ratio is considered as equation (76). The proposed metaheuristic algorithms are implemented for each Taguchi experiment, and then, the S/N ratios will be calculated by the Minitab 19.2020.1 software.

$$\frac{S}{N} = -10\log\left(\frac{1}{n}\sum_{i=1}^{n} y_i^2\right). \tag{76}$$

6. Results Analysis and Comparisons

The model is first solved in small and medium dimensions aimed at evaluating the accuracy and precision of the

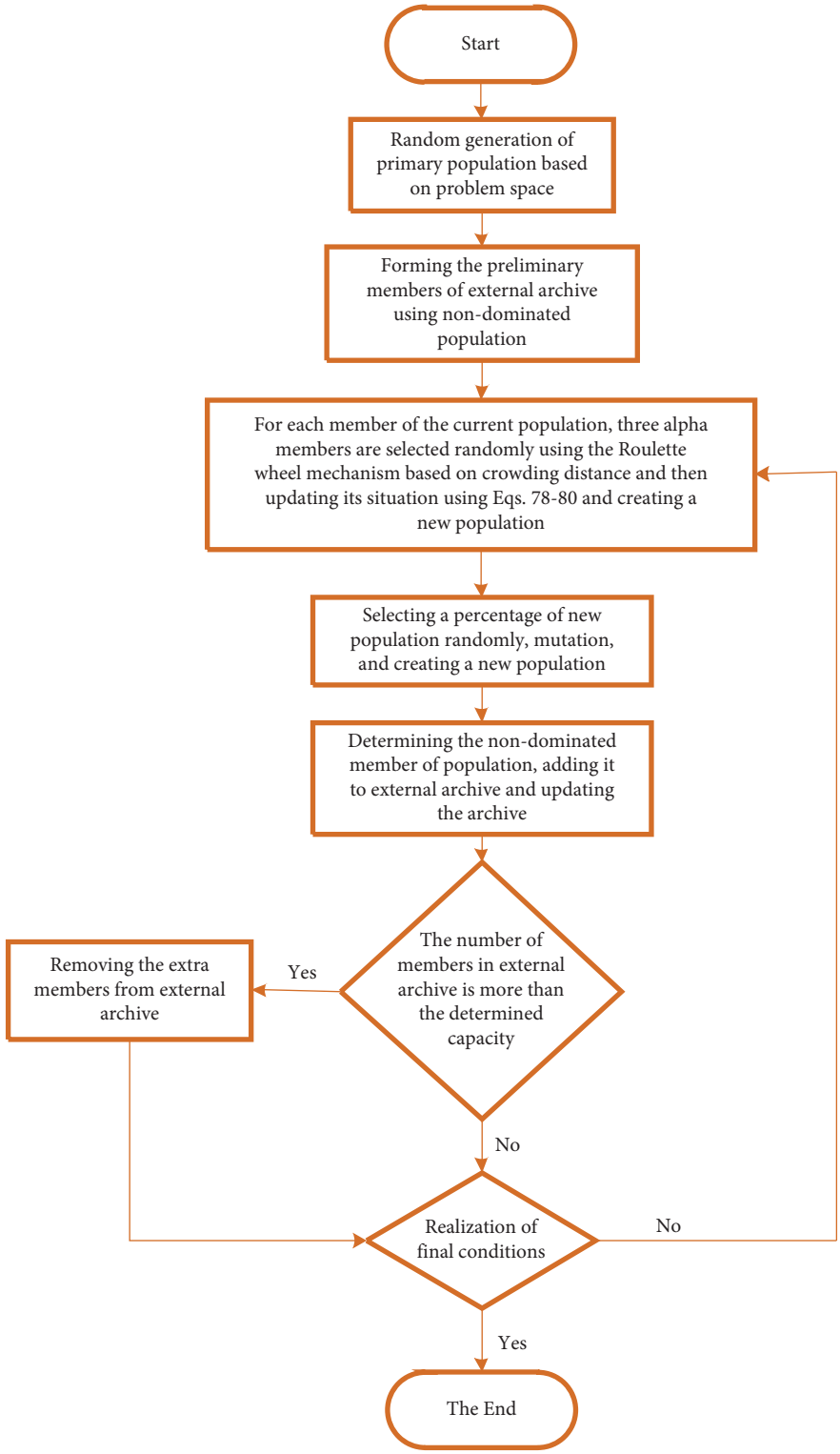

Figure 7: Flowchart of proposed algorithm GW-NS.

proposed model. Table 3 shows the problems with small dimensions (samples 1–5) and medium dimensions (samples 6–10). For example, there is a customer, a manufacturer, a supplier, a recycling center, a hub, a repair center, a distributor, and a landfill center in sample number 1.

Figure 8 shows the model solution time for NSGA-II, MOPSO, GW-NS algorithms, and the Epsilon constraint

Table 2: The algorithm parameter table.

Parameter	Level 1	Level 2	Level 3
MOPSO algorithm parameters			
Max—iteration	100	150	200
Population size (npop)	50	80	100
Repository size (nRep)	60	85	100
Inertia coefficient (w)	0.3	0.5	0.8
Inertia weight damping ratio (wdamp)	0.8	0.9	0.99
Number of grids per dimension (nGride)	3	5	7
Grid increase rate (alpha)	0.1	0.2	0.3
Leader selection pressure (beta)	2	4	5
Leader removal pressure (gamma)	2	4	5
Mutation rate (mu)	0.1	0.15	0.2
Individual learning coefficient (c1)	1	2	4
Collective learning coefficient (c2)	2	3	5
NSGA-II algorithm parameters			
Max—iteration	100	130	150
Population size (npop)	50	100	150
Mutation rate (pm)	0.8	0.85	0.9
Crossover rate (pc)	0.1	0.15	0.2
—	—	—	—
GW-NS algorithm parameters			
Max—iteration	100	140	160
Population size (npop)	54	96	165
Mutation rate (pm)	0.8	0.86	0.89
Crossover rate (pc)	0.1	0.16	0.2
Number of wolf(N)	20	36	50
Gray wolf pack size(G)	10	16	21
Path coefficient(a)	0.3	0.4	0.5

Table 3: The dimensions of the problem.

Number of the problem	Customers	Manufacturers	Suppliers	Recycling centers	Hub	Repair centers	Distribution centers	Burial centers
1	1	1	1	1	1	1	1	1
2	1	2	1	2	1	2	1	2
3	2	2	2	3	2	2	2	1
4	3	2	1	3	2	3	3	2
5	3	3	3	3	3	3	3	3
6	3	2	3	4	3	3	4	3
7	4	3	4	3	4	4	4	4
8	5	4	5	4	4	5	5	4
9	5	5	5	5	5	5	5	5
10	6	5	6	5	6	5	5	5

method. As can be seen, the solution time by the Epsilon constraint method is increasing exponentially as the dimension of the problem increases. Algorithms are programmed using GAMS and MATLAB (R2020 a) and implemented on a PC under Windows 7, Intel Core i3, 3.3 GHz, 4 GB RAM.

6.1. Multiobjective Performance Metrics. The performance of the algorithms used to solve the proposed model was evaluated by the following criteria, which are described below.

6.1.1. Mean Ideal Distance (MID). This criterion measures the degree of closeness between the solutions found on the Pareto front and the ideal points $(f_1^{\text{best}}, f_2^{\text{best}}, f_3^{\text{best}})$, which is calculated by equation (77). The lower the value of this criterion for an algorithm, the better the performance of that algorithm would be.

$$\text{MID} = \frac{\sqrt{\left(f_{1i} - f_1^{\text{best}}/f_1^{\text{nadir}} - f_1^{\text{best}}\right)^2 + \left(f_{2i} - f_2^{\text{best}}/f_2^{\text{nadir}} - f_2^{\text{best}}\right)^2 + \left(f_{3i} - f_3^{\text{best}}/f_3^{\text{nadir}} - f_3^{\text{best}}\right)^2}}{n}. \tag{77}$$

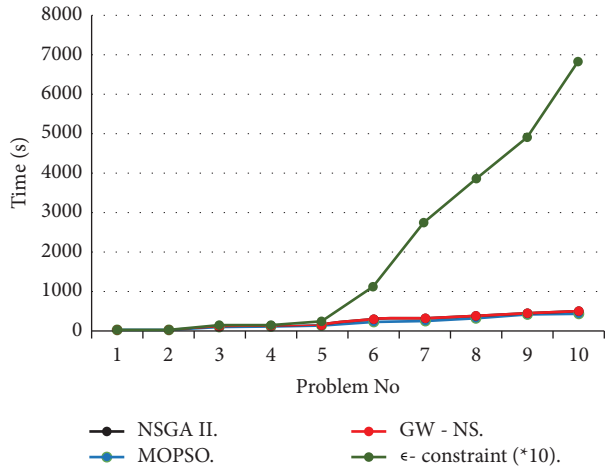

Figure 8: The model solution time in terms of increasing the problem dimension.

In equation (77), n is the number of nondominated solutions, while f_i^{best} and f_i^{nadir} are the best and worst values of the i^{th} objective function, respectively [42].

6.1.2. Diversification Metric (DM). This criterion measures the scattering of the Pareto solutions, which is calculated by the following equation.

$$DM = \sqrt{\left(\frac{\max\{f_{1i}\} - \min\{f_{1i}\}}{f_1^{nadir} - f_1^{best}}\right)^2 + \left(\frac{\max\{f_{2i}\} - \min\{f_{2i}\}}{f_2^{nadir} - f_2^{best}}\right)^2 + \left(\frac{\max\{f_{3i}\} - \min\{f_{3i}\}}{f_3^{nadir} - f_3^{best}}\right)^2}. \quad (78)$$

According to equation (78), a higher value of DM indicates the better performance of the algorithm [42].

6.1.3. Spacing Metric (SM). This criterion measures the scattering pattern of the nondominated solutions, which is calculated by the following equation.

$$SM = \frac{\sum_{i=1}^{n-1} |d_i - \overline{d}|}{(n-1)\overline{d}}. \quad (79)$$

In equation (79), d_i determines the Euclidean distance between successive solutions in the set of the nondominated solutions obtained by the algorithm and $\overline{d}$ is the average of these distances. According to the definition of SM, the lower the value of this index, the better the algorithm would be [42].

In order to compare the results of the algorithms, three metaheuristics are applied to solve 10 problems in various dimensions, and the obtained results are reported in Table 4. For a closer look at the results of the three algorithms, the following hypothesis was tested according to DM, SM, and MID indexes.

Hypothesis 1. There is a significant difference between the DM of the solutions generated by the three algorithms GW-NS, MOPSO, and NSGA-II.

Hypothesis 2. There is a significant difference between the MID of the solutions generated by the three algorithms GW-NS, MOPSO, and NSGA-II.

Hypothesis 3. There is a significant difference between the SM of the solutions generated by the three algorithms GW–NS, MOPSO, and NSGA-II.

Table 4 shows the values of MID, DM, and SM indices for the problems listed in Table 3.

The MID and SM indices, respectively, increase with low and high slopes as the size of the problem enhances according to Figures 9 and 10. To put it better, increasing the dimensions of the problem reduces the efficiency of algorithms in terms of MID and SM indices, while the MID index shows less sensitivity to the increase in dimensions. According to Figure 11, the increased size of the problem enhances the efficiency of the algorithms based on the DM index. In other words, increasing the dimensions of the problem exhibited a higher potential for exploring and extracting the region of the solution.

6.2. Statistical Analysis Comparisons. For the purpose of statistical analysis, one-way variance analysis technique and SPSS software are applied. As well, to confirm the parametric results, a nonparametric test called Kruskal—Wallis test was used. If data are suitable for variance analysis, nonparametric test is used where there is no precondition for uniformity of the variance or normal distribution. Results of one-way variance analysis and nonparametric test for three measures are provided in Tables 5–8.

Based on Tables 5–8 for all three indices SM, DM, and MID, the P value of ANOVA and Kruskal—Wallis tests are all more than 0.05, Thus, there is no significant difference

Table 4: The computational results of comparison measurement criteria of MOPSO, NSGA-II, and GW-NS algorithms.

Problem No	*NSGA-II*			*MOPSO*			*GW-NS*		
	SM	MID	DM	SM	MID	DM	SM	MID	DM
1	0.1	6.46	1.29	0	6.49	0.47	0	6.47	1.34
2	0.1	6.49	1.06	0.09	6.49	0.68	0.11	6.45	0.95
3	0.11	6.69	1.28	0.12	6.73	0.74	0.13	6.51	1.31
4	0.13	6.68	1.8	0.16	6.75	0.93	0.14	6.71	1.41
5	0.19	6.72	1.51	0.22	6.76	1.12	0.23	6.73	1.62
6	0.17	6.69	1.63	0.21	6.75	1.27	0.25	6.71	1.78
7	0.21	6.78	2.12	0.27	6.82	1.45	0.26	6.75	2.33
8	0.2	6.76	2.24	0.24	6.82	1.82	0.26	6.77	2.31
9	0.22	6.85	2.29	0.26	6.87	2.2	0.28	6.81	2.71
10	0.21	6.84	3.2	0.31	6.92	2.79	0.29	6.83	3.91
Ave	0.164	6.696	1.842	0.188	6.74	1.347	0.195	6.674	1.967

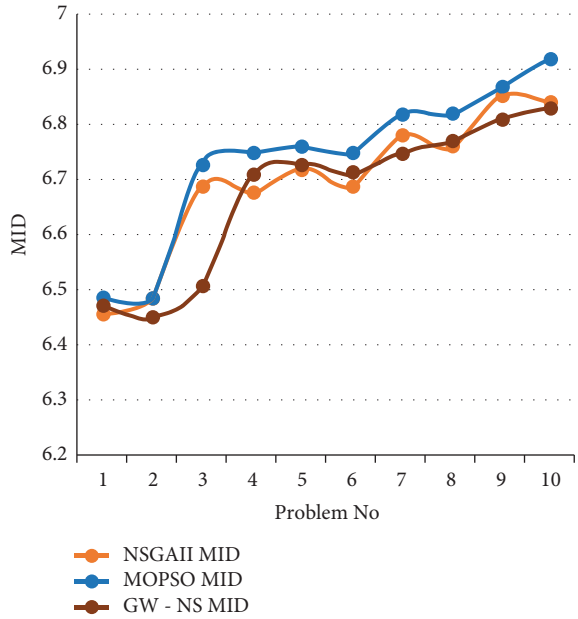

Figure 9: The result of comparing the algorithms in terms of MID.

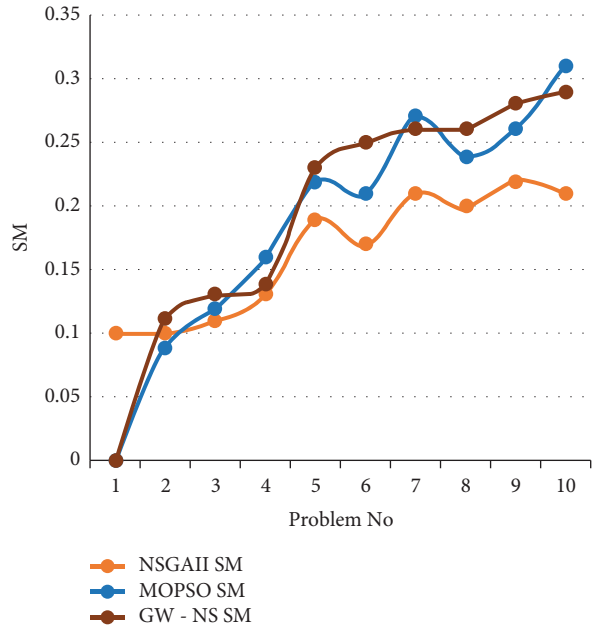

Figure 10: The result of comparing the algorithms in terms of SM.

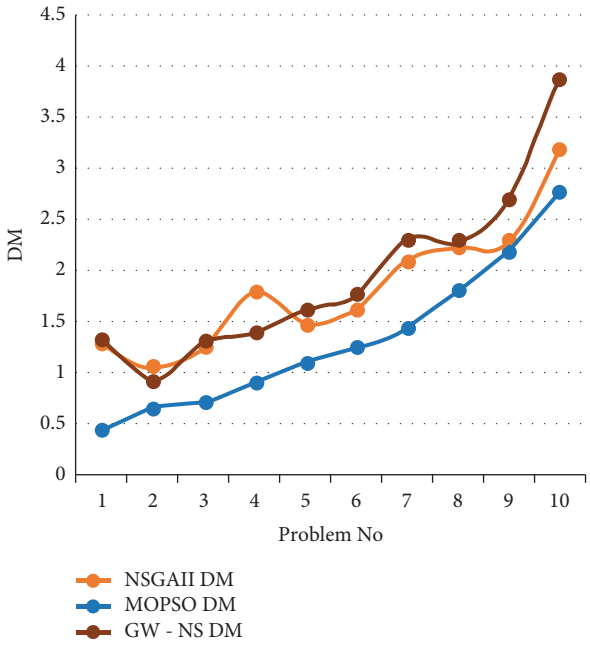

Figure 11: The result of comparing the algorithms in terms of DM.

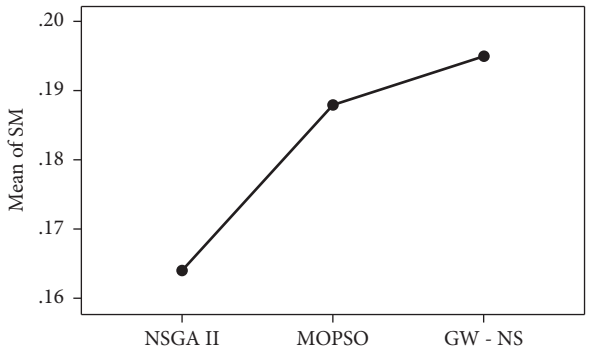

Figure 12: Mean changes in the performance index of SM algorithms.

Table 5: Results of one-way variance analysis for MID, DM, and SM.

Source	SS	DF	MS	F	P value
MID					
Solver	0.023	2	0.011	0.581	0.566
Error	0.525	27	0.019		
Total	0.547	29			
DM					
Solve	2.150	2	1.075	1.881	0.172
Error	15.429	27	0.571		
Total	17.579	29			
SM					
Solve	0.005	2	0.003	0.387	0.683
Error	0.184	27	0.007		
Total	0.190	29			

Table 6: Kruskal–Wallis nonparametric test for MID.

Solver	N	Mean rank	Chi-square	P value
NSGA-II	10	14.35	1.97	0.385
MOPSO	10	18.6		
GW-NS	10	13.55		
Total	30			

Table 7: Kruskal–Wallis nonparametric test for DM.

Solver	N	Mean rank	Chi-square	P value
NSGA-II	10	17.30	4.16	0.125
MOPSO	10	10.9		
GW-NS	10	18.3		
Total	30			

Table 8: Kruskal–Wallis nonparametric test for SM.

Solver	N	Mean rank	Chi-square	P value
NSGA-II	10	12.05	2.446	0.294
MOPSO	10	16.5		
GW-NS	10	17.95		
Total	30			

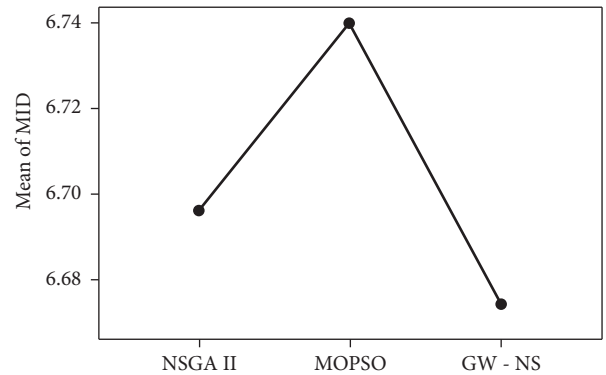

Figure 13: Mean changes in the MID performance index of algorithms.

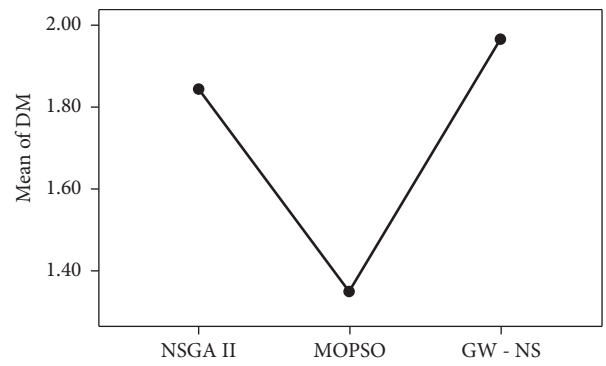

Figure 14: Mean changes in the performance index of DM algorithms.

between the performances of the three algorithms at the 5% error level. Figures 12–14 indicate that GW-NS, NSGA-II, and MOPSO algorithms have better performance in terms of MID index, respectively. In other words, this algorithm exhibited higher potentials for convergence to the ideal solution compared to other algorithms. The GW-NS

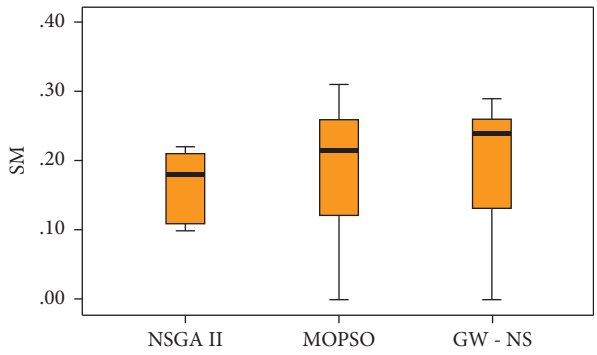

Figure 15: Boxplot of SM algorithms performance indicators.

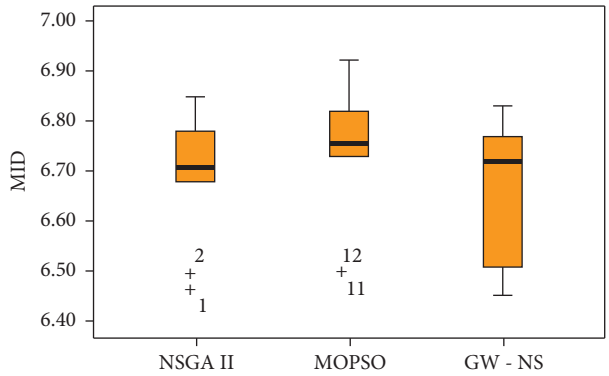

Figure 16: Boxplot of MID algorithms performance indicators.

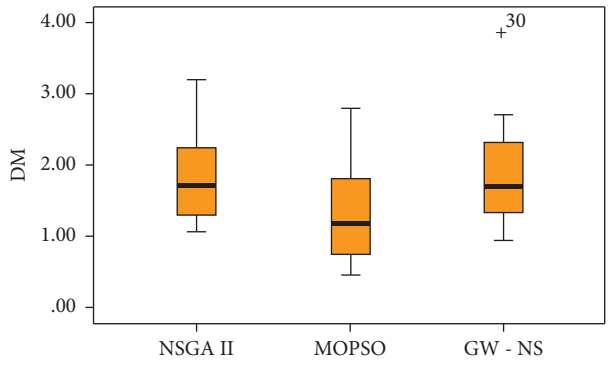

Figure 17: Boxplot of DM algorithms performance indicators.

algorithm also offered higher-diversity solutions(DM) than the NSGA-II and MOPSO algorithms. In other words, this algorithm exhibited higher potentials for exploring and extracting the region of the solution as compared with the NSGA-II and MOPSO algorithms. In addition, in terms of SM index, NSGA-II, MOPSO, and GW-NS algorithms indicate better performance, respectively. In other words, the NSGA-II algorithm generated more uniform solutions as compared with the GW-NS and MOPSO algorithms. Box plots Figures 15–17 show that the variability of the DM index is almost the same in all three algorithms. But in the MID index, the GW-NS algorithm and in the SM index, the MOPSO algorithms have the highest changes and less stability.

7. Conclusion and Future Works

In this study, a new multiobjective, multiperiod, multiproduct scenario-based fuzzy mathematical model for CLSC was presented. In the proposed model, in addition to the three aspects of sustainability, namely social, economic and environmental impact, reliability, quality of returned products by customers, and routing of goods flow in the supply chain were considered. In this network, the demand parameter was considered as fuzzy. In order to solve the proposed model, in addition to the two metaheuristic algorithms NSGA-II and MOPSO, a new hybrid metaheuristic algorithm using the strengths of the GWO algorithms (using multiple guides and avoiding falling into the optimal local trap) and NSGA-II (guaranteeing the quality of unused solutions crowding distance mechanism) was presented. After tuning their parameters by Taguchi method, their performance in problems with different dimensions was tested and evaluated by MID, DM, and SM criteria. The results of statistical analysis of indices indicated that no significant difference between the performance of the three algorithms at 5% error level. In general, GW-NS, NSGA-II, and MOPSO algorithms had better performance in terms of MID index, respectively. In addition, GW-NS, NSGA-II, and MOPSO algorithms performed better in terms of DM index. NSGA-II, MOPSO, and GW-NS algorithms performed better in terms of SM index, respectively. The model proposed in this paper can be developed in future research by considering several decision-makers in the closed loop network and the use of the concept of the game. The robust planning approach can be also used to deal with the supply chain uncertainty, making the model more powerful and flexible in the face of uncertainty. Also, instead of the exponential distribution assumed to model the reliability of the direct logistics elements, other probability distributions such as Erlang or Weibull can be considered. Multiple financial, environmental, and social goals combined with dynamic constraints can provide more effective and practical solutions. At the end, identify the strengths of other metaheuristic algorithms with the aim of using them to propose new hybrid algorithms. Combining two or more performance indicators of metaheuristic algorithms with each other and using them to compare algorithms can be considered for future study.

Abbreviations

Indices

R: Routes $r \in R$
L: Customers $l \in L$
J: Manufacturers $j \in J$
Q: The set of quality levels $Q_1, Q_2, Q_3\ Q_4$, $Q = Q_1 \cup Q_2 \cup Q_3 \cup Q_4$
Q_1: Quality level of products that are sent from hub stations to repair stations
Q_2: Quality level of products that are sent directly from the hub stations to the production stations

Q_3: Quality level of products that are sent from hub stations to recycling stations
Q_4: Quality level of products that are sent from hub stations to disposal stations, (where $Q_1 \succ Q_2 \succ Q_3 \succ Q_4 \succ$ is the quality level of the comparison operator)
I: Suppliers $i \in I$
O: The set of raw materials $o \in O$
P: Candidate points for recycling stations $p \in P$
M: Candidate points for hubs $m \in M$
W: Candidate points for repair stations $w \in W$
v: The set of means of transportation $v \in V$
C: Products set index $c \in C$
N: Candidate points for landfill and disposal stations $n \in N$
K: Candidate points of distribution stations $k \in K$
S: Set of scenarios $s \in S$
T: Term index $t \in T$

Parameters

$aq_{jj,s}$: Distance of the production station j from its own warehouse in scenario s
$a_{lm,s}$: Distance from the customer station l to the hub m in scenario s
$a_{mj,s}$: Distance of the hub station m from the production station j in scenario s
$a_{kl,s}$: Distance of the distribution station k from the customer station l in scenario s
$a_{ij,s}$: Distance of the supplier i from the production station of j in scenario s
$a_{jk,s}$: Distance of the production station j from the distribution station k in scenario s
$a_{mn,s}$: Distance of the hub m from the landfill canter n in scenario s
$a_{pj,s}$: Distance of the recycling station p from the production station j in scenario s
$a_{mp,s}$: Distance of the hub m from the recycling station p in scenario s
$a_{mw,s}$: Distance of the hub m from the repair station w in scenario s
$a_{wk,s}$: Distance of the repair station w from the distribution station k in scenario s
$dq_{jk,s}$: Distance of the producer warehouse j from the distribution station k in scenario s
EM_p: CO_2 emitted during the construction of the recycling station p
EM_k: CO_2 emitted during the construction of the distribution station k
EM_m: CO_2 emitted during the construction of the hub m
EM_n: The CO_2 emitted during the construction of the landfill and disposal station n
EM_W: CO_2 emitted during the construction of the repair station w
EMS_v: CO_2 emitted from the shipment of a yield unit by a type v vehicle over one kilometer
γ: CO_2 emitted from transporting a unit of product from the production station j to its own warehouse
u_p^t: Valency of the recycling station p in the term t
u_n^t: Valency of the landfill and disposal station n in the term t
u_k^t: Valency of the distribution station k in the term t
u_i^t: Valency of the supply station i in the term t
u_w^t: Valency of the repair station w in the term t
u_{jj}^t: Valency of the producer's j warehouse in the term t
u_j^t: Valency of the production station j in the term t
u_m^t: Valency of the hub m in the term t
cr_j^t: Valency of remanufacturing products in the production station j in the term t
E_n^t: Fixed cost of constructing the landfill and disposal (demolition) station n in the term t
E_m^t: Fixed cost of constructing the hub station m in the term t
E_k^t: Fixed cost of constructing the distribution station k in the term t
E_p^t: Fixed cost of constructing the recycling station p in the term t
E_w^t: Fixed cost of constructing the repair station w in the term t
$\widetilde{d_{l,s}^{ct}}$: Amount of demand for the yield c by the customer l in the term t in scenario s
$r_{lq,s}^{ct}$: Return rate of the yield c with the quality q from the customer station l in the term t in scenario s
rb_{mj}^{ct}: Return rate of the yield c from the hub station m to the production station j in the term t
rb_{mn}^{ct}: Return rate of the yield c from the hub station m to the landfill and disposal station n in the term t
rb_{mp}^{ct}: Return rate of the yield c from the hub station m to the recycling station p in the term t
rb_{mw}^{ct}: Return rate of the yield c from the hub station m to the repair station w in the term t
$fp_{lmq,s}^{ct}$: Return cost of each unit of the returned yield c with quality q from the customer station l to the hub station m in the term t in scenario s
$f_{j,s}^{ct}$: Maintenance cost of each unit of the yield c in the producer's warehouse at location j in the term t in scenario s
$h_{mnq,s}^{c}$: Transfer fee per unit of the returned yield c with quality q from the hub station m to the landfill station n in scenario s
$h_{kl,s}^{c}$: Transfer fee per unit of the yield c from the distribution station k to the customer station l in scenario s
$h_{ij,s}^{o}$: Transfer fee per unit of the raw materials o from the supply station i to the production station j in scenario s
$h_{jk,s}^{c}$: Transfer fee per unit of the yield c from the production station j to the distribution station k in scenario s
$h_{mjq,s}^{c}$: Transfer fee per unit of the comeback yield c with quality q from the hub station m to the production station j in scenario s
$h_{mpq,s}^{c}$: Transfer fee per unit of the comeback yield c with quality q from the hub station m to the recycling station p in scenario s

$h^c_{pj,s}$: Transfer fee per unit of the comeback yield c from the recycling station p to the production station j in scenario s

$h^c_{mwq,s}$: Transfer fee per unit of the comeback yield c with quality q from the hub station m to the repair station w in scenario s

$h^c_{wk,s}$: Transfer fee per unit of the yield c from the repair station w to the distribution station k in scenario s

$cq^c_{jk,s}$: Transfer fee per unit of the yield c from the warehouse of the producer j to the distribution station k in scenario s

$cq^c_{jj,s}$: Transfer fee per unit of the yield c from the production station j to its own warehouse in scenario s

$h^c_{lmq,s}$: Transfer fee per unit of the returned yield c from the customer l to the hub station m in scenario s

$cj_{ct,s}$: Transfer fee per unit of the yield c in the production station j in the term t in scenario s

$rcj_{ct,s}$: Transfer fee per unit of the yield c in the reproduction station j in the term t in scenario s

$cn_{ct,s}$: Transfer fee per unit of the yield c at the demolition station n in the term t in scenario s

$cm_{ct,s}$: Cost of collecting and sending a unit of the yield c to the hub station m in the term t in scenario s

$cp_{ct,s}$: Cost of recycling a unit of the yield c at the recycling station p in the term t in scenario s

$cw_{ct,s}$: Cost of repairing a unit of the yield c in the repair station w in the term t in scenario s

$ck_{ct,s}$: Cost of distributing a unit of the yield c in the distribution station k in the term t in scenario s

$\alpha j_{m,s}$: Fixed number of permanent job founded if established the hub station m in scenario s

$\alpha j_{p,s}$: Fixed number of permanent job founded if established the recycling station p in scenario s

$\alpha j_{w,s}$: Fixed number of permanent job founded if established the repair station w in scenario s

$\alpha j_{n,s}$: Fixed number of permanent job founded if established the demolition station n in scenario s

$\alpha j_{k,s}$: Fixed number of permanent job founded if established the distribution station k in scenario s

$\beta j_{m,s}$: Variable number of permanent job founded if established the hub station m in scenario s

$\beta j_{p,s}$: Variable number of permanent job founded if established the recycling station p in scenario s

$\beta j_{w,s}$: Variable number of permanent job founded if established the repair station w in scenario s

$\beta j_{n,s}$: Variable number of permanent job founded the demolition station n in scenario s

$\beta j_{k,s}$: Variable number of permanent job founded if established the distribution station k in scenario s

dl^t_j: Missed working days due to work injury in the production station j in the term t

Variables

$ro^{rt}_{vij,s}$: Equivalent to 1 if the vehicle of type v goes from the supplier i to the manufacturer j from the route r in the term t in scenario s, otherwise 0

$ro^{rt}_{vjk,s}$: Equivalent to 1 if the vehicle of type v goes from the manufacturer j to the distributor k from the route r in the term t in scenario s, otherwise 0

$Ro^{rt}_{vjk,s}$: Equivalent to 1 if the vehicle of type v goes from the warehouse of the manufacturer j to the distributor k of the route r in the term t in scenario s, otherwise 0

$ro^{rt}_{vkl,s}$: Equivalent to 1 if the vehicle of type v goes from the distributor k to the customer l from the route r in the term t in scenario s, otherwise 0

$ro^{rt}_{vlm,s}$: Equivalent to 1 if the vehicle of type v goes from the customer l to the hub m from the route r in the term t in scenario s, otherwise 0

$ro^{rt}_{vmp,s}$: Equivalent to 1 if the vehicle of type v goes from the hub m to the recycling station p from the route r in the term t in scenario s, otherwise 0

$ro^{rt}_{vpj,s}$: Equivalent to 1 if the vehicle of type v goes from the recycling station p to the manufacturer j from the route r in the term t in scenario s, otherwise 0

$ro^{rt}_{vmj,s}$: Equivalent to 1 if the vehicle of type v goes from the hub m to the manufacturer j from the route r in the term t in scenario s, otherwise 0

$ro^{rt}_{vmn,s}$: Equivalent to 1 if the vehicle of type v goes from the hub m to the demolition station n from the route r in the term t in scenario s, otherwise 0

$ro^{rt}_{vmw,s}$: Equivalent to 1 if the vehicle type v goes from the hub m to the repair station w from the route r in the term t in scenario s, otherwise 0

$ro^{rt}_{vwk,s}$: Equivalent to 1 if the vehicle type v goes from the repair station w to the distributor k from the route r in the term t in scenario s, otherwise 0

$z^{ct}_{lmq,s}$: Flow amount of the returned yield c with the quality of the type q from the customer l to the hub m in the term t in scenario s

$z^{ct}_{mpq,s}$: Flow amount of the returned yield c with the quality of the type q from the hub m to the recycling station p in the term t in scenario s

$z^{ot}_{ij,s}$: Flow amount of the raw materials o from the supply station i to the production station j in the term t in scenario s

$z^{ct}_{pj,s}$: Flow amount of the reused yield c from the recycling station p to the production station j in the term t in scenario s

$z^{ct}_{mnq,s}$: Flow amount of the returned yield c with the quality of the type q from the hub m to the demolition station n in the term t in scenario s

$z^{ct}_{mjq,s}$: Flow amount of the returned yield c with the quality of the type q from the hub m to the production station j in the term t in scenario s

$z^{ct}_{mwq,s}$: Flow amount of the returned yield c with the quality of the type q from the hub m to the repair station w in the term t in scenario s

$z^{ct}_{wk,s}$: Flow amount of the yield c from the repair station w to the distribution station k in the term t in scenario s

$z^{ct}_{jk,s}$: Flow amount of the yield c from the production station j to the distribution station k in the term t in scenario s

$z^{ct}_{kl,s}$: Flow amount of the yield c from the distribution station k to the customer l in the term t in scenario s

$Q^{ct}_{jk,s}$: Flow amount of the yield c from the warehouse of the producer j to the distribution station k in the term t in scenario s

$Q^{ct}_{jj,s}$: Flow amount of the yield c from the production station j to its own warehouse in the term t in scenario s

x^t_k: If the distribution station is established at the location k in the term t, its value would be equal to 1, otherwise 0

x^t_p: If the recycling station is established at the location p in the term t, its value would be equal to 1, otherwise 0

x^t_m: If the hub is established at the location m in the term t, its value would be equal to 1, otherwise 0

x^t_n: If the landfill and demolition station is established at the location n in the term t, its value would be equal to 1, otherwise 0

x^t_w: If the repair station is established at the location w in the term t, its value would be equal to 1, otherwise 0.

Data Availability

The data used to support the findings of this study will be made available from the corresponding author upon request.

Conflicts of Interest

The authors declare that they have no conflicts of interest.

References

[1] M. Rabbani, S. A. A. Hosseini-Mokhallesun, A. H. Ordibazar, and H. Farrokhi-Asl, "A hybrid robust possibilistic approach for a sustainable supply chain location-allocation network design," *International Journal of Systems Science: Operations and Logistics*, vol. 7, no. 1, pp. 60–75, 2020.

[2] K. Govindan, H. Mina, A. Esmaeili, and S. M. Gholami-Zanjani, "An integrated hybrid approach for circular supplier selection and closed loop supply chain network design under uncertainty," *Journal of Cleaner Production*, vol. 242, Article ID 118317, 2020.

[3] A. P. Chobar, M. A. Adibi, and A. Kazemi, "Multi-objective Hub-Spoke Network Design of Perishable Tourism Products Using Combination Machine Learning and Meta-Heuristic Algorithms," *Environment, Development and Sustainability*, pp. 1–28, 2022.

[4] M. Biuki, A. Kazemi, and A. Alinezhad, "An integrated location-routing-inventory model for sustainable design of a perishable products supply chain network," *Journal of Cleaner Production*, vol. 260, Article ID 120842, 2020.

[5] E. J. Mamaghani and S. Davari, "The bi-objective periodic closed loop network design problem," *Expert Systems with Applications*, vol. 144, Article ID 113068, 2020.

[6] H. Peng, N. Shen, H. Liao, H. Xue, and Q. Wang, "Uncertainty factors, methods, and solutions of closed-loop supply chain — a review for current situation and future prospects," *Journal of Cleaner Production*, vol. 254, Article ID 120032, 2020.

[7] H. Alzoubi, G. Ahmed, A. Al-Gasaymeh, and B. Al Kurdi, "Empirical study on sustainable supply chain strategies and its impact on competitive priorities: the mediating role of supply chain collaboration," *Management Science Letters*, vol. 10, no. 3, pp. 703–708, 2020.

[8] H. Dündar, M. Ömürgönülşen, and M. Soysal, "A review on sustainable urban vehicle routing," *Journal of Cleaner Production*, vol. 285, Article ID 125444, 2021.

[9] A. Pourghader Chobar, M. A. Adibi, and A. Kazemi, "A novel multi-objective model for hub location problem considering dynamic demand and environmental issues," *Journal of Industrial Engineering and Management Studies*, vol. 8, no. 1, pp. 1–31, 2021.

[10] M. Abdel-Basset and R. Mohamed, "A novel plithogenic TOPSIS-CRITIC model for sustainable supply chain risk management," *Journal of Cleaner Production*, vol. 247, Article ID 119586, 2020.

[11] A. Jabbarzadeh, B. Fahimnia, and F. Sabouhi, "Resilient and sustainable supply chain design: sustainability analysis under disruption risks," *International Journal of Production Research*, vol. 56, no. 17, pp. 5945–5968, 2018.

[12] J. Gaur, M. Amini, and A. K. Rao, "The impact of supply chain disruption on the closed-loop supply chain configuration profit: a study of sourcing policies," *International Journal of Production Research*, vol. 58, no. 17, pp. 5380–5400, 2020.

[13] F. Maadanpour Safari, F. Etebari, and A. Pourghader Chobar, "Modelling and optimization of a tri-objective Transportation-Location-Routing Problem considering route reliability: using MOGWO, MOPSO, MOWCA and NSGA-II," *Journal of Optimization in Industrial Engineering*, vol. 14, no. 2, pp. 99–114, 2021.

[14] Y. Zhang, W. Yadav, and Y. Bharosh, "Application of circular economy and uncertainty planning in analyzing the sustainable closed-loop supply chain network design," *Mathematical Problems in Engineering*, vol. 2022, Article ID 5320974, 16 pages, 2022.

[15] B. Hassangaviar, B. Naderi, F. Etebari, and B. Vahdani, "A multiobjective model for optimizing green closed-loop supply chain network under uncertain environment by NSGA-II metaheuristic algorithm," *Discrete Dynamics in Nature and Society*, vol. 2022, pp. 1–16, 2022.

[16] D. G. Mogale, A. De, A. Ghadge, and E. Aktas, "Multi-objective modelling of sustainable closed-loop supply chain network with price-sensitive demand and consumer's incentives," *Computers and Industrial Engineering*, vol. 168, Article ID 108105, 2022.

[17] Y. Kazancoglu, D. Yuksel, M. D. Sezer, S. K. Mangla, and L. Hua, "A green dual-channel closed-loop supply chain network design model," *Journal of Cleaner Production*, vol. 332, Article ID 130062, 2022.

[18] A. Khalili Nasr, M. Tavana, B. Alavi, and H. Mina, "A novel fuzzy multi-objective circular supplier selection and order allocation model for sustainable closed-loop supply chains," *Journal of Cleaner Production*, vol. 287, Article ID 124994, 2021.

[19] S. Sadeghi Ahangar, A. Sadati, and M. Rabbani, "Sustainable design of a municipal solid waste management system in an integrated closed-loop supply chain network using a fuzzy approach: a case study," *Journal of Industrial and Production Engineering*, vol. 38, no. 5, pp. 323–340, 2021.

[20] A. Goli, H. K. Zare, R. Tavakkoli-Moghaddam, and A. Sadegheih, "Multiobjective fuzzy mathematical model for a financially constrained closed-loop supply chain with labor employment," *Computational Intelligence*, vol. 36, no. 1, pp. 4–34, 2020.

[21] S. S. Ali, T. Paksoy, B. Torğul, and R. Kaur, "Reverse Logistics Optimization of an Industrial Air Conditioner Manufacturing

Company for Designing Sustainable Supply Chain: A Fuzzy Hybrid Multi-Criteria Decision-Making Approach," *Wireless Networks*, vol. 26, pp. 1–24, 2020.

[22] Y. Yun, A. Chuluunsukh, and M. Gen, "Sustainable closed-loop supply chain design problem: a hybrid genetic algorithm approach," *Mathematics*, vol. 8, no. 1, p. 84, 2020.

[23] H. Reyhani, Y. Jabarzadeh, N. Ghaffarinasab, V. Kumar, and J. A. Garza-Reyes, "A multi-objective linear optimization model for designing a sustainable closed-loop agricultural supply chain," in *Proceedings of the 10th Conference on Industrial Engineering and Operations Management Dubai, UAE*, pp. 1–12, Dubai, UAE, March 2020.

[24] P. Wang, J. Huang, Z. Cui, L. Xie, and J. Chen, "A Gaussian error correction multi-objective positioning model with NSGA-II," *Concurrency and Computation: Practice and Experience*, vol. 32, no. 5, p. e5464, 2020.

[25] Z. Mohtashami, A. Aghsami, and F. Jolai, "A green closed loop supply chain design using queuing system for reducing environmental impact and energy consumption," *Journal of Cleaner Production*, vol. 242, Article ID 118452, 2020.

[26] R. Sadeghi Rad and N. Nahavandi, "A novel multi-objective optimization model for integrated problem of green closed loop supply chain network design and quantity discount," *Journal of Cleaner Production*, vol. 196, pp. 1549–1565, 2018.

[27] M. Hajiaghaei-Keshteli and A. M. Fathollahi Fard, "Sustainable closed-loop supply chain network design with discount supposition," *Neural Computing and Applications*, vol. 31, no. 9, pp. 5343–5377, 2019.

[28] M. Ghomi-Avili, S. G. Jalali Naeini, R. Tavakkoli-Moghaddam, and A. Jabbarzadeh, "A fuzzy pricing model for a green competitive closed-loop supply chain network design in the presence of disruptions," *Journal of Cleaner Production*, vol. 188, pp. 425–442, 2018.

[29] M. Rahimi and V. Ghezavati, "Sustainable multi-period reverse logistics network design and planning under uncertainty utilizing conditional value at risk (CVaR) for recycling construction and demolition waste," *Journal of Cleaner Production*, vol. 172, pp. 1567–1581, 2018.

[30] G. Wang and A. Gunasekaran, "Operations scheduling in reverse supply chains: identical demand and delivery deadlines," *International Journal of Production Economics*, vol. 183, pp. 375–381, 2017.

[31] J. G. Dijkman, H. Van Haeringen, S. J. De Lange, and L. Zadeh, "Fuzzy numbers," *Journal of Mathematical Analysis and Applications*, vol. 92, Article ID 301e341, 1983.

[32] M. Hanss, "Applied Fuzzy Arithmetic," *An Introduction with Engineering Applications*, Springer, New York, NY, USA, 2005.

[33] A. Al-Qudaimi, K. Kaur, and S. Bhat, "Triangular fuzzy numbers multiplication: QKB method," *Fuzzy Optimization and Modeling Journal*, vol. 2, no. 2, pp. 34–40, 2021.

[34] T. F. Liang, "Distribution planning decisions using interactive fuzzy multi-objective linear programming," *Fuzzy Sets and Systems*, vol. 157, no. 10, pp. 1303–1316, 2006.

[35] R. C. Wang and T. F. Liang, "Applying possibilistic linear programming to aggregate production planning," *International Journal of Production Economics*, vol. 98, no. 3, pp. 328–341, 2005.

[36] M. Laumanns, L. Thiele, and E. Zitzler, "An efficient, adaptive parameter variation scheme for metaheuristics based on the epsilon-constraint method," *European Journal of Operational Research*, vol. 169, no. 3, pp. 932–942, 2006.

[37] M. Fakhrzad and A. Sadri Esfahani, "Modeling the time windows vehicle routing problem in cross-docking strategy using two meta-heuristic algorithms," *International Journal of Engineering-Transactions A: Basics*, vol. 27, no. 7, pp. 1113–1126, 2013.

[38] C. A. Coello, G. Pulido, and M. Lechuga, "Handling multiple objectives with particle swarm optimization," *IEEE Transactions on Evolutionary Computation*, vol. 8, no. 3, pp. 256–279, 2004.

[39] M. Z. Malik, M. Kumar, A. M. Soomro et al., "Strategic planning of renewable distributed generation in radial distribution system using advanced MOPSO method," *Energy Reports*, vol. 6, pp. 2872–2886, 2020.

[40] S. Mirjalili, S. M. Mirjalili, and A. Lewis, "Grey wolf optimizer," *Advances in Engineering Software*, vol. 69, pp. 46–61, 2014.

[41] S. Fraley, M. Oom, B. Terrien, and J. Date, *Design of Experiments via Taguchi Methods: Orthogonal Arrays: The Michigan Chemical Process Dynamic and Controls*, Open Text Book, Siyavula, South Africa, 2006.

[42] F. Habibi, F. Barzinpour, and S. Sadjadi, "A Multi-objective optimization model for project scheduling with time-varying resource requirements and capacities," *Journal of Industrial and Systems Engineering*, vol. 10, pp. 92–118, 2017.